1994

Computation of laminar viscous flows using Von Mises coordinates.

Paul Stephen. Carson
University of Windsor

COMPUTATION OF LAMINAR VISCOUS FLOWS USING VON MISES COORDINATES

by

Paul Stephen Carson

A Dissertation
Submitted to the Faculty of Graduate Studies and Research
Through the Department of Mathematics & Statistics
in Partial Fulfillment
of the Requirements for the degree of
Doctor of Philosophy
at the University of Windsor

Windsor, Ontario, Canada

1994

ISBN 0-612-01428-2

Name Paul Carson

Dissertation Abstracts International is arranged by broad, general subject categories. Please select the one subject which most nearly describes the content of your dissertation. Enter the corresponding four-digit code in the spaces provided.

Mathematics | 0405 | U·M·I

SUBJECT TERM | SUBJECT CODE

Subject Categories

THE HUMANITIES AND SOCIAL SCIENCES

COMMUNICATIONS AND THE ARTS
Architecture 0729
Art History 0377
Cinema 0900
Dance 0378
Fine Arts 0357
Information Science 0723
Journalism 0391
Library Science 0399
Mass Communications 0708
Music 0413
Speech Communication 0459
Theater 0465

EDUCATION
General 0515
Administration 0514
Adult and Continuing 0516
Agricultural 0517
Art 0273
Bilingual and Multicultural 0282
Business 0688
Community College 0275
Curriculum and Instruction 0727
Early Childhood 0518
Elementary 0524
Finance 0277
Guidance and Counseling 0519
Health 0680
Higher 0745
History of 0520
Home Economics 0278
Industrial 0521
Language and Literature 0279
Mathematics 0280
Music 0522
Philosophy of 0998
Physical 0523
Psychology 0525
Reading 0535
Religious 0527
Sciences 0714
Secondary 0533
Social Sciences 0534
Sociology of 0340
Special 0529
Teacher Training 0530
Technology 0710
Tests and Measurements 0288
Vocational 0747

LANGUAGE, LITERATURE AND LINGUISTICS
Language
General 0679
Ancient 0289
Linguistics 0290
Modern 0291
Literature
General 0401
Classical 0294
Comparative 0295
Medieval 0297
Modern 0298
African 0316
American 0591
Asian 0305
Canadian (English) 0352
Canadian (French) 0355
English 0593
Germanic 0311
Latin American 0312
Middle Eastern 0315
Romance 0313
Slavic and East European 0314

PHILOSOPHY, RELIGION AND THEOLOGY
Philosophy 0422
Religion
General 0318
Biblical Studies 0321
Clergy 0319
History of 0320
Philosophy of 0322
Theology 0469

SOCIAL SCIENCES
American Studies 0323
Anthropology
Archaeology 0324
Cultural 0326
Physical 0327
Business Administration
General 0310
Accounting 0272
Banking 0770
Management 0454
Marketing 0338
Canadian Studies 0385
Economics
General 0501
Agricultural 0503
Commerce-Business 0505
Finance 0508
History 0509
Labor 0510
Theory 0511
Folklore 0358
Geography 0366
Gerontology 0351
History
General 0578
Ancient 0579
Medieval 0581
Modern 0582
Black 0328
African 0331
Asia, Australia and Oceania 0332
Canadian 0334
European 0335
Latin American 0336
Middle Eastern 0333
United States 0337
History of Science 0585
Law 0398
Political Science
General 0615
International Law and Relations 0616
Public Administration 0617
Recreation 0814
Social Work 0452
Sociology
General 0626
Criminology and Penology 0627
Demography 0938
Ethnic and Racial Studies 0631
Individual and Family Studies 0628
Industrial and Labor Relations 0629
Public and Social Welfare 0630
Social Structure and Development 0700
Theory and Methods 0344
Transportation 0709
Urban and Regional Planning 0999
Women's Studies 0453

THE SCIENCES AND ENGINEERING

BIOLOGICAL SCIENCES
Agriculture
General 0473
Agronomy 0285
Animal Culture and Nutrition 0475
Animal Pathology 0476
Food Science and Technology 0359
Forestry and Wildlife 0478
Plant Culture 0479
Plant Pathology 0480
Plant Physiology 0817
Range Management 0777
Wood Technology 0746
Biology
General 0306
Anatomy 0287
Biostatistics 0308
Botany 0309
Cell 0379
Ecology 0329
Entomology 0353
Genetics 0369
Limnology 0793
Microbiology 0410
Molecular 0307
Neuroscience 0317
Oceanography 0416
Physiology 0433
Radiation 0821
Veterinary Science 0778
Zoology 0472
Biophysics
General 0786
Medical 0760

EARTH SCIENCES
Biogeochemistry 0425
Geochemistry 0996
Geodesy 0370
Geology 0372
Geophysics 0373
Hydrology 0388
Mineralogy 0411
Paleobotany 0345
Paleoecology 0426
Paleontology 0418
Paleozoology 0985
Palynology 0427
Physical Geography 0368
Physical Oceanography 0415

HEALTH AND ENVIRONMENTAL SCIENCES
Environmental Sciences 0768
Health Sciences
General 0566
Audiology 0300
Chemotherapy 0992
Dentistry 0567
Education 0350
Hospital Management 0769
Human Development 0758
Immunology 0982
Medicine and Surgery 0564
Mental Health 0347
Nursing 0569
Nutrition 0570
Obstetrics and Gynecology 0380
Occupational Health and Therapy 0354
Ophthalmology 0381
Pathology 0571
Pharmacology 0419
Pharmacy 0572
Physical Therapy 0382
Public Health 0573
Radiology 0574
Recreation 0575
Speech Pathology 0460
Toxicology 0383
Home Economics 0386

PHYSICAL SCIENCES
Pure Sciences
Chemistry
General 0485
Agricultural 0749
Analytical 0486
Biochemistry 0487
Inorganic 0488
Nuclear 0738
Organic 0490
Pharmaceutical 0491
Physical 0494
Polymer 0495
Radiation 0754
Mathematics 0405
Physics
General 0605
Acoustics 0986
Astronomy and Astrophysics 0606
Atmospheric Science 0608
Atomic 0748
Electronics and Electricity 0607
Elementary Particles and High Energy 0798
Fluid and Plasma 0759
Molecular 0609
Nuclear 0610
Optics 0752
Radiation 0756
Solid State 0611
Statistics 0463

Applied Sciences
Applied Mechanics 0346
Computer Science 0984

Engineering
General 0537
Aerospace 0538
Agricultural 0539
Automotive 0540
Biomedical 0541
Chemical 0542
Civil 0543
Electronics and Electrical 0544
Heat and Thermodynamics 0348
Hydraulic 0545
Industrial 0546
Marine 0547
Materials Science 0794
Mechanical 0548
Metallurgy 0743
Mining 0551
Nuclear 0552
Packaging 0549
Petroleum 0765
Sanitary and Municipal 0554
System Science 0790
Geotechnology 0428
Operations Research 0796
Plastics Technology 0795
Textile Technology 0994

PSYCHOLOGY
General 0621
Behavioral 0384
Clinical 0622
Developmental 0620
Experimental 0623
Industrial 0624
Personality 0625
Physiological 0989
Psychobiology 0349
Psychometrics 0632
Social 0451

ABSTRACT

In this thesis, we address the problem of computing laminar incompressible viscous flows. For such flows, there are various possibilities for the formulation of the problem. These include primitive variable (velocity and pressure), velocity-vorticity and stream function- vorticity formulations. Each has its own strengths and weaknesses.

In the stream function-vorticity formulation for two-dimensional flow, the difficulty is primarily associated with determination of vorticity at a boundary. In this thesis, we employ a variation of the stream function-vorticity formulation whereby incompressible, viscous flow in an internal complex geometry is formulated in terms of von Mises coordinates. That is, stream function is used as an independent rather than dependent variable. This formulation provides a rectangular computational domain with both Dirichlet and von Neumann boundary conditions for unknown functions, the vertical cartesian coordinate and the vorticity, in terms of the horizontal cartesian coordinate and the stream function. The governing second order nonlinear partial differential equations are solved by SLOR on uniform and, if required, clustered grids. A number of procedures for surmounting the problem of determining vorticity at a boundary are available. A novel approach to this problem is applied in this thesis.

A difficult, but well-documented, test problem was chosen to study the applicability of the von Mises formulation in viscous flows. It has been shown that extreme care must be taken in applying von Mises coordinates to viscous flow situations. In particular, viscosity is known to generate vorticity in the flow field and to cause, under appropriate conditions, flow separation. Of these two phenomenon, rotational flow and viscous separation, it is shown that rotational effects can be handled with no more

difficulty than experienced by conventional methods. However, separation cannot be handled directly by the von Mises formulation, and erroneous results may be obtained if not used carefully. This presents a challenging problem which has been overcome by developing an innovative way to predict the location of the streamline which divides the main flow from the recirculating region. In this way, the von Mises formulation can be used to study separated 2D viscous flows. This approach is used to predict the re-attachment length for the flow over a backward facing step and the results, when compared to other numerical data, confirm the applicability and accuracy of the method.

DEDICATION

To the memory of my Dad. I don't think he knew what he was letting himself in for when he told me to stay in school. I also don't think he meant for me to do it for as long as I have. Many of my friends have told me they wish they had parents like mine, not perfect, but there when you needed them. And I needed them! Thanks.

ACKNOWLEDGEMENTS

I owe everyone. They know who they are, so there is no point in trying to list them all. Maybe one day, if I keep paying back what I have received, I will go out even. Only God keeps that score.

TABLE OF CONTENTS

Page

LIST OF FIGURES

LIST OF TABLES

LIST OF DIAGRAMS

LIST OF APPENDICES

LIST OF SYMBOLS OR NOMENCLATURE

E, F, G	coefficients of First Fundamental Form
h	energy function
J	Jacobian
L	characteristic length
p	pressure function
q	speed function
r	radial component of polar coordinate
U_∞	constant flow speed at infinity
u	velocity component in x direction
v	velocity component in y direction
W	$\pm J$
x	cartesian coordinate
x_{LE}	value of x at the leading edge
x_{TE}	value of x at the trailing edge
y	cartesian coordinate

<u>Greek letters</u>

α	local angle of inclination of streamline with x-axis
ε	error
η	stretching coordinate
θ	angular component of polar coordinate, angle between coordinate curves in (ϕ,ψ) net
κ	curvature

μ	constant viscosity
ξ	stretching coordinate
ρ	constant fluid density
ϕ	curvilinear coordinate
ψ	curvilinear coordinate, stream function
ω	vorticity function

CHAPTER I

INTRODUCTION

The basic tools used by engineering and mathematical researchers to gain an understanding of the various physical phenomena associated with the dynamics of fluid flow are mathematical analysis (exact or non-exact solution methods), experimental (testing) and computational methods. Before the development of high-speed computers, experimentalists developed various simple devices to make measurements of flow quantities of particular interest to them. Analytical researchers then tried to duplicate these experimental results using fairly simple mathematical models and analysis to provide further guidelines to the experimentalists. Then the process was repeated, sometimes with the analysis leading the experimentation.

As the design of modern high-speed computers has become more and more sophisticated, there has been a greater demand for more detailed and accurate numerical analysis of the flow fields under investigation instead of using costly experimental methods, e.g., wind tunnel testing and prototype development. This need has made computational methods more than an equal partner with experimental methods in efforts to analyze complex fluid flow geometries.

Prior to about 1970, many papers appeared on the numerical solution of the Navier-Stokes equations governing the flow of a viscous incompressible fluid in an internal complex geometry. See, for example, a list of over 300 papers in the Ph.D. dissertation by P.J. Roache [I.1]. In the past ten years or so, more authors have taken an interest in this type of problem. For example, in order to stimulate a fruitful debate among computational fluid dynamics (CFD) specialists and to assess the capabilities of various numerical methods to deal with laminar flows in complex geometries, the International Association of Hydraulic Research (IAHR) Working Group on Refined Modelling of Flows decided to devote its Fifth Meeting to this subject in 1982. This meeting will be discussed in detail in Chapter III of this thesis.

There are various possibilities for the formulation of the problem of viscous incompressible flow. These include primitive variable (velocity and pressure), velocity-vorticity and stream function-vorticity formulations. The general solution procedure consists of discretizing the differential equations and boundary conditions over the fluid flow region and solving the resulting system of algebraic equations. Finite difference methods are employed in the discretization in this thesis. In general, when the full Navier-Stokes equations in terms of velocity and pressure (primitive variables) are solved, a specified velocity or velocity gradient (usually zero) must be given at the last downstream station due to the elliptic effect of the streamwise diffusion term. The upstream boundary conditions consist of specified velocity profiles at the upstream location. Along a non-porous body surface, the no-slip boundary conditions $u = v = 0$ are applied. For a line of symmetry, the normal velocity component and the normal derivative of the longitudinal velocity component must be zero. A downstream pressure boundary condition is needed. This boundary condition can either be a specified value of the pressure or a specified value of the pressure gradient in the direction of flow. This specification of boundary conditions on pressure can lead to serious numerical difficulties. However, the primitive variable approach offers the fewest complications in extending the calculations to three dimensions.

The velocity-vorticity approach requires the vorticity equation, the continuity equation, and the equations that define vorticity in terms of velocity gradients. A combination of the continuity equation and the definition of vorticity can be made after differentiation of both equations. This yield elliptic equations for the velocity components. An inconvenience of the velocity-vorticity formulation is that pressure is not directly obtained and consequently additional calculations are required for its determination.

For two-dimensional and for axi-symmetric flows, in order to overcome some of the above difficulties, it is convenient to introduce stream function and vorticity as dependent variables. The equation of continuity is automatically satisfied and the resulting system consists of two coupled nonlinear equations which are solved numerically by some iterative procedure. In the stream function-vorticity formulation, the difficulty is primarily associated with determination of vorticity at a boundary. In this thesis, we employ a variation of the stream function-vorticity formulation whereby the flow is formulated in terms of von Mises coordinates.

Aside from the fact that these coupled equations are nonlinear, there are several other difficulties associated with their solution. One of the major difficulties is that the values of vorticity on no-slip boundaries are not known a priori, while these values are needed in order to solve the discretized problem. In terms of von Mises coordinates another major difficulty is specification of the vertical cartesian coordinate, once the transformation has been made, on dividing streamlines between recirculating and non-recirculating flow and on free surfaces. The flow domain of the problem can also introduce other additional difficulties in the numerical method. Some authors prefer the use of velocity-pressure formulation of the Navier-Stokes equations in order to avoid the difficulties arising from the introduction of vorticity. However, as noted earlier, the pressure equation is complicated and introduces its own additional difficulties.

In order to test a numerical method, it is customary to choose a simple model problem. Whatever choice is made mathematically, it is usually non-trivial because of singularities that often arise at corners. Several numerical methods have been proposed in the literature differing in the choice of discretization schemes, the boundary approximations used to define vorticity on no-slip walls and the methods used to solve the resulting system of algebraic equations. Whatever test problem is chosen to be solved by whatever computational method, the numerical solutions are usually compared in terms of the values of stream function or vorticity at some representative points and also by comparing the values of certain parameters of the flow. Both techniques are employed in this thesis.

A primary difficulty in most cases is to choose a coordinate frame that simplifies both the correlation of measured data and the construction of predictive models. In analyzing fluid motions theoretically, cartesian coordinates are commonly adopted. However, Cartesian coordinates are not always the best choice. For example, the rectangular cartesian coordinate system may not be the appropriate choice since the physical interpretation of many quantities becomes elusive when flow direction and coordinate direction do not coincide. To estimate changes in properties of the flow between two points on a streamline requires integration along a curve, generally a complicated operation. Also, there are practical difficulties in aligning instruments accurately with some externally imposed rectangular frame.

The obvious choice has been to choose curvilinear coordinates. If one coordinate direction can be chosen almost parallel to the mean flow direction, then extra terms arising from deviation of the mean flow from the coordinates may be small enough to be approximated in calculation schemes or ignored in interpretation of measurements.

For instance, it is better to use cylindrical coordinates for flow around a circular cylinder or the flow in a circular pipe and to use spherical coordinates for the flow around a sphere. This is because proper coordinates can be chosen corresponding to the shape of boundaries.

In the early 1970's, Martin [I.2] introduced a natural curvilinear coordinate system (ϕ,ψ) in the physical plane (x,y) where ψ is the stream function, to study the geometry of certain steady two-dimensional, incompressible, viscous flows. This formulation has been used by Grossman and Barron [I.3] to numerically investigate incompressible, irrotational, inviscid flow over symmetric airfoils at zero angle of incidence. They have chosen the coordinate system to be orthogonal which, in their case, implies that the curves $\phi(x,y)$ = constant are potential curves. They found that it was not possible to determine analytically where the leading and trailing edges are mapped into the (ϕ,ψ) system and that numerically obtained values for the leading and trailing edges are not very accurate, resulting in inaccuracies in the solution near these points. During a further study of incompressible, irrotational, inviscid flows, Barron [I.4] introduced von Mises coordinates (x,ψ). Using these independent variables, one knows exactly where the leading and trailing edges are mapped in the (x,ψ) plane and inaccuracies in the solution near these points can be eliminated [I.5].

The purpose of this dissertation is to study the feasibility and advisability of applying stream function coordinate methods to viscous flow problems. This dissertation extends Barron's approach from that of two-dimensional, steady, incompressible, irrotational, inviscid flows to the case of viscous flows. In Barron's approach the coordinate ψ is taken as the stream function for the flow being considered. This approach automatically provides a rectangular computational domain (x,ψ), and the need to do grid generation is avoided except possibly in regions of recirculating flow. This is very significant since it reduces the equations to be solved by two. The flow equations are transformed into von Mises coordinates and solved subject to appropriate boundary conditions, which can be formulated as Dirichlet and von Neumann conditions. Since a boundary coincides with a streamline, as long as separation does not occur, the theoretical treatment becomes easier when choosing streamlines as coordinate axes. However, the basic equations become more complicated, which makes them more difficult to solve. This means the method has merits for some types of flow.

Each of the chapters of the dissertation is now briefly described. In Chapter II, the two-dimensional, steady, incompressible, viscous flow equations, first in (ϕ,ψ) system and then in the (x,ψ) system (unstretched), are derived. The flow equations are also given in the (x,ψ) system in stretched coordinates (ξ,η). A description of the numerical discretization and basic solution algorithm are also provided in Chapter II. Chapter III discusses a well defined test problem, the laminar flow through a non-trivial configuration, namely flow through a smooth expansion channel. Difficulties with flow in the weakly separated region (i.e., small region of recirculation) are discussed. This problem is not fully resolved by the method of solution proposed in Chapter II. Chapter IV presents a solution to a problem in the inviscid limit of zero viscosity. Since the problem of recirculation is not fully resolved with the test problem in Chapter III, this problem is chosen since the flow is still rotational, but no viscosity is allowed. Hence, recirculating flow is eliminated. The problem is hyperbolic-cosine shear flow about a circular cylinder. Chapter V presents the solution to the flow over a backward facing step along with appropriate boundary conditions. The reattachment point of the primary recirculating region is predicted and the calculated results compared to values obtained experimentally or by other numerical methods. Difficulties with flow near regions of discontinuity resulting in singularities in the flow parameters are discussed.

CHAPTER II

GOVERNING EQUATIONS

2.1 DIFFERENTIAL GEOMETRY

We first refer to some results from differential geometry which are essential for our purposes (cf. [I.2] and [I.4]).

Consider a coordinate transformation between cartesian coordinates (x,y) and some arbitrary curvilinear coordinates (ϕ,ψ) defined by

$$\vec{r} = \vec{r}(\phi,\psi) \tag{2.1.1}$$

where $\vec{r} = (x,y)$, i.e., $x = x(\phi,\psi)$ $y = y(\phi,\psi)$ (See Diagram 2.1.1). Assume that the Jacobian J, defined by $J = | \vec{r}_\phi \times \vec{r}_\psi | = x_\phi y_\psi - x_\psi y_\phi$ is non-zero in the region of interest. The squared element of arc length along any curve can be represented by

$$ds^2 = d\vec{r} \cdot d\vec{r} = E(\phi,\psi)d\phi^2 + 2F(\phi,\psi)d\phi d\psi + G(\phi,\psi)d\psi^2 \tag{2.1.2}$$

where

$$E = \vec{r}_\phi \cdot \vec{r}_\phi = x_\phi^2 + y_\phi^2$$

$$F = \vec{r}_\phi \cdot \vec{r}_\psi = x_\phi x_\psi + y_\phi y_\psi \tag{2.1.3}$$

$$G = \vec{r}_\psi \cdot \vec{r}_\psi = x_\psi^2 + y_\psi^2$$

are the metrics of the space under consideration (coefficients of the first fundamental form).

2.2 FLOW EQUATIONS FOR TWO-DIMENSIONAL, STEADY, INCOMPRESSIBLE, VISCOUS FLOW

The Navier-Stokes and mass conservation flow equations for the two-dimensional, steady (meaning stationary), incompressible (constant density), viscous flow in terms of physical or rectangular coordinates (x,y) are, in dimensional form,

$$\bar{u}_{\bar{x}} + \bar{v}_{\bar{y}} = 0 \qquad \text{(continuity)} \qquad (2.2.1a)$$

$$\begin{aligned} \bar{\rho}\left(\bar{u}\bar{u}_{\bar{x}} + \bar{v}\bar{u}_{\bar{y}}\right) + \bar{p}_{\bar{x}} &= \mu\left(\bar{u}_{\bar{x}\bar{x}} + \bar{u}_{\bar{y}\bar{y}}\right) \\ \bar{\rho}\left(\bar{u}\bar{v}_{\bar{x}} + \bar{v}\bar{v}_{\bar{y}}\right) + \bar{p}_{\bar{y}} &= \mu\left(\bar{v}_{\bar{x}\bar{x}} + \bar{v}_{\bar{y}\bar{y}}\right) \end{aligned} \qquad \text{(momentum equations)} \qquad (2.2.2a)$$

where $\bar{u}$, $\bar{v}$ are velocity components in the x and y coordinate directions respectively, $\bar{p}$ is pressure, $\bar{\rho}$ is the constant density and μ is the viscosity. The bar over a variable indicates its dimensional form. Defining a vorticity function $\bar{\omega} = \bar{\omega}(\bar{x},\bar{y})$ and energy function $\bar{h} = \bar{h}(\bar{x},\bar{y})$ by

$$\bar{\omega} = \bar{v}_{\bar{x}} - \bar{u}_{\bar{y}} \qquad \text{(vorticity)} \qquad (2.2.3a)$$

$$\bar{h} = \tfrac{1}{2}\bar{\rho}(\bar{u}^2 + \bar{v}^2) + \bar{p} \qquad \text{(energy)} \qquad (2.2.4a)$$

equations (2.2.2a) can be written, eliminating pressure $\bar{p}$, as

$$\begin{aligned} \bar{h}_{\bar{x}} - \bar{\rho}\bar{v}\bar{\omega} &= -\mu\,\bar{\omega}_{\bar{y}} \\ \bar{h}_{\bar{y}} + \bar{\rho}\bar{u}\bar{\omega} &= \mu\bar{\omega}_{\bar{x}} \end{aligned} \qquad \text{(momentum)} \qquad (2.2.2b)$$

Equations (2.2.1a), (2.2.3a) and (2.2.2b) constitute a system of four non-linear partial differential equations in four unknown functions: $\bar{u}$ and $\bar{v}$ are the velocity components,

$\bar{\omega}$ is the vorticity and $\bar{h}$ is the energy. The state equation ($\bar{\rho}$ = constant) and energy equation (2.2.4a) along with the preceding system of four equations constitute a complete system of equations.

Nondimensionalizing with respect to a characteristic length L and speed U_∞ according to

$$
\begin{aligned}
\bar{x} &= Lx \\
\bar{y} &= Ly \\
\bar{u} &= U_\infty u \\
\bar{v} &= U_\infty v \\
\bar{h} &= \bar{\rho} U_\infty^2 h \\
\bar{\omega} &= U_\infty \omega / L \\
\bar{p} &= \bar{\rho}\, U^2{}_\infty p
\end{aligned}
\tag{2.2.5}
$$

flow equations (2.2.1a), (2.2.3a), (2.2.4a) and (2.2.2b) become

$$u_x + v_y = 0 \qquad \text{(continuity)} \tag{2.2.1b}$$

$$h_x - v\omega = -\frac{1}{R_e}\,\omega_y$$

$$\text{(momentum)} \tag{2.2.2c}$$

$$h_y + u\omega = \frac{1}{R_e}\,\omega_x$$

$$\omega = v_x - u_y \qquad \text{(vorticity)} \tag{2.2.3b}$$

where,

$$h = \tfrac{1}{2}(u^2 + v^2) + p \qquad \text{(energy)} \tag{2.2.4b}$$

and $R_e = \dfrac{\bar{\rho}U_\infty L}{\mu}$ is the Reynolds number.

The equation of continuity (2.2.1b) implies the existence of a stream function $\psi(x,y)$ such that

$$\begin{aligned} u &= \psi_y \\ v &= -\psi_x \end{aligned} \qquad (2.2.6)$$

Appendix A contains a presentation of equations (2.2.2c) and (2.2.3b) using (2.2.6) in an alternate form more familiar in the literature. We will use one of these forms later on in this thesis (equation (A.1)).

Following Martin [I.2], we now proceed to write equations (2.2.1b), (2.2.2c), (2.2.3b) and (2.2.4b) in the (ϕ,ψ) curvilinear coordinate system where $\phi = \phi(x,y)$, $\psi = \psi(x,y)$. The essential feature is that rather than consider an arbitrary (ϕ,ψ) net, Martin chose ψ = constant curves to correspond to the streamlines and the function $\psi(x,y)$ to be the stream function defined in equation (2.2.6). Since the flow moves along the streamlines, this is a natural choice of coordinate system on which to do a numerical calculation [I.4]. For the present, the curves $\phi(x,y)$ = constant are left arbitrary, to be chosen in a convenient manner later. We assume the Jacobian $J \neq 0$ anywhere in the flow region and that the fluid flows along streamlines ψ = constant in the direction of increasing ϕ so that $J > 0$. In this manner the curvilinear coordinate system is more definite, being tied analytically to the actual flow problem. According to Barron [I.4], a second important aspect of Martin's method (to be seen shortly) is that the physical variables (u,v) are replaced by the geometric variables E, F and G in the flow equations. Hence, the metric coefficients E, F and G are determined as part of the solution of the flow equations.

Considering E, F, G, h and ω as functions of ϕ and ψ, flow equations (2.2.1b), (2.2.2c) and (2.2.3b) along with (2.2.4b) are transformed to the (ϕ,ψ) coordinate system.

Martin [I.2] has shown that the continuity equation (2.2.1b) is equivalent to (nondimensionalizing)

$$q^2 = u^2 + v^2 = \frac{E}{J^2} \qquad \text{(continuity)} \qquad (2.2.1c)$$

where $J^2 = EG\text{-}F^2$.

Hence the energy equation (2.2.4b) can be written as

$$h = \frac{E}{2J^2} + p \qquad \text{(energy)} \qquad (2.2.4c)$$

Martin has also shown that the momentum and vorticity equations (2.2.2c) and (2.2.3b) become (again nondimensionalizing)

$$Gh_\phi - F(h_\psi + \omega) = -\frac{1}{R_e} J\omega_\psi$$

$$\text{(momentum)} \qquad (2.2.2d)$$

$$-Fh_\phi + E(h_\psi + \omega) = -\frac{1}{R_e} J\omega_\phi$$

$$\omega = \frac{1}{J}\left[\left(\frac{F}{J}\right)_\phi - \left(\frac{E}{J}\right)_\psi\right] \qquad \text{(vorticity)} \qquad (2.2.3c)$$

Equations (2.2.2d) can be written as (Barron [I.4]) (see Appendix B[1]),

$$h_\phi = \frac{1}{R_e}\frac{F}{J}\,\omega_\phi - \frac{1}{R_e}\frac{E}{J}\,\omega_\psi \qquad \text{(momentum)} \qquad (2.2.2e)$$

$$h_\psi = -\omega + \frac{1}{R_e}\frac{G}{J}\,\omega_\phi - \frac{1}{R_e}\frac{F}{J}\,\omega_\psi$$

Finally an equation referred to by Martin as the Gauss equation, states that the Gaussian curvature K is zero. That is,

$$K = \frac{1}{J}\left[\left(\frac{J}{E}\,\Gamma_{11}^2\right)_\psi - \left(\frac{J}{E}\,\Gamma_{12}^2\right)_\phi\right] = 0 \qquad \text{(Gauss)} \qquad (2.2.7)$$

where Γ_{11} and Γ_{12} are Christoffel symbols, and

$$\Gamma_{11}^2 = \frac{-FE_\phi + 2EF_\phi - EE_\psi}{2J^2}$$

$$\Gamma_{12}^2 = \frac{EG_\phi - FE_\psi}{2J^2}$$

For a plane provided with a curvilinear coordinate system (ϕ,ψ), the Gaussian curvature always equals zero.

Equations (2.2.2e), (2.2.3c) and (2.2.7) are four partial differential equations for the five unknown functions E, F, G, h and ω. This system is underdetermined because of the arbitrariness of the curves $\phi(x,y)$ = constant chosen to define the coordinate system. In the next section a choice for $\phi = \phi(x,y)$ is proposed which provides

---

[1]The reason for including what appear to be simple and obvious derivations in the appendices is either for completeness or because this is the first time the equation appears in the literature.

boundary conditions in a simple form for numerical calculations and removes this arbitrariness. It will be shown that Gauss' equation is automatically satisfied for this choice of ϕ since E, F and G will then be known in terms of a single unknown function. This will be shown to reduce the four equations eventually to two equations in terms of only two unknown functions, this new function and the vorticity ω.

Of course, other choices are possible (and perhaps desirable in certain flow configurations), such as requiring the grid system to be orthogonal. However, these lead to additional equations to be solved and the boundary conditions are more complicated.

2.3 THE VON MISES TRANSFORMATION

As indicated in the previous section, in order to remove the arbitrariness in $\phi = \phi(x,y)$, it is convenient to choose

$$\phi(x,y) = x \tag{2.3.1}$$

so that the equations of motion (2.2.2e) and (2.2.3c) and the Gauss' equation (2.2.7) are formulated with (x,ψ) as independent variables rather than (ϕ,ψ), i.e., von Mises coordinates.

Using equation (2.3.1) in the expressions for the metric coefficients E, F and G, equations (2.1.3) give the metrics in terms of a single unknown function $y = y(x,\psi)$:

$$\begin{aligned} E &= 1 + y_x^2 \\ F &= y_x y_\psi \\ G &= y_\psi^2 \end{aligned} \tag{2.3.2}$$

The Jacobian J becomes

$$J = y_\psi \tag{2.3.3}$$

The continuity equation (2.2.1c) becomes, using (2.3.2) and (2.3.3),

$$q^2 = u^2 + v^2 = \frac{1+y_x^2}{y_\psi^2} \qquad \text{(continuity)} \qquad (2.3.4)$$

From (2.2.6),

$$u = \frac{1}{y_\psi} = \psi_y$$

$$v = \frac{y_x}{y_\psi} = uy_x = -\psi_x \qquad (2.3.5)$$

Using (2.3.2) and (2.3.3), the energy equation (2.2.4c) becomes

$$h = \frac{1+y_x^2}{2y_\psi^2} + p \qquad \text{(energy)} \qquad (2.3.6)$$

The momentum equations (2.2.2e) become, using (2.3.2) and (2.3.3),

$$h_x = \frac{1}{R_e}\left[y_x\omega_x - \frac{\left(1+y_x^2\right)}{y_\psi}\omega_\psi\right] \qquad \text{(momentum)} \qquad (2.3.7a)$$

$$h_\psi = -\omega + \frac{1}{R_e}\left[y_\psi\omega_x - y_x\omega_\psi\right]$$

The vorticity equation (2.2.3c) becomes, using (2.3.2) and (2.3.3)

$$\omega = \frac{1}{y_\psi}\left[y_{xx} - \left(\frac{1+y_x^2}{y_\psi}\right)_\psi\right] \qquad \text{(vorticity)} \qquad (2.3.8a)$$

Finally, Gauss' equation (2.2.7) is automatically satisfied since it is equivalent to $y_{x\psi} = y_{\psi x}$ for all (x,ψ), i.e., the transformation identically satisfies (2.2.7). Since the coordinates (ϕ,ψ) satisfy Gauss' equation in order to form a curvilinear net, the von

Mises transformation also must satisfy it so as to form a curvilinear net (x,ψ) (cf. Appendix C).

It should be noted at this point that we have transformed the equations of motion in terms of rectangular cartesian coordinates (x,y) to a curvilinear coordinate system (ϕ,ψ) using Martin's method. Then, using the von Mises transformation, we further transform the flow equations to another curvilinear coordinate system (x,ψ).

(x,y)	$\rightarrow$	(ϕ,ψ)	$\rightarrow$	(x,ψ)
physical plane		curvilinear plane		computational plane

This is actually the starting point for this thesis. The streamlines ψ = constant, which are curved in the physical plane, are mapped to horizontal straight lines in the computational plane.

Equations (2.3.7a) and (2.3.8a) will now be written in a more convenient form to serve as the starting point for the numerical work which will follow.

Expand equation (2.3.8a) to get

$$y_\psi^3\omega = y_\psi^2 y_{xx} - 2y_x y_\psi y_{x\psi} + \left(1 + y_x^2\right) y_{\psi\psi} \tag{2.3.8b}$$

Define the operator

$$L\{\ \} \equiv y_\psi^2 \frac{\partial^2}{\partial x^2} - 2y_x y_\psi \frac{\partial^2}{\partial x \partial \psi} + \left(1 + y_x^2\right) \frac{\partial^2}{\partial \psi^2}$$

Then, equation (2.3.8b) can be written as

$$L\{y\} - y_\psi^3\omega = 0$$

For use later, the above equation is written as

$$L\{y\} - y_{\psi}^{2}\omega y_{\psi} = 0 \qquad \text{(vorticity)} \qquad (2.3.8c)$$

where $y = y(x,\psi)$.

Eliminating h from equations (2.3.7a), using $h_{x\psi} = h_{\psi x}$, yields

$$L\{\omega\} - R_c\, y_{\psi}\omega_x - y_{\psi}^{2}\omega\omega_{\psi} = 0 \qquad (2.3.7b)$$

where $\omega = \omega(x,\psi)$ (cf. Appendix D for a derivation of this equation).

Equations (2.3.8c) and (2.3.7b) are two elliptic partial differential equations which must be solved for the two unknown functions $y = y(x,\psi)$ and $\omega = \omega(x,\psi)$. The boundary conditions associated with these equations are problem specific and will be discussed in later chapters.

To find the pressure, we use the equations (2.3.7a) to get an equation for energy $h = h(x,\psi)$ and then use equation (2.3.6) to solve for the pressure $p = p(x,\psi)$ (cf. Appendix E).

2.4 NUMERICAL ALGORITHM

2.4.1 Finite Difference Formulation

The equations will be solved by approximating derivatives by finite differences. Hence, the equations to be solved, i.e., equations (2.3.8c) and (2.3.7b), in difference operator notation, are respectively:

$$\left[A_{ij}^{(n)}\delta_{xx} + B_{ij}^{(n)}\delta_{x\psi} + C_{ij}^{(n)}\delta_{\psi\psi} + E_{ij}^{(n)}\delta_{\psi}\right] y_{ij}^{(n+1)} = 0$$

and

$$\left[A_{ij}^{(n+1)}\delta_{xx} + B_{ij}^{(n+1)}\delta_{x\psi} + C_{ij}^{(n+1)}\delta_{\psi\psi} + \mathrm{Re}D_{ij}^{(n+1)}\delta_{x} + E_{ij}^{(n+1)}\delta_{\psi}\right]\omega_{ij}^{(n+1)} = 0$$

or rewriting these two equations in a more compact notation

$$\left[A_{ij}^{(k)}\delta_{xx} + B_{ij}^{(k)}\delta_{x\psi} + C_{ij}^{(k)}\delta_{\psi\psi} + \alpha\mathrm{Re}D_{ij}^{(k)}\delta_{x} + E_{ij}^{(k)}\delta_{\psi}\right]\phi_{ij}^{(n+1)} = 0 \qquad (2.4.1.1)$$

where,

$$\phi = \begin{cases} y(x,\psi) \text{ if } \alpha=0 \\ \omega(x,\psi) \text{ if } \alpha=1 \end{cases}$$

are the unknowns and,

$$k = \begin{cases} n \quad \text{if } \phi=y \\ n+1 \text{ if } \phi=\omega \quad \text{(except in } E_{ij}^{(k)} \text{ where } \omega_{ij} \text{ is at (n))} \end{cases}$$

is the iteration number.

The operators δ_{xx}, $\delta_{x\psi}$, $\delta_{\psi\psi}$, δ_x and δ_ψ represent 3-point central difference operators, and are difference approximations to the partial derivatives in (2.3.8c) and (2.3.7b).

The coefficients $A_{ij}^{(k)}$, $B_{ij}^{(k)}$, $C_{ij}^{(k)}$, $D_{ij}^{(k)}$ and $E_{ij}^{(k)}$ in (2.4.1.1) are:

$$\begin{aligned} A_{ij}^{(k)} &= \left(\delta_{\psi}y\right)_{ij}^2 \\ B_{ij}^{(k)} &= -2\left(\delta_{x}y\right)_{ij}\left(\delta_{\psi}y\right)_{ij} \\ C_{ij}^{(k)} &= 1 + \left(\delta_{x}y\right)_{ij}^2 \\ D_{ij}^{(k)} &= -\left(\delta_{\psi}y\right)_{ij} \\ E_{ij}^{(k)} &= -\left(\delta_{\psi}y\right)_{ij}^2\omega_{ij} \end{aligned} \qquad (2.4.1.2)$$

The $\delta_x y$ and $\delta_\psi y$ are approximated using 3-point central differences, namely,

$$\left(\delta_x y\right)_{ij} = \frac{y_{i+1,j} - y_{i-1,j}}{2\Delta x}$$

$$\left(\delta_\psi y\right)_{ij} = \frac{y_{i,j+1} - y_{i,j-1}}{2\Delta \psi}$$

Using 3-point central differences is acceptable for small R_e. However, as in the conventional stream function-vorticity formulation, the convective term in (2.4.1.1) may have to be upwind or backward differenced for larger R_e, i.e., upwind the vorticity term $(\delta_x \omega)_{ij}$ in the expression $R_e D_{ij}(\delta_x \omega)_{ij}$, namely

$$(\delta_x \omega)_{ij} = \frac{\omega_{ij} - \omega_{i-1,j}}{\Delta x} \quad \text{(2-point)}$$

$$(\delta_x \omega)_{ij} = \frac{3\omega_{ij} - 4\omega_{i-1,j} + \omega_{i-2,j}}{2\Delta x} \quad \text{(3-point)}$$

Numerical instabilities of explicit finite difference methods can be simply related to the familiar concepts of static and dynamic instabilities. Although not a consideration in this thesis, dynamic instabilities are caused by too large a time step. Static instabilities result from the form of the finite difference equation. For non-oscillatory solutions, limitations on the maximum Reynolds number, R_e, based on the finite difference cell size or the characteristic length Δx or $\Delta \psi$, called the cell Reynolds number or Peclet number, are necessary. Oscillatory solutions may occur if the cell R_e is too large. Whether they actually do occur depends on the flow geometry and imposition of boundary conditions.

However, a first-order accurate method, using upwind differences for the convective term in (2.4.1.1), although feasible in principle, is not recommended, insofar as the effective R_e of the numerical solution is lowered by the numerical viscosity introduced by the first-order accurate upwind differences. This point will be discussed more fully in Chapter III.

2.4.2 Solution Procedure

By using 3-point central difference approximations, equation (2.4.1.1) can be expressed as

$$\frac{A_{ij}^{(k)}}{\Delta x^2}(\phi_{i-1,j}-2\phi_{ij}+\phi_{i+1,j})^{(n+1)} + \frac{B_{ij}^{(k)}}{4\Delta x\Delta\psi}(\phi_{i+1,j+1}+\phi_{i-1,j-1}$$

$$-\phi_{i+1,j-1}-\phi_{i-1,j+1})^{(n+1)} + \frac{C_{ij}^{(k)}}{\Delta\psi^2}(\phi_{i,j-1}-2\phi_{ij}+\phi_{i,j+1})^{(n+1)}$$

$$+\frac{\alpha R_e D_{ij}^{(k)}}{2\Delta x}(\phi_{i+1,j}-\phi_{i-1,j})^{(n+1)} + \frac{E_{ij}^{(k)}}{2\Delta\psi}(\phi_{i,j+1}-\phi_{i,j-1})^{(n+1)} = 0$$

By rearranging, we have

$$B_{ij}^{(k)}\frac{\Delta x}{4\Delta\psi}\phi_{i-1,j-1}^{(n+1)} + \left[A_{ij}^{(k)} - \frac{\alpha R_e D_{ij}^{(k)}\Delta x}{2}\right]\phi_{i-1,j}^{(n+1)} - B_{ij}^{(k)}\frac{\Delta x}{4\Delta\psi}\phi_{i-1,j+1}^{(n+1)}$$

$$+\left[C_{ij}^{(k)}\frac{\Delta x^2}{\Delta\psi^2} - E_{ij}^{(k)}\frac{\Delta x^2}{2\Delta\psi}\right]\phi_{i,j-1}^{(n+1)} - 2\left[A_{ij}^{(k)} + C_{ij}^{(k)}\frac{\Delta x^2}{\Delta\psi^2}\right]\phi_{ij}^{(n+1)}$$

$$+\left[C_{ij}^{(k)}\frac{\Delta x^2}{\Delta\psi^2} + E_{ij}^{(k)}\frac{\Delta x^2}{2\Delta\psi}\right]\phi_{i,j+1}^{(n+1)} - B_{ij}^{(k)}\frac{\Delta x}{4\Delta\psi}\phi_{i+1,j-1}^{(n+1)} \qquad (2.4.2.1a)$$

$$+\left[A_{ij}^{(k)} + \frac{\alpha R_e D_{ij}^{(k)}\Delta x}{2}\right]\phi_{i+1,j}^{(n+1)} + B_{ij}^{(k)}\frac{\Delta x}{4\Delta\psi}\phi_{i+1,j+1}^{(n+1)} = 0$$

which can be abbreviated as follows, where ϕ is at (n+1)

$$
\begin{aligned}
& b_{ij}\,\phi_{i-1,j-1} \quad + \quad (a_{ij} - d_{ij})\,\phi_{i-1,j} \quad - \quad b_{ij}\,\phi_{i-1,j+1} \\
& +(c_{ij} - e_{ij})\phi_{i,j-1} \quad - \quad 2(a_{ij} + c_{ij})\,\phi_{ij} \quad + \quad (c_{ij} + e_{ij})\,\phi_{i,j+1} \\
& -b_{ij}\phi_{i+1,j-1} \quad + \quad (a_{ij} + d_{ij})\phi_{i+1,j} \quad + \quad b_{ij}\,\phi_{i+1,j+1} \; = \; 0
\end{aligned}
\tag{2.4.2.2a}
$$

where

$$
\begin{aligned}
a_{ij} &= A_{ij}^{(k)} \\
b_{ij} &= B_{ij}^{(k)}\,\frac{\Delta x}{4\Delta\psi} \\
c_{ij} &= C_{ij}^{(k)}\,\frac{\Delta x^2}{\Delta\psi^2} \\
d_{ij} &= \alpha R_e D_{ij}^{(k)}\,\frac{\Delta x}{2} \\
e_{ij} &= E_{ij}^{(k)}\,\frac{\Delta x^2}{2\Delta\psi}
\end{aligned}
\tag{2.4.2.3a}
$$

For a rectangular domain meshed with an IX x JX grid, with known boundary values ϕ_{ij} on the four boundaries where i = 1 or IX, and j = 1 or JX, the finite difference equations (2.4.2.2a) can be expressed in block tridiagonal matrix equation form as

$$
\begin{bmatrix}
B_2 & C_2 & & & & \\
A_3 & B_3 & C_3 & & & \\
 & A_4 & B_4 & \cdots & & \\
 & & \cdots & \cdots & \cdots & \\
 & & & A_{I2} & B_{I2} & C_{I2} \\
 & & & & A_{I1} & B_{I1}
\end{bmatrix}
\begin{bmatrix}
\vec{\phi}_2 \\ \vec{\phi}_3 \\ \vec{\phi}_4 \\ \vdots \\ \vec{\phi}_{I2} \\ \vec{\phi}_{I1}
\end{bmatrix}^{(n+1)}
=
\begin{bmatrix}
R\vec{H}S_2 \\ R\vec{H}S_3 \\ R\vec{H}S_4 \\ \vdots \\ R\vec{H}S_{I2} \\ R\vec{H}S_{I1}
\end{bmatrix}
\tag{2.4.2.4}
$$

where,

$$\overline{\phi}_i^{(n+1)} = \left[\phi_{i2}^{(n+1)},\ \ \phi_{i3}^{(n+1)},\ \ \cdots\ \ \phi_{i,J1}^{(n+1)}\right]^T$$

is the solution vector along grid line i for $i = 2,3 \ldots, I1$. Here $I1 = IX - 1$, $I2 = IX - 2$, $J1 = JX - 1$ and $J2 = JX - 2$.

Matrices $\mathbf{A}_i$, $\mathbf{B}_i$, and $\mathbf{C}_i$ are J2 x J2 tridiagonal matrices which can be expressed as

$$A_i = \text{trid}\ \left[\text{for } 3 \le i \le I1 \quad \left(\begin{array}{ccc} \scriptstyle 3\le j\le J1 & \scriptstyle 2\le j\le J1 & \scriptstyle 2\le j\le J2 \\ b_{ij} & a_{ij}-d_{ij} & -b_{ij} \end{array}\right)\right]$$

$$B_i = \text{trid}\ \left[\text{for } 2 \le i \le I1 \quad \left(\begin{array}{ccc} \scriptstyle 3\le j\le J1 & \scriptstyle 2\le j\le J1 & \scriptstyle 2\le j\le J2 \\ c_{ij}-e_{ij} & -2(a_{ij}+c_{ij}) & c_{ij}+e_{ij} \end{array}\right)\right]$$

$$C_i = \text{trid}\ \left[\text{for } 2 \le i \le I2 \quad \left(\begin{array}{ccc} \scriptstyle 3\le j\le J1 & \scriptstyle 2\le j\le J1 & \scriptstyle 2\le j\le J2 \\ -b_{ij} & a_{ij}+d_{ij} & b_{ij} \end{array}\right)\right]$$

Abbreviating the above, we have

$$A_i = \text{trid}\left(b_{ij},\ a_{ij}-d_{ij},\ -b_{ij}\right)$$

$$B_i = \text{trid}\left(c_{ij}-e_{ij},\ -2(a_{ij}+c_{ij}),\ c_{ij}+e_{ij}\right)$$

$$C_i = \text{trid}\left(-b_{ij},\ a_{ij}+d_{ij},\ b_{ij}\right)$$

For example, if $i = 3$, we have

$$A_3 = \begin{bmatrix} a_{32}-d_{32} & -b_{32} & & & \\ b_{33} & a_{33}-d_{33} & -b_{33} & & \\ & \cdots & \cdots & \cdots & \\ & & & b_{3,J1} & a_{3,J1}-d_{3,J1} \end{bmatrix}$$

$$B_3 = \begin{bmatrix} -2(a_{32}+c_{32}) & c_{32}+e_{32} & & & \\ c_{33}-e_{33} & -2(a_{33}+c_{33}) & c_{33}+e_{33} & & \\ & \cdots & \cdots & \cdots & \\ & & & c_{3,J1}-e_{3,J1} & -2(a_{3,J1}+c_{3,J1}) \end{bmatrix}$$

$$C_3 = \begin{bmatrix} a_{32}+d_{32} & b_{32} & & & \\ -b_{33} & a_{33}+d_{33} & b_{33} & & \\ & \cdots & \cdots & \cdots & \\ & & & -b_{3,J1} & a_{3,J1}+d_{3,J1} \end{bmatrix}$$

$R\vec{H}S_i$ is a J2 x 1 column vector which contains the boundary conditions and can be expressed as follows:

For i = 2 or i = I1, and j = 3,4,...,J2

$$R\vec{H}S_i = \begin{bmatrix} \gamma b_{i2}\phi_{i+\gamma,1}-(a_{i2}+\gamma d_{i2})\phi_{i+\gamma,2}-\gamma b_{i2}\phi_{i+\gamma,3} \\ -\gamma b_{i2}\phi_{i-\gamma,1}-(c_{i2}-e_{i2})\phi_{i1} \\ \vdots \\ \gamma b_{ij}\phi_{i+\gamma,j-1}-(a_{ij}+\gamma d_{ij})\phi_{i+\gamma,j}-\gamma b_{ij}\phi_{i+\gamma,j+1} \\ \vdots \\ \gamma b_{i,J1}\phi_{i+\gamma,J2}-(a_{i,J1}+\gamma d_{i,J1})\phi_{i+\gamma,J1}-\gamma b_{i,J1}\phi_{i+\gamma,JX} \\ +\gamma b_{i,J1}\phi_{i-\gamma,JX}-(c_{i,J1}+e_{i,J1})\phi_{i,JX} \end{bmatrix}$$

where

$$\gamma = \begin{cases} -1 & \text{if } i=2 \\ 1 & \text{if } i=I1 \end{cases}$$

Or more explicitly, if i = 2, then, for j = 3,4,...,J2

$$\widehat{RHS}_2 = \begin{bmatrix} b_{22}(\phi_{13}-\phi_{11})-(a_{22}-d_{22})\phi_{12} \\ +b_{22}\phi_{31}-(c_{22}-e_{22})\phi_{21} \\ \vdots \\ b_{2j}(\phi_{1,j+1}-\phi_{1,j-1})-(a_{2j}-d_{2j})\phi_{1j} \\ \vdots \\ b_{2,J1}(\phi_{1,JX}-\phi_{1,J2})-(a_{2,J1}-d_{2,J1})\phi_{1,J1} \\ -b_{2,J1}\phi_{3,JX}-(c_{2,J1}+e_{2,J1})\phi_{2,JX} \end{bmatrix}$$

If i = I1,

$$\widehat{RHS}_{I1} = \begin{bmatrix} b_{I1,2}(\phi_{IX,1}-\phi_{IX,3})-(a_{I1,2}+d_{I1,2})\phi_{IX,2} \\ -b_{I1,2}\phi_{I2,1}-(c_{I1,2}-e_{I1,2})\phi_{I1,1} \\ \vdots \\ b_{I1,j}(\phi_{IX,j-1}-\phi_{IX,j+1})-(a_{I1,j}+d_{I1,j})\phi_{IX,j} \\ \vdots \\ b_{I1,J1}(\phi_{IX,J2}-\phi_{IX,JX})-(a_{I1,J1}+d_{I1,J1})\phi_{IX,J1} \\ +b_{I1,J1}\phi_{I2,JX}-(c_{I1,J1}+e_{I1,J1})\phi_{I1,JX} \end{bmatrix}$$

For $3 \leq i \leq I2$,

$$\vec{RHS}_i = \begin{bmatrix} -b_{i2}\phi_{i-1,1} - (c_{i2} - e_{i2})\phi_{i1} + b_{i2}\phi_{i+1,1} \\ 0 \\ \cdot \\ \cdot \\ \cdot \\ 0 \\ b_{i,J1}\phi_{i-1,JX} - (c_{i,J1} + e_{i,J1})\phi_{i,JX} - b_{i,J1}\phi_{i+1,JX} \end{bmatrix}$$

The matrix equation is solved by an iterative method. The basic procedure is to obtain the solution using the method of successive line over-relaxation (SLOR), sweeping from left to right through the grid. The matrix equation (2.4.2.4) can be written vertically line by line so that on line i, we have

$$B_i\vec{\phi}_i^{(n+1)} = \vec{RHS}_i - A_i\vec{\phi}_{i-1}^{(n+1)} - C_i\vec{\phi}_{i+1}^{(n)}$$

In pointwise form, this can be written as

$$\begin{aligned}[B_i\vec{\phi}_i^{(n+1)}]_j &= RHS_{ij} + b_{ij}\left(\phi_{i-1,j+1}^{(n+1)} - \phi_{i-1,j-1}^{(n+1)}\right) - \left(a_{ij} - d_{ij}\right)\phi_{i-1,j}^{(n+1)} \\ &\quad + b_{ij}\left(\phi_{i+1,j-1}^{(n)} - \phi_{i+1,j+1}^{(n)}\right) - \left(a_{ij} + d_{ij}\right)\phi_{i+1,j}^{(n)} \\ &= RHS_{ij} + b_{ij}\left(\phi_{i-1,j+1}^{(n+1)} - \phi_{i-1,j-1}^{(n+1)} + \phi_{i+1,j-1}^{(n)} - \phi_{i+1,j+1}^{(n)}\right) \\ &\quad -\left(a_{ij} - d_{ij}\right)\phi_{i-1,j}^{(n+1)} - \left(a_{ij} + d_{ij}\right)\phi_{i+1,j}^{(n)}\end{aligned}$$

for all interior points, i.e., $i = 3,4,\ldots,I2$ and $j = 3,4,\ldots,J2$. Due to the boundary conditions along $j = 1$, $j = JX$, $i = 1$ and $i = IX$, we obtain the following.

If $j = 2$,

$$[B_i\vec{\phi}_i^{(n+1)}]_2 = RHS_{i2} - (a_{i2}-d_{i2})\phi_{i-1,2}^{(n+1)} - (a_{i2}+d_{i2})\phi_{i+1,2}^{(n)}$$
$$+b_{i2}\left(\phi_{i-1,3}^{(n+1)} - \phi_{i+1,3}^{(n)}\right)$$

If j = J1,

$$[B_i\vec{\phi}_i^{(n+1)}]_{J1} = RHS_{i,J1} - (a_{i,J1}-d_{i,J1})\phi_{i-1,J1}^{(n+1)} - (a_{i,J1}+d_{i,J1})\phi_{i+1,J1}^{(n)}$$
$$-b_{i,J1}\left(\phi_{i-1,J2}^{(n+1)} - \phi_{i+1,J2}^{(n)}\right)$$

For i = 2, for all j we have

$$[B_2\vec{\phi}_2^{(n+1)}]_j = RHS_{2,j} + b_{2j}\left(\phi_{3,j-1}^{(n)} - \phi_{3,j+1}^{(n)}\right) - (a_{2j} + d_{2j})\phi_{3,j}^{(n)}$$

If however j = 2, this further reduces to

$$[B_2\vec{\phi}_2^{(n+1)}]_2 = RHS_{22} - b_{22}\phi_{33}^{(n)} - (a_{22} + d_{22})\phi_{32}^{(n)}$$

or, if j = J1,

$$[B_2\vec{\phi}_2^{(n+1)}]_{J1} = RHS_{2,J1} + b_{2,J1}\phi_{3,J2}^{(n)} - (a_{2,J1} + d_{2,J1})\phi_{3,J1}^{(n)}$$

For i = I1, we have, for all j

$$[B_{I1}\vec{\phi}_{I1}^{(n+1)}]_j = RHS_{I1,j} + b_{I1,j}\left(\phi_{I2,j+1}^{(n+1)} - \phi_{I2,j-1}^{(n+1)}\right) - (a_{I1,j} - d_{I1,j})\phi_{I2,j}^{(n+1)}$$

If j = 2, this reduces to

$$[B_{I1}\vec{\phi}_{I1}^{(n+1)}]_2 = RHS_{I1,J} + b_{I1,2}\phi_{I2,3}^{(n+1)} - (a_{I1,2} - d_{I1,2})\phi_{I2,2}^{(n+1)}$$

and, if j = J1,

$$[B_{I1}\vec{\phi}_{I1}^{(n+1)}]_{J1} = RHS_{I1,J1} - b_{I1,J1}\phi_{I2,J2}^{(n+1)} - (a_{I1,J1} - d_{I1,J1})\phi_{I2,J1}^{(n+1)}$$

Having obtained $\vec{\phi}_i^{(n+1)}$, and calling these values $\vec{\Phi}_i^{(n+1)}$, a modified or relaxed value $\vec{\phi}_i^{(n+1)}$ can be obtained by using a relaxation factor β_α and the following expression:

$$\vec{\phi}_i^{(n+1)} = (1-\beta_\alpha)\vec{\phi}_i^{(n)} + \beta_\alpha\vec{\Phi}_i^{(n+1)}$$

where $1 \leq \beta_\alpha < 2$ if $\alpha = 0$ (i.e., $\phi = y$, $\beta_o \equiv \beta_y$) and $0 < \beta_\alpha \leq 1$ if $\alpha = 1$ (i.e., $\phi = \omega$, $\beta_1 = \beta_\omega$). That is, y is over-relaxed and ω is under-relaxed.

2.4.3 Iterative Procedure

1. Set $\alpha = 0$ (therefore $\phi = y$, $k = n$). Linearize by evaluating coefficients at previous iteration level (n) as indicated in equation (2.4.2.1a). Solve for $y_{ij}^{(n+1)}$ using SLOR.

2. Evaluate near-boundary values of the speed from

$$(q_{ij}^2)^{(n+1)} = \left[\frac{1 + (\delta_x y)^2}{(\delta_\psi y)^2}\right]_{ij}^{(n+1)} = \frac{C_{ij}^{(n+1)}}{A_{ij}^{(n+1)}} \qquad (2.4.3.1)$$

for j = 2, 3, 4, ..., (near lower boundary) and for j = J1, J2, J3, ..., (near upper boundary) as needed for evaluation of ω at the boundaries (cf. Section 2.4.5).

3. Evaluate boundary values of the vorticities ω_{i1} and $\omega_{i,JX}$ from appropriate formulas. Call these values $\bar{\omega}_{i1}^{(n+1)}$ and $\bar{\omega}_{i,JX}^{(n+1)}$. Obtain under-relaxed boundary values $\omega_{i1}^{(n+1)}$ and $\omega_{i,JX}^{(n+1)}$ by using a smoothing or damping parameter δ (see computational preliminaries in next section for choice of δ):

$$\omega_{ij}^{(n+1)} = (1-\delta)\omega_{ij}^{(n)} + \delta\bar{\omega}_{ij}^{(n+1)}, \quad 0<\delta\leq 1, \quad j=1 \text{ and } JX.$$

4. Set α = 1 (therefore $\phi = \omega$, k = n+1). Linearize by evaluating coefficients at iteration level (n+1) for y_{ij}'s and previous iteration level (n) for ω_{ij}'s and approximate the second order derivatives at level (n+1). Solve for $\omega_{ij}^{(n+1)}$ using SLOR.

5. Set n = n + 1 and repeat steps 1 to 4 until some specified convergence criteria is met, e.g., the iterations could be stopped when, for all (i,j), the maximum norm

$$\|\omega\| = \max_{ij} \left|\omega_{ij}^{(n+1)} - \omega_{ij}^{(n)}\right| < \varepsilon$$

where ε is user-specified, say ε = 0.2 x 10^{-4}. Using the above convergence criteria guarantees [II.1] that for all (i,j),

$$\|y\| = \max_{ij} \left|y_{ij}^{(n+1)} - y_{ij}^{(n)}\right| < \varepsilon$$

In some applications this convergence criteria may prove unsatisfactory. In that event, the iterations could be stopped when, for all (i,j), the maximum norms

$$\|y\| = \max_{ij}\left|y_{ij}^{(n+1)} - y_{ij}^{(n)}\right| < \varepsilon_y \qquad \text{and}$$

$$\|\omega\| = \max_{ij}\left|\omega_{ij}^{(n+1)} - \omega_{ij}^{(n)}\right| < \varepsilon_\omega$$

where ε_y and ε_ω are user-specified, say $\varepsilon_y = 0.2 \times 10^{-3}$ and $\varepsilon_\omega = 0.2 \times 10^{-2}$. The iterations start with some initial approximation $\omega_{ij}^{(n)}$ of the vorticity with n = 0. If no such approximation exists, set $\omega_{ij}^{(n)} = 0$.

Equations for y and ω are solved at interior points only, i.e., $2 \leq i \leq I1 = IX - 1$, $2 \leq j \leq J1 = JX - 1$. Hence, the fact that the Jacobian becomes infinite along the solid boundaries does not create a problem because we do not apply the partial differential equations on these boundaries, i.e., $u = \frac{1}{y_\psi} = 0$, $v = \frac{y_x}{y_\psi} = 0$, implying $y_\psi \to \infty$ on the boundaries, would make the Jacobian infinite. Also, it is well established by computational experience that the iterative convergence can be judged by examining only the vorticity on the wall.

2.4.4 Computational Preliminaries

A non-zero value of the damping parameter δ is essential for the convergence of the numerical procedure [II.1]. For an estimate of δ, one must determine the growth factor ρ for the y_{ij} iterations. The value of ρ is estimated by using $\delta = 0$ in step 3 of the iterative procedure for a small number of iterations. Compute, for large n

$$\rho \approx \frac{\|y_{ij}^{(n+1)} - y_{ij}^{(n)}\|}{\|y_{ij}^{(n)} - y_{ij}^{(n-1)}\|},$$

The norm used is the maximum norm $\|y\| = \max_{ij} |y_{ij}|$. Let

$$\mu = \frac{\rho - 1}{\rho + 1}$$

For convergence of the y_{ij} iterations, δ should be chosen such that $\mu \leq \delta \leq 1$ and a near optimal value of δ is given by

$$\delta_{opt} = \frac{\rho}{\rho + 2}$$

2.4.5 Boundary Conditions for Vorticity

The values of vorticity on the solid boundaries are generally unknown and must be obtained as part of the overall solution. As in the conventional (ψ,ω) formulation, these values of vorticity must be approximated along any solid boundaries.

By definition,

$$\omega(x,y) = v_x - u_y \tag{2.4.5.1}$$

Also, by definition of the stream function

$$\begin{aligned} u &= \psi_y \\ v &= -\psi_x \end{aligned} \tag{2.4.5.2}$$

Since $u = u(x,y)$, $v = v(x,y)$, and under the von Mises transformation, $y = y(x,\psi)$, we get $u = u(x,\psi)$, $v = v(x,\psi)$. Hence,

$$\begin{aligned} v_x &= v_x x_x + v_\psi \psi_x = v_x - v v_\psi \\ u_y &= u_x x_y + u_\psi \psi_y = u u_\psi \end{aligned} \tag{2.4.5.3}$$

using (2.4.5.2). Substituting (2.4.5.3) into (2.4.5.1), we get

$$\omega = \omega(x,\psi) = v_x - vv_\psi - uu_\psi \tag{2.4.5.4}$$

In [II.1] several solid boundary approximations are suggested for vorticity. However, expanding any of these suggested schemes in a Taylor series about the point (i,1) i = 1,2,3... and using the no-slip condition on this boundary, namely $u_{i1} = v_{i1} = 0$, equation (2.4.5.4) yields $\omega_{i1} = 0$ for all i. Obviously, this is no good for our purposes. The problem seems to be that even though $u = v = 0$ on the boundary, uu_ψ and vv_ψ do not tend to zero. In fact, from (2.4.5.3), $uu_\psi \rightarrow 0$ would imply $u_y \rightarrow 0$, which is obviously incorrect for physical reasons. Hence, an alternate approach is required.

Now, $q^2 = u^2 + v^2$, and therefore $(q^2)_\psi = 2uu_\psi + 2vv_\psi$ or

$$\tfrac{1}{2}(q^2)_\psi = uu_\psi + vv_\psi \tag{2.4.5.5}$$

Substituting (2.4.5.5) into (2.4.5.4) we get

$$\omega = \omega(x,\psi) = v_x - \tfrac{1}{2}(q^2)_\psi \tag{2.4.5.6a}$$

Along a solid boundary the stream function $\psi = \psi_b$ = constant. In most of our applications, solid boundaries occur when i = 1 or IX for all j and/or j = 1 or JX for all i. These usually correspond to curves where, for convenience, we take $\psi = 0$ or $\psi = \psi_{MAX}$.

The no-slip viscous boundary condition on solid boundaries, namely $u = v = 0$ must be imposed. In particular, this implies that $v_x = 0$ on $\psi = \psi_b$ = constant. Thus, (2.4.5.6a) reduces to

$$\omega(x,\psi_b) = -\frac{1}{2}\left.\frac{\partial q^2}{\partial \psi}\right|_{\psi=\psi_b} \tag{2.4.5.6b}$$

and clearly $\frac{\partial q^2}{\partial \psi} \neq 0$ at the boundary $\psi = \psi_b$.

Hence, the following formulas for vorticity can be obtained by Taylor series expansions using the no-slip boundary condition on solid boundaries, namely $q_{i1}^2 = q_{i,JX}^2 = 0$ for a bottom or top boundary, to obtain ω_{i1} and $\omega_{i,JX}$, respectively ($i = 2,3,4,\ldots$).

For the bottom boundary $\psi = 0$ ($j = 1$), one of the following approximate relations can be used (cf. Appendix F):

$$0(\Delta\psi): \quad \omega_{i1} \approx -\frac{1}{2\Delta\psi} q_{i2}^2 \tag{2.4.5.7a}$$

$$\omega_{i1} \approx -\frac{1}{2\Delta\psi}\left(q_{i3}^2 - q_{i2}^2\right) \tag{2.4.5.7b}$$

$$\omega_{i1} \approx -\frac{1}{2\Delta\psi}\left(q_{i4}^2 - q_{i3}^2\right) \tag{2.4.5.7c}$$

$$0(\Delta\psi^2): \quad \omega_{i1} \approx \frac{1}{4\Delta\psi}\left(q_{i3}^2 - 4q_{i2}^2\right) \tag{2.4.5.7d}$$

$$\omega_{i1} \approx \frac{1}{12\Delta\psi}\left(4q_{i4}^2 - 9q_{i3}^2\right) \tag{2.4.5.7e}$$

$$\omega_{i1} \approx \frac{1}{4\Delta\psi}\left(3q_{i4}^2 - 8q_{i3}^2 + 5q_{i2}^2\right) \tag{2.4.5.7f}$$

$$0(\Delta\psi^3): \quad \omega_{i1} \approx -\frac{1}{12\Delta\psi}\left(2q_{i4}^2 - 9q_{i3}^2 + 18q_{i2}^2\right) \tag{2.4.5.7g}$$

$$\omega_{i1} \approx -\frac{1}{12\Delta\psi}\left(11q_{i5}^2 - 42q_{i4}^2 + 57q_{i3}^2 - 26q_{i2}^2\right) \tag{2.4.5.7h}$$

$$0(\Delta\psi^4): \quad \omega_{i1} \approx -\frac{1}{72\Delta\psi}\left(q_{i5}^2 + 8q_{i4}^2 - 48q_{i3}^2 + 104q_{i2}^2\right) \tag{2.4.5.7i}$$

Similarly, for a top boundary $\psi = \psi_{MAX}$ ($j = JX$), one of the following approximate relations can be applied:

$$0(\Delta\psi): \quad \omega_{i,JX} \approx \frac{1}{2\Delta\psi} q_{i,J1}^2 \tag{2.4.5.8a}$$

$$\omega_{i,JX} \approx \frac{1}{2\Delta\psi}\left(q_{i,J2}^2 - q_{i,J1}^2\right) \tag{2.4.5.8b}$$

$$\omega_{i,JX} \approx \frac{1}{2\Delta\psi}\left(q_{i,J3}^2 - q_{i,J2}^2\right) \tag{2.4.5.8c}$$

$$0(\Delta\psi^2): \quad \omega_{i,JX} \approx -\frac{1}{4\Delta\psi}\left(q_{i,J2}^2 - 4q_{i,J1}^2\right) \tag{2.4.5.8d}$$

$$\omega_{i,JX} \approx -\frac{1}{12\Delta\psi}\left(4q_{i,J3}^2 - 9q_{i,J2}^2\right) \tag{2.4.5.8e}$$

$$\omega_{i,JX} \approx -\frac{1}{4\Delta\psi}\left(3q_{i,J3}^2 - 8q_{i,J2}^2 + 5q_{i,J1}^2\right) \tag{2.4.5.8f}$$

$$0(\Delta\psi^3): \quad \omega_{i,JX} \approx \frac{1}{12\Delta\psi}\left(2q_{i,J3}^2 - 9q_{i,J2}^2 + 18q_{i,J1}^2\right) \tag{2.4.5.8g}$$

$$\omega_{i,JX} \approx \frac{1}{12\Delta\psi}\left(11q_{i,J4}^2 - 42q_{i,J3}^2 + 57q_{i,J2}^2 - 26q_{i,J1}^2\right) \tag{2.4.5.8h}$$

$$0(\Delta\psi^4): \quad \omega_{i,JX} \approx \frac{1}{72\Delta\psi}\left(q_{i,J4}^2 + 8q_{i,J3}^2 - 48q_{i,J2}^2 + 104q_{i,J1}^2\right) \tag{2.4.5.8i}$$

Note that the positive and negative signs in equations (2.4.5.7) and (2.4.5.8) are correct as indicated.

At first glance, some of these approximations may appear wrong or inconsistent. For example, equations (2.4.5.7b) and (2.4.5.7d) involve the same points (i,2) and (i,3), but (2.4.5.7b) was obtained by writing

$$\omega_{i1} \approx aq_{i3}^2 + bq_{i2}^2$$

while (2.4.5.7d) was obtained by writing

$$\omega_{i1} \approx aq_{i3}^2 + bq_{i2}^2 + cq_{i1}^2$$

and, after finding the constants a, b, c, using the no-slip boundary condition to set $q_{i1}^2 = 0$. Derivation of equations (2.4.5.7b) and (2.4.5.7d) is contained in Appendix F to demonstrate more clearly the significance of this point. Obviously, (2.4.5.7d) is the correct result to use since it employs the non-slip condition while (2.4.5.7b) does not.

The formulas (2.4.5.7b, c, f, h) are symmetric in the sense that we do not use the term q_{i1}^2 in the derivation, whereas the formulas (2.4.5.7a, d, e, g, i) are non-symmetric in the sense that we take $q_{i1}^2 = 0$ after calculating the constant coefficients. Further, note that the value of the constants in the symmetric formulas sums to zero as they should, but in the non-symmetric formulas they do not; however, the coefficient of q_{i1}^2 can be easily calculated. For example, in formula (2.4.5.7d), summing the constants to zero implies that the constant coefficient for q_{i1}^2 must be +3, as noted in Appendix F. Although not a consideration for the problems in this thesis, if the values of the q_{ij}^2 ($j = 1,2,3,\ldots$) happen to be close to 1, the resulting value for ω_{i1} could be in error when using the symmetric formulas. More investigation of this situation is required in future research.

Some preliminary testing of the boundary conditions for vorticity ω_{i1} was undertaken for a simple test problem to try to determine the most appropriate formula to use. Knowing exact results for ω_{i1} at $x = 0$ (i.e., $i = 1$) the various formulas were tested one-by-one to determine the most accurate. Of all the formulas listed, equation

(2.4.5.7g) (and its corresponding formula (2.4.5.8g) for $\omega_{i,IX}$) came closest to the exact value. These equations will be used as applicable, for the lower and upper boundary values of vorticity, respectively.

However, the choice of boundary condition also affects numerical stability and the rate of convergence of the iterative process. Another possible subject for future research will be the systematic comparison of the solutions obtained using the different expressions for vorticity.

2.4.6 Clustered Grids

To achieve clustering of the grids in regions of high gradients, one-dimensional stretching functions are employed.

The flow equations with appropriate boundary conditions have been presented in unstretched coordinates. In order to formulate the equations in the stretched coordinates, general transformations can be introduced, defined by

$$\begin{aligned} x &= x(\xi) \\ \psi &= \psi(\eta) \end{aligned} \qquad (2.4.6.1)$$

The benefit of these transformations is that they can provide us with a dense mesh in the vicinity of any singularity and allow us to pack more points near an axis or any solid boundary.

Equation (2.4.1.1) and coefficients (2.4.1.2) are transformed from unstretched coordinates (x,ψ) to stretched coordinates (ξ,η) for later use. Initially, only the second transformation of equation (2.4.6.1) will be used and the required equations derived, then both transformations will be applied. Our reason for doing this is dictated by the nature of the particular problems to be solved, for example, some may require only the ψ

coordinate to be stretched, while some will require stretching both the x and ψ coordinate. Details and the resulting equations can be found in Appendix G.

2.4.7 Large Reynolds Number

The central differencing scheme employed to obtain (2.4.2.1a) works well for low R_e. For larger R_e, it becomes necessary to upwind or backward difference the convective term $(\delta_x\omega)_{ij}$ in (2.4.1.1). In this case $\alpha = 1$, $\phi = \omega(x,\psi)$ and equation (2.4.1.1) can be expressed as

$$\frac{A_{ij}^{(k)}}{\Delta x^2}(\omega_{i-1,j}-2\omega_{ij}+\omega_{i+1,j})^{(n+1)} + \frac{B_{ij}^{(k)}}{4\Delta x\Delta\psi}(\omega_{i+1,j+1}+\omega_{i-1,j-1}$$

$$-\omega_{i+1,j-1}-\omega_{i-1,j+1})^{(n+1)} + \frac{C_{ij}^{(k)}}{\Delta\psi^2}(\omega_{i,j-1}-2\omega_{ij}+\omega_{i,j+1})^{(n+1)}$$

$$+\frac{R_e D_{ij}^{(k)}}{\Delta x}(\omega_{ij}-\omega_{i-1,j})^{(n+1)} + \frac{E_{ij}^{(k)}}{2\Delta\psi}(\omega_{i,j+1}-\omega_{i,j-1})^{(n+1)} = 0$$

By rearranging, we have

$$B_{ij}^{(k)}\frac{\Delta x}{4\Delta\psi}\omega_{i-1,j-1}^{(n+1)} + \left(A_{ij}^{(k)}-R_e D_{ij}^{(k)}\Delta x\right)\omega_{i-1,j}^{(n+1)} - B_{ij}^{(k)}\frac{\Delta x}{4\Delta\psi}\omega_{i-1,j+1}^{(n+1)}$$

$$+\left[C_{ij}^{(k)}\frac{\Delta x^2}{\Delta\psi^2}-E_{ij}^{(k)}\frac{\Delta x^2}{2\Delta\psi}\right]\omega_{i,j-1}^{(n+1)} - 2\left[A_{ij}^{(k)} + C_{ij}^{(k)}\frac{\Delta x^2}{\Delta\psi^2} + R_e D_{ij}^{(k)}\Delta x\right]\omega_{ij}^{(n+1)}$$

$$+\left[C_{ij}^{(k)}\frac{\Delta x^2}{\Delta\psi^2}+E_{ij}^{(k)}\frac{\Delta x^2}{2\Delta\psi}\right]\omega_{i,j+1}^{(n+1)} - B_{ij}^{(k)}\frac{\Delta x}{4\Delta\psi}\omega_{i+1,j-1}^{(n+1)} \tag{2.4.2.1b}$$

$$+ A_{ij}^{(k)}\omega_{i+1,j}^{(n+1)} + B_{ij}^{(k)}\frac{\Delta x}{4\Delta\psi}\omega_{i+1,j+1}^{(n+1)} = 0$$

which can be abbreviated as

$$
\begin{aligned}
& b_{ij}\,\omega_{i-1,j-1} + (a_{ij} - d_{ij}^{*})\,\omega_{i-1,j} - b_{ij}\,\omega_{i-1,j+1} \\
& + (c_{ij} - e_{ij})\,\omega_{i,j-1} - 2(a_{ij} + c_{ij} + d_{ij}^{*})\,\omega_{ij} + (c_{ij} + e_{ij})\,\omega_{i,j+1} \\
& - b_{ij}\,\omega_{i+1,j-1} + a_{ij}\,\omega_{i+1,j} + b_{ij}\,\omega_{i+1,j+1} = 0
\end{aligned}
\tag{2.4.2.2b}
$$

where,

$$
\begin{aligned}
a_{ij} &= A_{ij}^{(k)} \\
b_{ij} &= B_{ij}^{(k)} \frac{\Delta x}{4\Delta\psi} \\
c_{ij} &= C_{ij}^{(k)} \frac{\Delta x^2}{\Delta\psi^2} \\
d_{ij}^{*} &= R_e D_{ij}^{(k)} \Delta x \\
e_{ij} &= E_{ij}^{(k)} \frac{\Delta x^2}{2\Delta\psi}
\end{aligned}
\tag{2.4.2.3b}
$$

Corresponding changes have to be made to the various tridiagonal matrices. Comparing equations (2.4.2.2a) and (2.4.2.2b), it is seen that the upwind differencing of the convective term only changes the coefficients of $\omega_{i-1,j}$, ω_{ij} and $\omega_{i+1,j}$. The * in d_{ij}^{*} is used so as not to cause confusion with the expression for d_{ij} stated previously in (2.4.2.3a).

CHAPTER III

PLANE DIVERGING VISCOUS LAMINAR CHANNEL FLOW OF COMPLEX GEOMETRY

3.1 INTRODUCTION

In 1982, the International Association for Hydraulic Research (IAHR) Working Group on Refined Modelling of Flows devoted the Fifth IAHR Meeting to a specific subject - to assess the capabilities of various numerical simulation methods to deal with laminar flows in "complex geometries". Here "complex geometries" means flow domains that do not coincide with coordinate axes in some simple coordinate system such as Cartesian or polar.

Why study such flows? Steady-state viscous flow in two-dimensional channels with arbitrary wall contours are representative of flush inlet geometries [III.1]. The water inlets for ships powered by water pumps are often mounted flush to the hull below the water line. The calculation of the flow in flush inlets is of interest for the prediction of the total drag of the ship and the performance of the pump. Flow separation can occur in the inlet, so that viscous effects cannot be ignored.

A single, well defined comparison test problem, namely the laminar flow in a channel with a smooth expansion, suggested by the work of Roache [III.2] on the scaling of Reynolds number in weakly separated (i.e., small recirculating region) channel flows, was chosen for testing various numerical methods. The purpose of the test problem was to evaluate the capabilities of various Navier-Stokes solvers and to highlight difficulties in the modelling of complex geometries. This problem has been used to test the present formulation. A comparison and discussion of the solutions obtained by the participants was reported by Napolitano and Orlandi [III.3]. As reported in [III.3], some of the participants felt that the problem under investigation was 'too easy' and therefore not suitable to assess the capability of each code to compute flows in complex geometries. As the author of this thesis and others discovered, and as the reader will verify after analysis of the results obtained, such an opinion was premature.

3.2 TEST PROBLEM

3.2.1 Problem Specification

The geometry is a diverging channel with length depending on the Reynolds number R_e, i.e., the length of the channel is scaled proportionally to R_e so that the channel becomes longer and straighter as R_e increases, i.e., $R_e = R_{ec}$ is a geometrical constant which determines the steepness of the curved wall of the expansion (see Diagram 3.1.1). For $R_e >> 1$, quasi-self-similar flow conditions and solutions can be obtained [III.2] by having the channel length x increase proportional to R_e so solutions become self-similar in the scaled longitudinal variable $x_{out} = R_{ec}/3$ (x_{out} = outlet of channel). This scaling is necessary to keep the separated flow region within the computational mesh. Weakly separated laminar two-dimensional incompressible channel flows display a self-similar solution.

Two flows were computed corresponding to relatively small values of R_e, i.e., $R_e = R_{ec} = 10$ and $R_e = R_{ec} = 100$. $R_e = 10$ was chosen because of its highly distorted geometry. $R_e = 100$ was chosen to assess the dependence of the convergence rate on R_e. A 21 x 21 finite difference mesh was prescribed. Computed results for the wall were obtained for equally spaced x/x_{out} locations.

Because the numerical results from these two problems should not depend too much on the treatment of advection terms, an optional third case was suggested, namely $R_e = 100$ inside the $R_{ec} = 10$ channel. Even though this case would be characterized by more significant advection, a case more strongly influenced by the modelling of non-linear terms, it was not considered simply because this third problem was not physically representative. As noted in [III.4], flow in a symmetric channel at high Reynolds number is not unique. In the case of laminar flow, the existence of asymmetric solutions implies non-uniqueness of solutions of the Navier-Stokes equations. Also, the symmetric solution modelled by the test problem is, in fact, unstable at high Reynolds number. Thus, the third test problem, although it can be studied computationally, is not physically realistic.

3.2.2 Boundary Conditions in the Physical Domain

The lower boundary (solid wall) coordinates of the channel are given analytically as

$$y = y_\ell(x) = \frac{1}{2}\left[\tanh\left[2-\frac{30x}{R_c}\right] - \tanh 2\right], \quad 0 \le x \le x_{out} = \frac{R_{cc}}{3} \qquad (3.2.2.1)$$

and no-slip conditions $u = v = 0$ are applied along this boundary. (See Appendix H for a discussion of this function).

The upper boundary (centreline or symmetry plane) is located at

$$y = y_u(x) = 1.0, \quad 0 \le x \le x_{out}$$

Inlet boundary conditions are given in terms of the Cartesian velocity components (u,v) as

$$\left.\begin{array}{l} u = 3\left[y - \dfrac{y^2}{2}\right] \\ v = 0 \end{array}\right\} \quad \text{for } x=0,\ 0 \le y \le 1$$

i.e., equilibrium flow of the inlet with an imposed fully developed parabolic Poiseuille flow velocity distribution. The origin of the physical coordinates (x,y) is on the lower wall at the inflow boundary, where the channel half height has been normalized to y = 1. The maximum inflow velocity is u(0,1) = 3/2. The length of the channel is $x = x_{out} = R_{cc}/3$.

Several investigators used a simple linear transformation or stretching to map (x,y) into a rectangular computational domain. We also obtain a rectangular region for the computational domain (Diagram 3.1.2), but the transformation to achieve this has been done on the original partial differential equations. Finally, it should be noted that Poiseuille flow implies constant area flow, which in the case of a diverging channel is a contradiction. This results in a particularly annoying difficulty, to be discussed later.

In terms of the stream function, the inlet conditions are

$$u = \psi_y = 3\left[y - \frac{y^2}{2}\right]$$
$$v = -\psi_x = 0$$

Therefore,

$$\psi = \psi(y) = \frac{1}{2}\left(3y^2 - y^3\right) \quad \text{for } x=0,\ 0 \le y \le 1$$

where we have taken $\psi = 0$ at $y = 0$.

The standard no-slip condition on solid walls (i.e., u = v = 0) is imposed at the wall $0 \le x \le x_{out}$ and $y = y_\ell(x)$. Symmetry is enforced at $0 \le x \le x_{out}$ and $y = y_u(x) = 1$.

The outlet section of the channel is located at

$$x = x_{out} = \frac{R_{cc}}{3}$$

so that, at the lower boundary

$$y = y_\ell(x_{out}) = \frac{1}{2}[\tanh(-8) - \tanh 2] = -0.98202$$

The outlet boundary conditions are left somewhat arbitrary [III.2]. For parallel flow

$$u_x = v_x = 0, \text{ for } x = x_{out} \quad \text{and} \quad y_\ell\left(\frac{R_{cc}}{3}\right) \leq y \leq 1 \ .$$

This implies $y_x = \omega_x = 0$. See Appendix I for a further discussion of this point.

3.2.3 Boundary Conditions in the Computational Domain

Boundary conditions for y:

- At $x = 0, 0 \leq \psi \leq 1$

$$\psi = \frac{1}{2}\left(3y^2 - y^3\right)$$

which can be solved explicitly for y as a function of ψ to give (see Appendix J)

$$y = 2\cos\left(\theta + \frac{4\pi}{3}\right) + 1 \tag{3.2.3.1}$$

where

$$\theta = \frac{1}{3}\arccos(1 - \psi)$$

- At $x = x_{out}$, $0 \le \psi \le 1$

$$y_x = 0$$

- At $\psi = 0$, $0 \le x \le x_{out}$

$$y = y_\ell(x) = \frac{1}{2}\left[\tanh\left[2 - \frac{30x}{R_e}\right] - \tanh 2\right]$$

- At $\psi = 1$, $0 \le x \le x_{out}$

$$y = y_u(x) = 1$$

Boundary conditions for ω:

- At $x = 0$, $0 \le \psi \le 1$, by definition $\omega = -\nabla^2\psi$ and $\psi = \psi(y)$ at the inlet, so that

$$\omega = -\psi_{yy} = -u_y = -3(1-y) \tag{3.2.3.2}$$

- At $x = x_{out}$, $0 \le \psi \le 1$

$$\omega_x = 0$$

- At $\psi = 0$, $0 \le x \le x_{out}$

$$\omega_{i1} \approx -\frac{1}{12\Delta\psi}\left(2q_{i4}^2 - 9q_{i3}^2 + 18q_{i2}^2\right)$$

- At $\psi = 1$, $0 \le x \le x_{out}$

$$\omega = 0 \text{ (symmetry condition)}$$

Note: At $x = x_{out}$, $0 \le \psi \le 1$, 3-point backward or upward differencing has been used for $y_x = \omega_x = 0$, i.e., $\dfrac{\phi_{I2,j} - 4\phi_{I1,j} + 3\phi_{IX,j}}{2\Delta x} = 0$, $\phi = \begin{cases} y \\ \omega \end{cases}$.

3.2.4 Vorticity Discontinuity at the Inlet

This section could have been placed under the heading of discussion. However, because of the significance of this issue, it was felt that a discussion of this topic should come earlier.

Unfortunately, the test problem had a defect [III.4]. As noted earlier, the validity of the inlet boundary conditions was questionable. Fully developed Poiseuille flow conditions have been prescribed for the inlet velocity profile in spite of the non-zero slope of the wall of the channel at $x = 0$. As a consequence of this inappropriate choice of inlet profile, there is a singularity at this point, which shows up either as a disturbed wall pressure distribution or as a discontinuity in vorticity on the channel wall at the inlet or origin. In fact, the choice of the outlet as the reference pressure point in a primitive-variable approach would also have caused difficulties because of the arbitrariness of the boundary conditions at the outlet that the stream function-vorticity approach could alleviate.

As noted in [III.4], the magnitude of the discontinuity in vorticity at the origin because of the nature of the boundary conditions is a function of the angle the wall makes with the horizontal at the inlet. The discontinuity only affects the local flow, which can be made plausible by considering the velocity close to the wall. The effect, however, is rather pronounced. At the inlet, the local flow is parallel to the x axis, but just inside the inlet it must be parallel to the channel wall, which is not parallel to the x axis. By constructing the local flow solution, Cliffe et al [III.4] proved that there is in fact a discontinuity in vorticity and obtained a value for the jump. For the case $R_e = R_{ec} = 10$, the value obtained was 0.9125 and for the case $R_e = R_{ec} = 100$, the value obtained was 0.0989. Both of these values are used in this thesis.

In addition to the results obtained for the jump in vorticity at the inlet, the inlet boundary condition for vorticity must be modified. At $x = 0$, $0 \leq \psi \leq 1$, we obtained equation (3.2.3.2), namely, $\omega = -3(1-y)$. This was obtained by noting that $\psi = \psi(y)$ only at the inlet and therefore that $\omega = -\psi_{yy} = -u_y$. Equally, this could have been obtained by using:

$$\omega = v_x - u_y$$

and the fact that,

$$u = 3\left[y - \frac{y^2}{2}\right] = u(y)$$
$$v = 0$$

at the inlet. Taking $v_x = 0$ gives

$$\omega = -u_y$$

Actually, this is incorrect since $v_x \neq 0$ unless the channel is perfectly straight for a couple of grid points to the right of the inlet (a method also tried without boundary condition modification). Hence, the boundary condition for ω at the inlet (equation (3.2.3.2)) is modified as follows:

At $x = 0, 0 \leq \psi \leq 1$,

$$\omega = -3(1-y) + v_x \tag{3.2.4.1}$$

where v_x is approximated by a one-sided or forward (downwind) difference formula, either 2-point or 3-point. (See Appendix K for a summary of the difference formulas used for v_x). Note that at $y = 0$ ($j=1$), from the no-slip boundary condition along the wall, $v = 0$ still. This implies $v_x = 0$. Hence at $x = 0$, $y = 0$ ($i=1, j=1$) we still have $\omega_{11} = -3$. However, for $i = 1, j = 2,3,\ldots, J1$, $v_x \neq 0$.

3.2.5 Clustered Grid Functions

The mesh distribution employed in the calculations is very important to modelling the separation region correctly. In particular, using a proper stretching in the direction normal to the wall could be essential. In this way a finer resolution is obtained in the region where a separation bubble is likely to develop.

Hence, it is desirable to concentrate grid lines close to the channel wall first, and second, to redistribute lines away from the inlet to the body of the domain [III.5]. The first objective can be achieved by choosing ψ in equation (2.4.6.1) to be

$$\psi = \eta_{MAX}\left[1 - e^{-\alpha(\eta_{MAX}-\eta)}\right] \tag{3.2.5.1}$$

where η_{MAX} is the largest value of η in the new computational domain. In our present case $\eta_{MAX} = 1.0$. The larger the value chosen for the constant α, the more grid lines will be concentrated towards the channel wall. The second objective can be achieved by setting x in equation (2.4.6.1) to be

$$x = \sinh\left[\beta(\xi-\xi_o)\right] \tag{3.2.5.2}$$

where ξ_o is the grid line around which concentration of the grid lines is desired and β is again a constant which determines the degree of concentration.

3.3 RESULTS AND DISCUSSIONS

3.3.1 Preliminaries

In the absence of an exact reference solution, the grid-independent results obtained by Cliffe et al in [III.4] have been taken as a benchmark, as recommended by Napolitano and Orlandi [III.3]. Cliffe et al used a finite element method in primitive variables, a Newton-Raphson linearization scheme and the frontal solution method for the resulting linear system. Such a solution has been used to compute the average percentage error ε_{ω_u} defined according to the relationship

$$\varepsilon_{\omega_{i1}} = \frac{100}{19} \sum_{i=2}^{20} \left| \frac{\omega_{i1} - \omega_{i1CJG}}{\omega_{i1CJG}} \right| \tag{3.3.1.1}$$

where ω_{i1} is the computed wall vorticity at 21 equally spaced $\frac{x}{x_{out}}$ locations along the wall and the subscript CJG refers to the benchmark solution of Cliffe et al noted above. The values of the gridpoints $x = 0$ and $x = x_{out}$ have not been included in the definition of $\varepsilon_{\omega_{i1}}$ to reduce the influences of the singularity at the inlet and of the arbitrary outlet boundary conditions. $\varepsilon_{\omega_{i1}}$ has been defined so as to account mostly for the region around and inside the separation bubble as the results of this thesis will indicate. Since this is a rational and appropriate choice, $\varepsilon_{\omega_{i1}}$ is a good quantity to judge the accuracy of the solutions for the present flow case (more so than, say, pressure). If the method under consideration ignores the separation phenomenon completely or if the length and the position of the separation region are not computed very accurately, then $\varepsilon_{\omega_{i1}}$ will be very large because very large relative errors for ω are probable near the separation and the reattachment points. One must appreciate the goal of trying to obtain accuracy away from thin boundary layers without actually resolving these boundary layers in detail.

3.3.2 Results

Results were obtained for the following problems:

1. Reynolds number: (i) $R_e = R_{ec} = 10$ and (ii) $R_e = R_{ec} = 100$ where $\Delta x = \frac{R_{ec}}{3}/20$. For example, for $R_{ec} = 10$, $\Delta x = 0.167$. For $R_{ec} = 100$, $\Delta x = 1.667$. $\Delta\psi = 0.05$ in both cases.

2. Inlet corrections: (i) No inlet correction, (ii) the inlet correction used by Cliffe et al [III.4] and (iii) the modified boundary condition given by equation (3.2.4.1).

For Reynolds number $R_e = R_{ec} = 10$, Figures (3.3.2.1), (3.3.2.2) and (3.3.2.3) contain plots of the streamlines y_{ij}, $j=1$ (the wall), $j=2$ (first streamline) to $j = 10$ for $i = 1,2,\ldots,20$.

Figure (3.3.2.4) is a plot of the wall vorticity ω_{i1}, $i = 1,2,\ldots,20$.

Figure (3.3.2.5) is a plot of the worst case wall vorticity values ω_{i1}, $i = 1,2,\ldots,20$ obtained by all the participants that reported in [III.3] against the results obtained in Figure (3.3.2.4) ($R_e = R_{ec} = 10$).

Table (3.3.2.1) contains a listing of the various parameters used to obtain the results.

Tables (3.3.2.2), (3.3.2.3) and (3.3.2.4) contain the error for each point of the wall vorticity and the total error. The number of iterations referred to in the tables is for one equation. Hence, the number of iterations for the system of equations is half the quoted value.

Table (3.3.2.5) contains a comparison of the separation and reattachment points and the relative errors where the vorticity $\omega = 0$ for various values of x.

All the results were obtained using an IBM PC-compatible/Intel 80286 (AT) computer.

3.3.3 Discussion of Results

3.3.3.1 $R_e = R_{ec} = 10$

As given in Tables (3.3.2.2), (3.3.2.3) and (3.3.2.4) all attempts to obtain results for the wall vorticity resulted in average percentage errors greater than 100%. The best case was obtained by using the modified boundary condition given by equation (3.2.4.1). However, the least number of iterations was obtained by using the modified inlet correction of Cliffe et al [III.4].

There are several explanations for the large average percentage errors. The first reason comes from the method of calculating the error. According to equation (3.3.1.1) the average percentage error is obtained by dividing by the benchmark values obtained by Cliffe et al [III.4]. The largest errors occur in the separated flow region because the value of the wall vorticity there is very small. Division by a small number leads to large error, especially in the recirculating region.

The second reason for the large average percentage error comes from the method of solution. In Section (2.2) it was noted that the Jacobian J must be greater than zero. In a region of recirculating flow, J can be either greater than zero or less than zero. Hence, the fluid cannot flow along streamlines ψ = constant in the direction of increasing $\phi(x,y) = x$, as noted in equation (2.3.1). At points in a recirculating region the flow along streamlines ψ = constant will be alternating between the direction of decreasing $\phi(x,y) = x$ and the direction of increasing $\phi(x,y) = x$.

Although the recirculating region is small, it is still significant enough to cause destabilizing effects on the solution. As seen in Figure (3.3.2.4), the plot of the wall vorticity, the best results are obtained after the recirculating region where errors were as small as 0.1% to 3.0%. As well, as seen in Figure (3.3.2.5), the plot of the worst case wall vorticity obtained by all the participants that reported in [III.3], the values of wall vorticity obtained in this study are quite comparable to results of other investigators.

Numerous attempts were made to improve the results. Clustering the grid according to equations (3.2.5.1) and (3.2.5.2) produced at best oscillating results which would not converge within the given error tolerances. As well, no improvement in the average percentage error was indicated. Attempts to minimize the effects of the recirculating region by shrinking its width, also met with no improvement. For example, choosing $R_e = 0.1$ and $R_{ec} = 300$ resulted in converging solutions, but no improvement in the average percentage error - the error was simply spread out more evenly among all the values of x. Also, the limit of Stokes flow ($R_e = 0$; infinite viscosity) was attempted for the case under consideration, namely $R_{ec} = 10$. In this limit, separation should not occur. The solution did converge, leading to the conclusion that viscous flow with no separation ought to be further investigated by the current method of solution.

Finally, predictions of the separation and reattachment points varied from a low of 13.2% to a high of 25.2% error. The separation point was best predicted using the inlet correction of Cliffe et al [III.4] and the reattachment point was best predicted using the boundary condition correction at the inlet.

3.3.3.2 $\underline{R_e = R_{ec} = 100}$

Converged results for this case could not be obtained. At first it was thought that the problem had to be with the vorticity term in equation (2.4.1.1) because of the larger Reynolds number $R_e = 100$. Since the results were oscillating but not converging, it was thought that upwind differencing of the vorticity term in (2.4.1.1) would prevent the oscillations from occurring.

A source of differences among algorithms is in the treatment of the derivatives of the convective terms. In the case where diffusion dominates convection, the use of second order accurate centered differences for the convective derivatives constitutes the best compromise between computational accuracy and economy. In cases where there is convective dominance, the use of centered differences for the convective terms may result in instability or non-physical/oscillatory behaviour. The most widely used way of avoiding this instability is the use of a first order accurate upwind formulation, so that a hybrid central/upwind differencing scheme is employed. Even though this approach results in unconditional stability, it can introduce artificial or numerical diffusion, an error that may become so dominant as to obscure the effects of the physical diffusivity on the flow. In any event, the oscillations for the case $R_e = R_{ec} = 100$ could not be prevented with this approach.

According to [III.6], there are limitations on the cell Reynolds number, or Peclet number, $R_{e\,cell}$, for non-oscillatory convergent solutions. In [III.6], $R_{e\,cell}$ must be less than or equal to a typical value of 10.

$R_{e\,cell}$ is based on the characteristic length of the cell Δx or $\Delta\psi$. Hence, in our case, $\frac{R_{e\,cell\,\Delta x}}{\Delta x}$ = constant and $\frac{R_{e\,cell\,\Delta\psi}}{\Delta\psi}$ = constant, so that taking their ratio, we obtain, $\frac{R_{e\,cell\,\Delta x}}{R_{e\,cell\,\Delta\psi}} = \frac{\Delta x}{\Delta\psi}$ = constant. This constant can be looked at as a cell aspect ratio, AR, and should be less than 1. For the case $R_e = R_{ec} = 10$, AR = $\frac{0.167}{0.05}$ = 3.34, which is near the value 1 and the method converged. For the case $R_e = R_{ec} =$ 100, AR = $\frac{1.667}{0.05}$ = 33.34 which is much greater than 1 and the method would not converge. Even though we were restricted by the geometry of the test problem, going to larger values of $\Delta\psi$ led to solutions that would eventually converge, but the results were not comparable to the benchmark values.

3.3.4 Conclusions

Contrary to what was reported by Napolitano and Orlandi in [III.3], this problem was not too easy. In fact, the proposed method of solution in this thesis could not handle the problem, resulting in average percentage errors in excess of 100% for the solutions that would converge. From these results, it appears that viscous flow problems that contain separated regions of flow cannot be treated, especially at the higher Reynolds numbers, using the formulation in this thesis. However, as we will show in Chapter V, this formulation can be modified in such a way as to allow flow separation. In the next chapter we solve a flow problem which illustrates that the difficulties encountered in this chapter are related to the viscous effects, rather than in handling flow fields with non-zero vorticity.

CHAPTER IV

CIRCULAR CYLINDER IN HYPERBOLIC-COSINE SHEAR FLOW

4.1 INTRODUCTION

Since the problem of recirculation is not fully resolved in Chapter III, a problem is solved where the flow is rotational, but no viscosity is allowed. Here, recirculating flow is eliminated. The problem is hyperbolic-cosine shear flow about a circular cylinder as discussed by Van Dyke [IV.1].

4.2 FLOW EQUATIONS

4.2.1 Differential Equations

If no viscosity is allowed, we are considering flow in the inviscid limit of $R_e \rightarrow \infty$.

The equation (2.3.7b), namely,

$$L\{\omega\} - R_e y_\psi \omega_x - y_\psi^2 \omega \omega_\psi = 0$$

where $\omega = \omega(x,\psi)$, reduces to $y_\psi \omega_x = 0$. Since $y_\psi = 1/u \neq 0$, $\omega_x = 0$ which implies $\omega = \omega(\psi)$ only. This condition guarantees that at any x station (i.e., x = constant), the vorticity profile is exactly the same as at the inlet (i.e., ω = constant along each streamline). Thus, once we know ω at infinity, we know it throughout the flow field. This is a dynamical condition for steady motion.

Hence, equation (2.3.8c),

$$L\{y\} - y_\psi^2 \omega y_\psi = 0$$

where $y = y(x,\psi)$ or,

$$y_\psi^2 y_{xx} - 2y_x y_\psi y_{x\psi} + (1+y_x^2)y_{\psi\psi} - y_\psi^2 \omega y_\psi = 0$$

or in difference form,

$$\left(A_{ij}^{(n)}\delta_{xx} + B_{ij}^{(n)}\delta_{x\psi} + C_{ij}^{(n)}\delta_{\psi\psi} + E_{ij}^{(n)}\delta_\psi\right)y_{ij}^{(n+1)} = 0 \qquad (4.2.1.1)$$

where the coefficients and subscripts are as previously defined, becomes the only equation to be solved for the unknown $y = y(x,\psi)$. (Note: We have taken $\phi = y(x,\psi)$, i.e., $\alpha = 0$, $k = n$ in equation (4.2.1.1)). The vorticity ω in the coefficient E_{ij} is known at each (i,j). Again, we can start with some initial approximation of the vorticity ω for $n = 0$, e.g., $\omega = 0$ when $n = 0$, just to get the iteration for y started, afterwards $\omega = \omega(\psi)$ is known along each streamline.

4.2.2 Circular Cylinder in Hyperbolic-Cosine Shear Flow

The solution of the circular cylinder in hyperbolic-cosine shear flow is developed in Appendix L from the uniform flow problem at infinity to demonstrate the problem's increasing analytic complexity and which the numerical method utilized in this thesis handles very nicely.

Note that we are not solving an irrotational inviscid problem, but a rotational, inviscid problem because of the upstream boundary condition on vorticity at $x = -\infty$. This is not a truly physical situation, but is used to simulate an inviscid non-recirculating flow in which vorticity is present.

For flow over a symmetric body, like a circular cylinder, with the flow at infinity symmetric about $y = 0$, we only need to consider the upper half (x,ψ) plane. The symmetric body is taken as a section of the streamline $\psi = 0$.

4.2.3 Boundary Conditions in the Computational Domain

Given the symmetric body geometry, i.e., $y = f(x)$, the boundary conditions associated with equation (4.2.1.1) can be expressed as follows (see Diagram (4.2.3.1)).

The values of x at the leading and trailing edges are denoted by x_{LE} and x_{TE}, respectively.

Boundary conditions for y: (nondimensionalized):

1. Hyperbolic-cosine shear flow at infinity (equation (L3) from Appendix L):

$$y = \frac{1}{\epsilon^{\frac{1}{2}}} \sinh^{-1}\left(\epsilon^{\frac{1}{2}}\psi\right) \text{ at } x = \pm\infty \text{ and at } \psi = +\infty$$

where ϵ = vorticity number (perturbation parameter).

2. Flow symmetry and flow tangency:

$$y(x,0) = \begin{cases} 0 \text{ for } -\infty < x < x_{LE} \quad x_{TE} < x < \infty \\ f(x) = \sqrt{0.25-x^2} \text{ for } x_{LE} \leq x \leq x_{TE} \end{cases}$$

Boundary conditions for ω: (non-dimensionalized).

At all x stations, ω = constant along a streamline (equation (L4) from Appendix L):

$$\omega = -\epsilon^{\frac{1}{2}}\sinh(\epsilon^{\frac{1}{2}}y)$$

for all x.

In discrete form, this is

$$\omega_{ij} = \omega_{1j} = -\epsilon^{\frac{1}{2}}\sinh\left(\epsilon^{\frac{1}{2}}y_{1j}\right)$$

for all j where i = 1 corresponds to $x = -\infty$.

The speed is given by

$$q^2 = u^2 + v^2 = \frac{1+y_x^2}{y_\psi^2} \qquad (4.2.3.1)$$

We calculate $q = q_s$, the speed on the surface of the circular cylinder, using equation (4.2.3.1)

$$q^2 = q_s^2 = \frac{1+f'(x)^2}{y_\psi^2} \qquad (4.2.3.2)$$

In discrete form the surface speed is $q_{s,i1}$ for all i, where j = 1 corresponds to the surface of the circular cylinder.

4.3 RESULTS AND DISCUSSION

4.3.1 Results

Results were obtained for the following:

1. Equal uniform grid spacing in the x and ψ directions, $\Delta x = \Delta\psi = 0.05$.
2. The dimensionless vorticity number or perturbation parameter $\epsilon = 0.1$.
3. The radius of the circular cylinder was $r = a = ½$.

All results were obtained using an IBM-PC-compatible/Intel 80286 (AT) computer. The numerical results for the speed on the surface of the circular cylinder in hyperbolic-cosine shear flow are presented in the following tables and figures and compared with the second order solution determined by Van Dyke [IV.1] (perturbation or analytic (approximate) solution obtained using equation (L2) in Appendix L).

Table (4.3.1.1) contains a listing of the various parameters used to obtain the results.

Tables (4.3.1.2) and (4.3.1.3) contain the numerical results compared to the perturbation or analytic results obtained from Van Dyke. The error at each point was compared (the total error was not a consideration in this problem).

Figures (4.3.1.1) and (4.3.1.2) contain a plot of the results tabulated in Tables (4.3.1.2) and (4.3.1.3).

4.3.2 Discussion of Results

As seen either from Tables (4.3.1.2) and (4.3.1.3) or Figures (4.3.1.1) and (4.3.1.2), agreement is best over the main body of the circular cylinder with accuracy decreasing towards the leading and trailing edges. The validity of all these solutions can be questioned near the stagnation points at the leading and trailing edges. As noted in [I.3], the inaccuracy at the leading and trailing edge could be overcome by an extrapolation of the accurate values over the centre of the profile to the stagnation points at the leading and trailing edges. Also, refining the grid near the leading and trailing edges or using a staggered grid spacing would improve the accuracy at these two locations. However, since the main reason for attempting this problem was to validate the method of solution in regions of non-recirculating flow, no further refinements were attempted.

4.3.3 Conclusions

The numerical results are found to be almost exactly the same as the perturbation results except near the leading and trailing edges. The results obtained in [I.3] indicated that the numerical results consistently underestimated the perturbation results. This was not the case for the results obtained here. Making the grid finer or packing lines which would improve the numerical solution in the sense of making it closer to the perturbation results is suggested. However, the perturbation results are themselves only approximate analytic solutions. The numerical results represent the flow accurately in regions not near singularities, i.e., over the top of various profiles, while the perturbation results can be used to advantage when singularities arise. Hence, we conclude that the numerical results agree very well with the analytical results.

The results of this chapter confirm our assertion that the difficulties encountered in Chapter III are due to the flow separation rather than the flow vorticity. In the next chapter we propose a method which allows treatment of the re-circulating region.

CHAPTER V

STEADY FLOW PAST A BACKWARD FACING STEP

5.1 INTRODUCTION

The flow over a backward facing step (BFS) in a channel or the flow through a channel containing a sudden expansion or corner provides an excellent test case for the accuracy of numerical methods because of the dependence of the reattachment length of the dividing streamline on the Reynolds number R_e. Excessive numerical smoothing in favour of stability will result in failure to predict the correct reattachment length.

As noted in [V.1], experimental studies over a BFS yielded two-dimensional laminar flows only at Reynolds numbers $R_e < 400$ and $R_e > 6000$. In the laminar range, the velocity field was close to that of a fully developed channel flow with only a slight deviation from that of parabolic flow.

In between these Reynolds numbers, the transition to turbulent flow was found to be strongly three-dimensional where velocity fluctuations began to increase, while maintaining symmetry to the centre plane of the test section. It was initially believed that the BFS flow, with its simple geometry, would yield a simple flow pattern showing a single separation region attached to the step. Other regions of detached flow were not expected.

Although numerical prediction procedures encounter false diffusion as discussed in Chapter II of this thesis, good agreement between the predicted and measured flow field for Reynolds numbers $R_e < 400$ were obtained in [V.1], demonstrating that truncation errors due to false diffusion can be kept very low. For Reynolds numbers $R_e > 400$, two-dimensional predictions were also obtained, but the results showed multiple regions of recirculating flow. Some of the differences were explained as being caused by the three-dimensionality of the flow, where additional recirculating flow regions were measured downstream of the primary region of separation caused by the sharp change in the flow direction. For example, an additional recirculating flow region was measured at the upper wall downstream of the expansion, developing late in the laminar range ($R_e = 400$) and remaining in existence throughout the transition region ($400 < R_e < 6000$). This was due to the adverse pressure change or gradient downstream of, and created by, the sudden expansion. It was largely dependent on the expansion ratio of the BFS flow geometry.

For the above reasons, it was decided to try to duplicate the results obtained in [V.2] with a Reynolds number of $R_e = 50$. See Diagrams (5.1.1) and (5.1.2) for the physical and computational domains in terms of nondimensional coordinates $x = \frac{\bar{x}}{L}$ and $y = \frac{\bar{y}}{H}$, i.e., the coordinates have been nondimensionalized in terms of the channel length L and height H.

5.2 TEST PROBLEM

5.2.1 Problem Specification

Fully developed Poiseuille flow has been specified at the entrance and the exit of the channel. This means, in theory, that equilibrium flow exists at the inlet and exit. Hence, the boundary conditions are such that an imposed fully developed parabolic velocity distribution is prescribed at a section $x = 0$ a short distance upstream of the step and also again far downstream at a section $x = x_{MAX}$. In reality, the downstream reversion to Poiseuille flow at low R_e is achieved in an asymptotic manner (as also is the change upstream). This sort of downstream boundary condition becomes invalidated at high Reynolds number R_e when ultimately turbulence sets in.

As discussed in [V.1], the length measured from the step to the end of the calculation domain should be selected to be equivalent to at least four times the experimentally measured reattachment length of the primary recirculatory region. The boundary condition at that far downstream cross-section can then be taken as that of fully developed parabolic flow, i.e., $\frac{\partial u}{\partial x} = \frac{\partial v}{\partial x} = 0$. This distance has been shown to be sufficient to make the reattachment length independent of the length of the calculation domain. For small Reynolds number, the section length downstream of the step, at the outlet to the channel can be made sufficiently long to permit the flow to redevelop into a fully developed channel flow. For higher Reynolds numbers, no matter how reasonably long the channel, small deviations could be present.

Similar to the discussion by Roache [I.1], the adequacy of the boundary conditions on $y = y(x,\psi)$ and $\omega = \omega(x,\psi)$ in this thesis will depend on the Reynolds number of the problem, the differencing method used, and on the initial conditions. The limit of zero upstream wall boundary layer thickness can be simulated by using a "slip" wall condition. The slip wall condition is that used on the solid wall upper surface or lid. The upstream wall, the base and the centreline will also be solid walls.

The upstream inflow boundary cannot have a unique solution since its characteristics will change depending on the physical flow upstream of the inflow cross-section, and upon the separated flow solution itself. The problem is unclear mathematically. For example, it is not clear that one should completely specify the input, lest the elliptic nature of the equations be restricted. Yet, something must be specified. The upstream inflow boundary is partly determined by specifying a boundary-layer inflow velocity profile shape, and partly develops as part of the solution. By velocity profile, we will mean values of the x-component of velocity suitably normalized, i.e., on the maximum inlet velocity.

The inflow stream function is determined by integration of the second-order Poiseuille flow boundary-layer solution for u. It should be noted that the boundary-layer equations do not correctly represent the flow at low R_e and we do not suggest that the input velocity profile used represents an accurate solution of the flat plate flow ahead of the base of the channel. It is merely a convenient one-parameter family of u velocity profiles by which one can study the effects of upstream velocity profile shape on the separated flow. It qualitatively represents a meaningful flow condition [I.1].

We could neglect the details of farther downstream flow continuation and still obtain realistic answers upstream. However, catastrophic instabilities may be propagated upstream from the outflow boundary and destroy the solution. The aim should be to allow the most free flow adjustment at the downstream continuation surface which still gives a solution. However, the safest method from the viewpoint of stability is to completely specify the outflow conditions (which is the approach taken in this thesis). For example, we will not assume that $\omega_{IX,j} = \omega_{I1,j}$, which is equivalent to stating that vorticity is merely advected out of the mesh region, assuming no viscous production of vorticity between (IX,j) and (I1,j). Hence, at the outlet of the channel, a fully developed velocity profile will be specified.

We will force separation at the sharp corner. As indicated in stream function plots contained in [V.3], the extrapolated separation point moves down from or below the sharp corner off the base. The incompressible numerical results show a regular movement of the separation point down the base as R_e is decreased, in agreement with the well known incompressible result at $R_e = 0$ for Stokes flow over a sphere, in which no separation occurs. For all the different methods of treating the sharp corner vorticity, separation was indicated below the sharp corner, including one method intended to bias the solution toward separation at the corner and two methods intended to force separation at the sharp corner. At $R_c = 100$, the numerical solution in [V.3] indicated separation occurring at somewhere less than one cell height below the sharp corner. This viscous effect was somewhat exaggerated because of the implicit artificial viscosity effect of the upwind differencing used in [V.3]. The location of separation will thus depend on the cell size, and can only be interpreted qualitatively at $R_c = 100$. On the other hand, at $R_c = 0.1$, the artificial viscosity effect is negligible, so the use of $R_c = 50$ in this thesis seems a reasonable compromise.

Failure to preserve conservation can lead to numerical instabilities. To stabilize the calculations while using methods that do not preserve these properties, artificial viscosity is often introduced, either explicitly or implicitly, by using dissipative finite-difference schemes, especially for high R_c flows. For low R_c flows it is possible that a non-conservative scheme can produce a stable solution without artificial viscosity, since the viscous terms are relatively large anyway and can quickly eliminate the error terms introduced. However, it is interesting to note that even though there are not enough cells between the sharp corner and true separation point to accurately resolve the distance, separation is still indicated experimentally between 2 or 3 cells below the corner. Hence, the phenomenon does not appear to be merely an abberation of the computational mesh [V.3]. Thus, it appears that the Stokes flow limit does give separation below the sharp corner. Also, the backward facing step geometry in [V.3] did not necessarily imply a flow configuration devoid of separation. This phenomenon is not investigated further in this thesis and could be a topic for further study. Instead, we will assume indicted separation occurring less than a cell spacing below the corner can be ignored, and the dividing streamline (DSL) can be faired into the assumed corner separation.

At the centre of the recirculatory region, or eye of the separation bubble, there is a strong flow reversal. Because of the conclusions established in Chapter II, this region of the flow field will not be investigated using the mathematical formulation in this thesis.

Finally, at a separation (or reattachment) point in a continuum flow, the vorticity is zero. That is, at the separation and reattachment point, there is a stress free velocity profile. Although the method is not used in this thesis, the reattachment point may be determined by locating the point at which $\omega=0$ along a wall. The present formulation provides a more convenient condition for locating the reattachment point, as will be discussed later.

5.2.2 Boundary Conditions in the Physical Domain

Consider steady Poiseuille flow given by the equation

$$\frac{d^2u}{dy^2} = \frac{1}{\mu}\frac{dp}{dx} = -C,\ v=0 \tag{5.2.2.1}$$

where C is a constant.

Integrating (5.2.2.1), we have

$$u = u(y) = -\frac{C}{2}y^2 + a_m y + b_m \tag{5.2.2.2}$$

where a_m and b_m ($m = 1$ or 2) are arbitrary constants of integration. Equation (5.2.2.2) will be applied at both the inlet ($m=1$) and the outlet ($m=2$).

At the inlet $x = 0$ we have $u = 0$ at $y = h$. Hence, (5.2.2.2) gives,

$$\frac{-C_1}{2} h^2 + a_1 h + b_1 = 0 \qquad (5.2.2.3a)$$

where $C_1 \equiv C$.

Also, $u = 0$ at $y = 1+h$, $x = 0$, which gives

$$\frac{-C_1}{2} (1+h)^2 + a_1(1+h) + b_1 = 0 \qquad (5.2.2.3b)$$

Solving (5.2.2.3a) and (5.2.2.3b) for a_1 and b_1 we get

$$a_1 = \frac{C_1}{2}(1+2h) \text{ and } b_1 = \frac{-C_1}{2}(1+h)h$$

Substituting the above into equation (5.2.2.2) we have

$$u = u_{inlet}(y) = \frac{-C_1}{2}\left[y^2 - (1+2h)y + (1+h)h\right] \qquad (5.2.2.4a)$$

At the outlet $x = x_{MAX}$ we have $u = 0$ at $y = 0$, which gives using (5.2.2.2),

$$b_2 = 0 \qquad (5.2.2.5a)$$

and $u = 0$ at $y = 1+h$, which gives

$$\frac{-C_2}{2}(1+h)^2 + a_2(1+h) = 0 \qquad (5.2.2.5b)$$

with $C \equiv C_2$.

Solving (5.2.2.5b) for a_2 we get

$$a_2 = \frac{C_2}{2}(1+h)$$

Substituting the above into equation (5.2.2.2) we have

$$u = u_{outlet}(y) = \frac{-C_2}{2}\left[y^2 - (1+h)y\right] \qquad (5.2.2.6a)$$

One way to choose C_1 is to require unit mass flux at the inlet. For example, we take

$$\psi(y = 1+h) - \psi(y=h) = 1 \text{ at the inlet} \qquad (5.2.2.7)$$

Using (5.2.2.4a) and the definition $u = \psi_y$ we get

$$\begin{aligned}\psi_{inlet}(y) &= \int_h^y u_{inlet}(y)\,dy \\ &= \frac{-C_1}{2}\left[\frac{y^3}{3} - \frac{1}{2}(1+2h)y^2 + (1+h)hy - \frac{h^3}{3} - \frac{h^2}{2}\right]\end{aligned} \qquad (5.2.2.8a)$$

With $\psi_{inlet}(y=h) = 0$ and choosing C_1 such that $\psi_{inlet}(y=1+h) = 1$ we can solve (5.2.2.7)

and (5.2.2.8a) for $\frac{C_1}{2} = 6$.

Then equations (5.2.2.4a) and (5.2.2.8a) become

$$u = u_{inlet}(y) = -6[y^2 - (1+2h)y + (1+h)h] \qquad (5.2.2.4b)$$

and

$$\psi = \psi_{inlet}(y) = -2y^3 + 3(1+2h)y^2 - 6(1+h)hy + (3+2h)h^2 \qquad (5.2.2.8b)$$

Similarly, by the conservation of mass, C_2 must be chosen to give unit mass flux at the outlet. That is, we take

$$\psi(y = 1+h) - \psi(y = 0) = 1 \text{ at the exit} \qquad (5.2.2.9)$$

From (5.2.2.6a), using definition $u = \psi_y$ we get

$$\psi_{outlet}(y) = \int_0^y u_{outlet} dy$$
$$= \frac{-C_2}{2}\left[\frac{y^3}{3} - (1+h)\frac{y^2}{2}\right] \qquad (5.2.2.10a)$$

With $\psi_{outlet}(y=0) = 0$ and choosing C_2 such that $\psi_{outlet}(y = 1+h) = 1$ we can solve (5.2.2.9) and (5.2.2.10a) for $\frac{C_2}{2} = \frac{6}{(1+h)^3}$.

Then equations (5.2.2.6a) and (5.2.2.10a) become

$$u = u_{outlet}(y) = \frac{-6}{(1+h)^3}\left[y^2-(1+h)y\right] \qquad (5.2.2.6b)$$

and

$$\psi = \psi_{outlet}(y) = -\frac{1}{(1+h)^3}\left[2y^3-3(1+h)y^2\right] \qquad (5.2.2.10b)$$

By definition $\omega = -\nabla^2\psi$. But $\psi = \psi(y)$ only at the inlet $x = 0$. Hence,

$$\omega = \omega_{inlet}(y) = -\psi_{yy} = -u_y$$
$$= 6\left[2y - (1+2h)\right] \qquad (5.2.2.11)$$

from either equation (5.2.2.4b) or (5.2.2.8b).

Similarly, $\psi = \psi(y)$ only at the outlet $x = x_{MAX}$.

Hence,
$$\omega = \omega_{outlet}(y) = -\psi_{yy} = -u_y$$
$$= \frac{6}{(1+h)^2}\left[2y-(1+h)\right] \qquad (5.2.2.12)$$

from either equation (5.2.2.6b) or (5.2.2.10b).

5.2.3 Boundary Conditions in the Computational Domain

Boundary conditions for y:

- Inlet boundary where $x = 0,\ 0 \le \psi \le \psi_{MAX} = 1$

From equation (5.2.2.8b) ψ is a cubic function of y given by

$\psi = -2y^3 + 3(1+2h)y^2 - 6h(1+h)y + (3+2h)h^2$

This can be solved explicitly for y as a function of ψ as per the method in Appendix J to give (for h = 0.4)

$$y = \cos(\theta + \frac{4}{3}\pi) + \frac{9}{10}$$

where

$$\theta = \frac{1}{3}\arccos(1 - 2\psi)$$

- Outlet boundary where $x = x_{MAX} = 6,\ 0 \le \psi \le \psi_{MAX} = 1$

From equation (5.2.2.10b), ψ is a cubic function of y given by

$$\psi = -\frac{1}{(1+h)^3}\left[2y^3 - 3(1+h)y^2\right]$$

This can be solved explicitly for y as a function of ψ as per the method in Appendix J to give (for h = 0.4)

$$y = \frac{7}{5}\cos(\theta + \frac{4}{3}\pi) + \frac{7}{10}$$

where

$$\theta = \frac{1}{3}\arccos(1-2\psi)$$

Alternatively, the downstream continuation problem could be treated in a manner following [V.3] where linear extrapolation for y is used which approximates $v_x = \left[\frac{y_x}{y_\psi}\right]_x = 0$ or $y_{xx} = 0$ since $\psi = \psi(y)$ (or $y = y(\psi)$) at the outlet $x = x_{MAX}$. This gives the difference equation

$$y_{IX,j} = 2y_{I1,j} - y_{I2,j}$$

- <u>Upper boundary lid where $\psi = \psi_{MAX} = 1,\ 0 \le x \le x_{MAX} = 6$</u>

  $y = 1+h = 1.4$

- <u>Lower boundary wall where $\psi = 0$ (j=1)</u>

$$y = \begin{cases} h = 0.4 & \text{for } 0 \le x \le x_{SEP} = 2 \\ 0 & \text{for } 2 + L_x = x_A \le x \le x_{MAX} = 6 \end{cases}$$

For $2 = x_{SEP} < x < x_A = 2 + L_x$ on the dividing streamline (DSL), see section (5.2.4) for an evaluation of $y = y_{i1}$.

<u>Boundary conditions for ω:</u>

- <u>Inlet boundary where $x = 0,\ 0 \le \psi \le \psi_{MAX} = 1$</u>

  From equation (5.2.2.11)

  $\omega = 6[2y - (1+2h)]$

- <u>Outlet boundary where $x = x_{MAX} = 6$, $0 \leq \psi \leq \psi_{MAX} = 1$</u>

From equation (5.2.2.12)

$$\omega = \frac{6}{(1+h)^2}\left[2y-(1+h)\right]$$

Alternatively, in a manner following [V.3] we could impose zero streamwise gradient for ω, namely $\omega_x = 0$, which has finite difference approximation

$$\omega_{IX,j} = \omega_{I1,j}$$

- <u>Upper boundary lid where $\psi = \psi_{MAX} = 1$ ($j = JX$), $0 \leq x \leq x_{MAX} = 6$</u>

In [V.3] the boundary condition at the upper boundary was reported as disappointing, resulting in destabilizing solutions. It was not possible to model the backstep with no upper boundary or in the free flight case (inflow through the mesh of the lid). The most nearly free condition in [V.3] was to use an impermeable slip wall at the lid.

Since $v = 0$ on $\psi = \psi_{MAX}$, the following condition for ω at the lid was used in [V.3], namely $\omega_{i,JX} = 0$, which implies $\frac{\partial u}{\partial y} = 0$ since

$$\omega = -\frac{\partial u}{\partial y} + \frac{\partial v}{\partial x} = -\frac{\partial u}{\partial y} = 0 \quad \text{(since } v = 0 \text{ for all } x \text{ along the lid).}$$

Because the wall in our case is assumed not to be impermeable, $\omega_{i,JX} = \omega_{i,J1}$ is a less restrictive condition, which approximately implies $\frac{\partial^2 u}{\partial y^2} = 0$ at the lid since

$$\frac{\partial \omega}{\partial y} = -\frac{\partial^2 u}{\partial y^2} + \frac{\partial^2 v}{\partial x \partial y} = -\frac{\partial^2 u}{\partial y^2} = 0 \quad \text{(since } v = v(y) \text{ only).}$$

- Lower boundary wall where $\psi = 0$ ($j = 1$)

From equation (2.4.5.7g)

$$\omega_{i1} \approx -\frac{1}{12\Delta\psi}\left(2q_{i4}^2 - 9q_{i3}^2 + 18q_{i2}^2\right)$$

for $0 \le x < x_{SEP} = 2$ and $2 + L_x = x_A < x \le x_{MAX} = 6$

$\omega = 0$ for $x = x_{SEP} = 2$ (modified to allow for the singularity) and $x = x_A = 2+L_x$

For $2 = x_{SEP} < x < x_A = 2 + L_x$ on the DSL we use equation (2.4.5.6a), namely

$$\omega = v_x - \frac{1}{2}q_\psi^2$$

which is approximated as follows:

$$\omega_{i1} \approx \frac{v_{i+1,1} - v_{i-1,1}}{2\Delta x} - \frac{1}{2}\,\frac{q_{i2}^2 - q_{i1}^2}{\Delta\psi}$$

where

$$v_{k1} \approx \frac{y_{k+1,1} - y_{k-1,1}}{2\Delta x} \cdot \frac{\Delta\psi}{y_{k2} - y_{k1}} \quad \text{for } k = i-1 \text{ and } i+1$$

From equation (2.4.3.1), the speed is approximated using

$$q_{i1}^2 \approx \frac{1 + \left[\dfrac{y_{i+1,1} - y_{i-1,1}}{2\Delta x}\right]^2}{\left[\dfrac{y_{i2} - y_{i1}}{\Delta\psi}\right]^2}$$

and

$$q_{i2}^2 \approx \frac{1 + \left[\dfrac{y_{i+1,2} - y_{i-1,2}}{2\Delta x}\right]^2}{\left[\dfrac{y_{i3} - y_{i1}}{2\Delta\psi}\right]^2}$$

Alternatively, from equation (2.4.5.7g), with $q_{i1}^2 \neq 0$, the second term in ω could be approximated by

$$\frac{1}{24\Delta\psi}\left(2q_{i4}^2 - 9q_{i3}^2 + 18q^{2a} - 11q_{i1}^2\right)$$

As discussed in [V.4], it is worth noting here that as R_e decreases (≤ 100) the reattachment point moves forward towards the base. Hence, the vorticity contour lines have a distinct similarity to streamlines indicating less dominance of advective transport. For example, the plots of various DSLs appear similar (they are virtually identical) to the dividing vorticity contours plotted in [V.3] for similar Reynolds numbers. Hence, for ease of computation we could take $\omega = 0$ on the DSL without creating any significant error for the Reynolds number under consideration.

5.2.4 Expression for $y = y_{i1}$ on the Lower Boundary

From the conservation of mass, considering the conduction of constant mass flux applied to the stream tube adjacent to the lower boundary, we obtain

$$\Delta\psi = \int_{y_{i1}}^{y_{i2}} u(x_i,y)\, dy \qquad (5.2.4.1)$$

where we take $y_{i2} > y_{i1}$.

Using the Trapezoidal Rule to approximate the integral in (5.2.4.1), we obtain

$$\Delta\psi \approx \frac{\Delta y}{2}(u_{i1}+u_{i2})$$

Hence, approximately, we have

$$\Delta\psi = \left[\frac{y_{i2}-y_{i1}}{2}\right]\left[\frac{1}{y_\psi}\Big|_{i1}+\frac{1}{y_\psi}\Big|_{i2}\right] \qquad (5.2.4.2)$$

where we have used $u = \dfrac{1}{y_\psi}$ from (2.3.5).

Approximating $y_\psi\,|_{i1}$ using a 2-point forward difference, $(\delta_\psi y)_{i1} = \dfrac{y_{i2}-y_{i1}}{\Delta\psi}$, and $y_\psi\,|_{i2}$ using a 2-point central difference, $(\delta_\psi y)_{i2} = \dfrac{y_{i3}-y_{i1}}{2\Delta\psi}$, and simplifying, we obtain from equation (5.2.4.2)

$$y_{i1} = 2y_{i2}-y_{i3} \qquad (5.2.4.3)$$

It should be noted that equation (5.2.4.3) is the 3-point central difference formula for $(\delta y_{\psi\psi})_{i2} = 0$ and is valid on the lower boundary $\psi = 0$ ($j = 1$) for all x, including the interval $2 = x_{SEP} < x < x_A = 2 + L_x$. It is, therefore, an equation for the dividing or separation streamline in the physical plane.

Having obtained y_{i1}, call these values $\bar{y}_{i1}^{(n+1)}$. A modified or relaxed value $y_{i1}^{(n+1)}$ can be obtained by using the relaxation factor β_y with the following expression:

$$y_{i1}^{(n+1)} = (1-\beta_y)\, y_{i1}^{(n)} + \beta_y\, \bar{y}_{i1}^{(n+1)} \qquad (5.2.4.4)$$

The reattachment point, where $x = x_A = 2 + L_x$, is determined from the value of i at which $y_{i1}^{(n+1)} = 0$. The reattachment length is $L_x = x_A - 2$. Note that $y_{i1}^{(n+1)} = 0.4$ at $x = x_{SEP} = 2$ and the initial guess for $y_{i1}^{(1)}$ (n=0), in order to begin the iteration procedure, was chosen to lie on an ellipse (see Appendix M).

5.2.5 Modification of Equation (5.2.4.3) for $y = y_{i1}$ on the Lower Boundary Dividing Streamline

Equation (5.2.4.3), namely,

$$y_{i1} = 2y_{i2} - y_{i3}$$

expresses the conservation of mass, approximately. Hence, it should hold for all i, in particular, at the inlet.

Since, at the inlet $\psi = \psi(y)$ only, we have

$$\Delta\psi = \frac{d\psi}{dy}\Delta y = u\Delta y \qquad (5.2.5.1a)$$

In the computational domain $\Delta\psi$ = constant as j increases from 1 to J1, but Δy is not constant. Define

$$\Delta y_j = y_{j+1} - y_j \qquad (5.2.5.2a)$$

where we have dropped the i index for convenience.

Rearranging equation (5.2.5.1a) we have

$$y_{j+1} = y_j + \Delta y_j, \quad j=1,2,\ldots,J1 \qquad (5.2.5.2b)$$

For variable Δy_j, we can rearrange equation (5.2.5.1a) as

$$\Delta y_j = \frac{\Delta\psi}{u_j} \tag{5.2.5.1b}$$

Now, as y_j increases (i.e., as j increases), we know u increases in the lower half of the channel. For example, from equation (5.2.2.11)

$$\frac{du}{dy} = -6\left[2y-(1+2h)\right] = 6-12(y-h) > 0$$

for $|y-h| < ½$, i.e., $h \leq y < h+½$.

Thus, as y_j increases, u_j increases and hence, Δy_j decreases from equation (5.2.5.1b). Therefore, up to the centre of the channel $j = j_c$, we have

$$\Delta y_1 > \Delta y_2 > \ldots. > \Delta y_{jc} \tag{5.2.5.3}$$

Now consider equation (5.2.4.3) at the inlet (dropping the i index), namely,

$$y_1 = 2y_2 - y_3 \tag{5.2.5.4}$$

From equation (5.2.5.2b) we have

$$\begin{aligned} y_1 &= h \\ y_2 &= y_1+\Delta y_1 \\ &= h+\Delta y_1 \\ y_3 &= y_2+\Delta y_2 \\ &= h+\Delta y_1+\Delta y_2 \end{aligned} \tag{5.2.5.5}$$

Substituting (5.2.5.5) into (5.2.5.4) we have

$$h = 2(h+\Delta y_1) - (h+\Delta y_1+\Delta y_2)$$

which leads to

$$\Delta y_1 = \Delta y_2$$

in contradiction to inequalities (5.2.5.3).

The same kind of analysis can be applied at the separation point $x = x_{SEP} = 2$. We would still expect that

$$\Delta y_1 > \Delta y_2 > \ldots \Delta y_{jc} \quad \text{at } x = x_{SEP} = 2$$

Then equation (5.2.5.4), namely

$$\begin{aligned} y_1 &= 2y_2 - y_3 \\ &= 2(h+\Delta y_1) - (h+\Delta y_1+\Delta y_2) \\ &= h + \Delta y_1 - \Delta y_2 \\ &> h \text{ since } \Delta y_1 > \Delta y_2 \end{aligned}$$

This means that equation (5.2.4.3), or as modified in (5.2.5.4), predicts that the dividing or separation streamline rises rather than falls just after the separation point $x=x_{SEP}=2$. Obviously, this is not physically realistic. The problem lies in the fact that constant $\Delta\psi$'s correspond to a widening of the streamtubes near the walls, where u is small, and a narrowing near the mid-stream. This is precisely the opposite of what we want to occur. To alleviate this problem, define a new variable η by

$$\eta = \eta(\psi) \tag{5.2.5.6}$$

such that

$$\psi = \psi_{inlet}(\eta) = -2\eta^3 + 3(1+2h)\eta^2 - 6(1+h)h\eta + (3+2h)h^2 \quad (5.2.5.7)$$

Equation (5.2.5.7) is equation (5.2.2.8b) with y replaced by η.

The new variable η will be used to replace ψ, that is, we perform the following change of independent variables:

(x,y)	$\mapsto$	(x,ψ)	$\mapsto$	(x,η)
physical domain		intermediate computational domain		final computational domain

The overall effect of this sequence of transformations is that we will have uniform spacing Δx and uniform spacing Δy only at inlet in the physical domain, uniform spacing Δx but variable spacing $\Delta\psi$ in the intermediate computational domain, and uniform spacing Δx and uniform spacing $\Delta\eta$, in the final computational domain. That is, the effect of uniform or constant spacing $\Delta\eta$ in the (x,η) plane is to give variable spacing $\Delta\psi$ in the (x,ψ) plane, whereas previously the spacing in the (x,ψ) plane was uniform or constant. Hence, we have effectively packed the grid near the walls.

On the lower boundary $(j=1)$ in the (x,η) plane we now have, for all i,

$$\eta_1 = h$$

and,

$$\eta_2 = \eta_1 + \Delta\eta = h+\Delta\eta \quad (5.2.5.8a)$$

where $\Delta\eta = \eta_2 - \eta_1$.

On the lower boundary $(j=1)$ in the (x,ψ) plane we have, for all i, $\psi_1 = 0$, and $\Delta\psi = \psi_2 - \psi_1$,

$$\text{so that } \psi_2 = \psi_1 + \Delta\psi = \Delta\psi \qquad (5.2.5.8b)$$

Again, from the conservation of mass, considering the condition of constant mass flux applied to the stream tube adjacent to the lower boundary, we obtain

$$\begin{aligned}
\Delta\psi &= \int_{y_u}^{y_n} u\,dy \\
&= \psi_2, \quad \text{from (5.2.5.8b)} \\
&= \psi(\eta_2) \\
&= \psi(h+\Delta\eta), \quad \text{from (5.2.5.8a)} \\
&= (3-2\Delta\eta)\,\Delta\eta^2, \quad \text{using equation (5.2.5.7)}
\end{aligned}$$

Using $u = \dfrac{1}{y_\psi}$ we have

$$y_\psi = \frac{\partial y}{\partial \psi} = \frac{d\eta}{d\psi}\frac{\partial y}{\partial \eta} = \frac{y_\eta}{\dfrac{d\psi}{d\eta}} = \frac{y_\eta}{\psi'(\eta)}$$

Hence, combining the above results,

$$\Delta\psi = \int_{y_u}^{y_n} u\,dy = \int_{y_u}^{y_n} \frac{1}{y_\psi}\,dy = \int_{y_u}^{y_n} \frac{\psi'(n)}{y_\eta}\,dy = (3-2\Delta\eta)\Delta\eta^2$$

Using the trapezoidal rule to approximate the above integral, we obtain

$$\left[\frac{y_{i2}-y_{i1}}{2}\right]\left[\frac{\psi'(\eta)}{y_\eta}\Big|_{i1}+\frac{\psi'(\eta)}{y_\eta}\Big|_{i2}\right] \approx (3-2\Delta\eta)\Delta\eta^2 \qquad (5.2.5.9)$$

From equation (5.2.5.7)

$$\psi' = \psi'(\eta) = -6\left[\eta^2-(1+2h)\eta+(1+h)h\right] \qquad (5.2.5.10)$$

so that $\psi'(\eta)\big|_{i1} = \psi'(\eta_1) = \psi'(h) = 0$.

Therefore, equation (5.2.5.9) reduces to

$$\left[\frac{y_{i2}-y_{i1}}{2}\right]\frac{\psi'(\eta)}{y_\eta}\Big|_{i2} \approx (3-2\Delta\eta)\Delta\eta^2 \qquad (5.2.5.11)$$

Now $\psi'(\eta)\big|_{i2} = \psi'(\eta_2) = \psi'(h+\Delta\eta)$

$= 6(1-\Delta\eta)\Delta\eta,$ from (5.2.5.10)

Approximating $y_\eta\big|_{i2}$ using a central difference (i.e., $\left(\delta_\eta y\right)_{i2} = \dfrac{y_{i3}-y_{i1}}{2\Delta\eta}$) and using the above expression for $\psi'(\eta)\big|_{i2}$, we obtain from (5.2.5.11)

$$y_{i1} = \frac{6(1-\Delta\eta)y_{i2} - (3-2\Delta\eta)y_{i3}}{3 - 4\Delta\eta} \qquad (5.2.5.12)$$

Note that if $\Delta\eta = 0$, equation (5.2.5.12) reduces to equation (5.2.4.3). Numerically, it is possible to find values of $\Delta\eta$ such that equation (5.2.5.12) predicts a decrease in $y = y_{i1}$ for $x \geq x_{SEP} = 2$, i.e., $y = y_{i1} < h$ for $x \geq x_{SEP} = 2$. Hence, the dividing or separation streamline falls rather than rises just after the separation point.

5.3 RESULTS AND DISCUSSION

5.3.1 Preliminaries

For the geometry and data depicted in Diagram (5.1.1), a stream function-vorticity method with equally spaced mesh sizes (=0.1) in both coordinate directions was used in [V.2]. After 328 iterations, the length of the recirculatory region was determined to be $L_x = 0.765$. Other results range from a low of $L_x = 0.580$ to a high of $L_x = 0.770$.

As noted in [V.4], a Reynolds number based on the expansion ratio $E = \frac{h}{H} = \frac{h}{1+h}$, or step height h, as a single parameter that defines the reattachment length in a laminar two-dimensional flow, is unlikely. The reattachment length in laminar two-dimensional BFS flows is probably not a function of a single variable, but more likely a function of several variables, including the expansion ratio and the inlet section Reynolds number R_e (based on the maximum inlet velocity and twice the inlet channel height or twice the hydraulic radius of the inlet or small channel 2(H-h)).

The relevant limits for the examination of the planar laminar BFS flow field are $E \to 0$ and $R_e \to 0$, for which $L_x \to 0$. Experimental evidence indicates that the flow field becomes three-dimensional and turbulent for sufficiently large values of E and R_e [V.4]. The best parametric fit for the range of expansion ratios and Reynolds numbers covered by data in [V.4] is given by a correlation of the form

$$\frac{L_x}{2(H-h)} = C_1 R_e^{C_2}\left(e^{C_3 E}-1\right) \tag{5.3.1}$$

where $C_1 = 0.004$, $C_2 = 0.75$ and $C_3 = 4.75$. Again, for the geometry depicted in Diagram (5.1.1), equation (5.3.1) with $E = \frac{h}{H} = \frac{0.4}{1.4}$ and $R_e = 50$ gives $L_x = 0.434$.

The above should give some indication in the variability of the results obtained for the length of the primary recirculating region.

5.3.2 Results

Results were obtained for equal-sized grid spacing in the x and η directions, i.e., $\Delta x = \Delta\eta = 0.1$. All results were obtained using an IBM PC-compatible/Intel 80286 (AT) computer.

The numerical results for the solution of the flow over a BFS in a channel or the flow through a channel containing a sudden expansion or corner are presented in the following table and figure.

Table (5.3.2.1) contains a listing of the various parameters used to obtain the results.

Figure (5.3.2.1) contains a plot of the streamlines y_{ij}, for $j = 1$, the lower boundary, (the upstream wall surface, dividing streamline and downstream wall surface) and $j = 2$ (first streamline) to $j = 10$ (upper surface) for $i = 1,2, \ldots, 60$.

Figure (5.3.2.2) contains a plot of the vorticity distribution ω_{ij} along the lower boundary (upstream and downstream walls and dividing streamline, i.e., $j = 1$), and the upper wall ($j = 10$), for $i = 1,2,\ldots,60$.

Using the original boundary conditions described in section 5.2.3 rather than the alternative ones from (V.3), after the 11th iteration, the dividing or separation streamline (DSL) crossed the x axis for the first time. After 363 iterations, the value of L_x fell between 0.75 to 0.80 ($x = 2.75$ to 2.80). Using the mid-value for L_x (0.755), this gave an error of 1.3% when compared to the results obtained in [V.2]. Similar (but not as accurate) results were obtained using various combinations of the alternative boundary conditions.

5.3.3 Discussion of Results

Difficulties were encountered in achieving global convergence. Although it did not seem to matter which combination of boundary conditions were used, as described in section (5.2.3), the vortex length or reattachment length L_x simply oscillated back and forth about the nominal value reported in the previous section, regardless of the number of iterations. As noted in [V.5] and [V.6] the use of smooth boundaries enabled the authors to remove the vorticity singularities at sharp corners at which the boundary slope is discontinuous. At the corners the vorticity is infinite. This was done by using either a boundary curve with a continuous slope or replacing the corner by a blunt stagnation point. The model with smooth boundaries gave the authors in [V.5] and [V.6] a more realistic representation of the physical flow being modelled. In our case, following this lead, the singularity in vorticity at the step $x=2$ was removed using a boundary curve with a continuous slope, and global convergence was achieved. Overall results for y_{i1} changed very little, probably because the stream function is not singular anywhere so an alternative method is only needed for deriving the vorticity at points where the difference equations employ values of ω at the singular points themselves as noted in [V.5].

As noted in [V.4], at a specified expansion ratio E, L_x grows in a moderately nonlinear manner as R_e increases. That is, in the laminar flow regime, the length of the flow development or reattachment downstream of the step increases with increasing Reynolds number; however, the increase is not linear. At a given or constant R_e, a monotonic increase (nearly exponentially) in L_x occurs with increasing E, because an increase in E causes an increase in the maximum velocity at the inflow or channel inlet. Both of the above effects are observed in our case when the parameters E and R_e are varied.

As noted in [V.4], the DSL appeared concave upwards near reattachment. This result is not observed in our case, where the results for y_{i1} simply decrease steadily for increasing x.

Reattachment occurs between one and two base heights downstream of the corner for the input velocity problem (second order) [V.3]. Although not attempted in this thesis, if the order of the input profile increases, reattachment occurs further downstream of the corner, i.e., for a fourth order profile, reattachment should occur between seven and eight base heights downstream.

Finally, it should be noted that following Chapter IV, when the formulas for ω_{i1} were removed, global convergence also resulted, indicating that there is possibly some instability created in the use of the formulas reported in equations (2.4.5.7a) through (2.4.5.8i). This problem with the approximations used for boundary vorticity values has been noted by several authors, for example, see [II.1].

5.3.4 Conclusions

Once the correct and accurate formulas are obtained for locating the position of the dividing streamline which bounds the recirculation zone, and the problem of singularity in vorticity at the corner of the BFS is removed, the numerical results are found to be almost exactly the same as the results presented in [V.2]. Problems with discontinuities in the flow geometry resulting in singularities in one of the flow parameters are to be avoided unless special care is taken to handle the difficulties that will arise.

CHAPTER VI

CONCLUSIONS

The work in this thesis was undertaken to investigate the feasibility, practicality and advisability of applying stream function coordinate methods in viscous flow problems. The natural curvilinear coordinate system (ϕ,ψ) introduced by Martin [I.2] and the use of von Mises coordinates (x,ψ) introduced by Barron [I.4] has been extended to the consideration of two-dimensional, steady, incompressible, laminar viscous flows.

In Chapter III, difficulties associated with a weakly separated region in the flow field are discussed. It has been shown, by considering the well-documented test problem of flow in a smoothly expanding channel, that the stream function coordinate method in its conventional form cannot accurately predict viscous flows if the flow has separated. The question arises, however, as to whether the difficulties are associated with the numerics or the physics. In particular, the failure to achieve an accurate converged solution could be due to the sensitivity of the vorticity transport equation solution and/or the choice of numerical approximation for the wall vorticity (numerics), or the presence of viscosity which leads to no-slip conditions on the solid walls (physics). Nevertheless, the conclusion can be drawn that flow separation leading to the development of a recirculating region must be handled carefully, or completely avoided if possible. It was further observed that the ratio of the grid spacing $\frac{\Delta x}{\Delta \psi}$ should not be too large, preferably as near as possible to one as the calculations will allow.

The study of an inviscid shear flow over an obstacle in Chapter IV indicates that the primary difficulty in applying von Mises coordinates is related to the viscosity and the recirculating flow region rather than the presence of vorticity in the flow.

In Chapter V, problems in which the flow configuration results in singularities in one of the flow parameters are discussed. The classical problem of flow over a backward facing step is considered. The stream function coordinate method is modified to account for flow separation and reattachment. A novel scheme is devised, based on conservation of mass flux, to accurately predict the location of the dividing streamline and its point of reattachment to the wall.

This thesis successfully demonstrates the application of the theory as developed in Chapter II and represented by equations (2.3.8c) and (2.3.7b). Stream function coordinate methods can be used for both attached and separated flows provided appropriate attention is paid to modelling the separation and recirculating region. The method cannot be used to study the recirculating flow itself. However, it does allow one to accurately identify the region of recirculation which can then be solved by conventional methods. The importance of the stream function coordinate method for viscous flows is that it allows efficient grid usage since the main part of the flow field can be predicted by this method. Numerical grid generation is only required in the relatively small recirculating regions which can be tightly gridded and accurately resolved using conventional formulations and methods.

REFERENCES

[I.1] Roache, P.J., Numerical Solutions of Compressible and Incompressible Laminar Separated Flows, Ph.D. Dissertation, Department of Aero-Space Engineering, University of Notre Dame, Notre Dame, Indiana, November, 1967.

[I.2] Martin, M.H., The Flow of a Viscous Fluid I, Archives of Rational Mechanics and Analysis, Vol. 41, pp. 266-286, 1971.

[I.3] Grossman, G.W. and Barron, R.M., A New Approach to the Solution of Navier-Stokes Equations, International Journal for Numerical Methods in Fluids, Vol. 7, pp. 1315-1324, 1987.

[I.4] Barron, R.M., Computation of Incompressible Potential Flow Using von Mises Coordinates, Mathematics and Computers in Simulation, Vol. 31, pp. 177-188, 1989.

[I.5] Barron, R.M. and Naeem, R.K., Numerical Solution of Transonic Flows on a Stream Function Coordinate System, International Journal for Numerical Methods in Fluids, Vol. 9, pp. 1183-1193, 1989.

[II.1] Gupta, M.M. and Manohar, R.P., Boundary Approximations and Accuracy in Viscous Flow Computations, Journal of Computational Physics, Volume 31, pp. 265-288, 1979.

[III.1] Roache, P.J., A Semidirect Method for Internal Flows in Flush Inlets, AIAA Paper 77-647, pp. 149-155, 1977.

[III.2] Roache, P.J., Scaling of High-Reynolds-Number Weakly Separated Channel Flows, Symposium on Numerical and Physical Aspects of Aerodynamic Flows, Springer-Verlag, pp. 87-98, 1982.

[III.3] Napolitano, M. and Orlandi, P., Laminar Flow in a Complex Geometry: A Comparison, International Journal For Numerical Methods in Fluids, Volume 5, pp. 667-683, 1985.

[III.4] Cliffe, K.A., Jackson, C.P. and Greenfield, A.C., Finite Element Solutions for Flows in a Symmetric Channel with a Smooth Expansion, U.K. Atomic Energy Authority (AERE), Theoretical Physics Division, Harwell, AERE-R-10608, 1982.

[III.5] Porter, J.D., Sykes, J. and Wilkes, N.S., Calculation of Fluid Flows Using Finite Differences and the Method of Co-ordinate Transformations, U.K. Atomic Energy Authority, (AERE), Engineering Sciences Division, Harwell, AERE-R-10760, 1983.

[III.6] Fletcher, C.A.J., Computational Techniques for Fluid Dynamics 1, Fundamental and General Techniques, Springer-Verlag, pp. 294-296, 1991.

[IV.1] Van Dyke, M., Perturbation Methods in Fluid Mechanics, The Parabolic Press, Stanford, California, pp. 9-13, 20, 98, 217, 1975.

[V.1] Armaly, B.F., Durst, F., Pereira, J.C.F. and Schonung, B., Experimental and Theoretical Investigation of Backward-Facing Step Flow, Journal of Fluid Mechanics, Vol. 127, pp. 473-496, 1983.

[V.2] Takemitsu, N., Finite Difference Method to Solve Incompressible Fluid Flow, Journal of Computational Physics, Vol. 61, pp. 499-518, 1985.

[V.3] Roache, P.J. and Mueller, T.J., Numerical Solutions of Laminar Separated Flows, AIAA Journal, Vol. 8, No. 3, pp. 530-538, 1970.

[V.4] Thangam, S. and Knight, D.D., A Computational Scheme on Generalized Coordinates For Viscous Incompressible Flows, Computers and Fluids, Vol. 18, No. 4, pp. 317-327, 1990.

[V.5] Bramley, J.S. and Dennis, S.C.R., The Numerical Solution of Two-Dimensional Flow in a Branching Channel, Computers and Fluids, Vol. 12, No. 4, pp. 339-355, 1984.

[V.6] Bramley, J.S. and Sloan, P.M., Numerical Solution for Two-Dimensional Flow in a Branching Channel Using Boundary-Fitted Coordinates, Computers and Fluids, Vol. 15, No. 3, pp. 297-311, 1987.

FIGURES

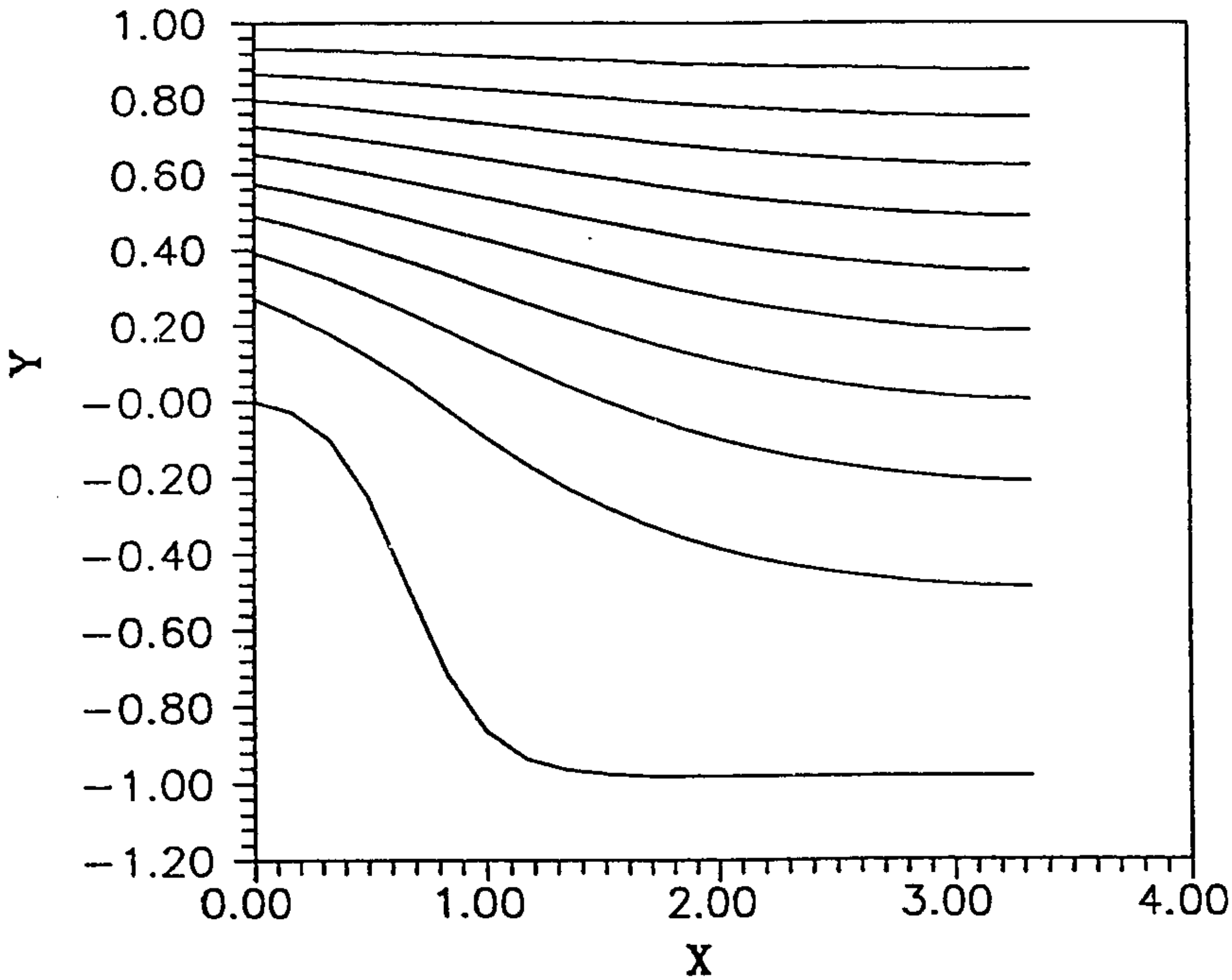

Figure (3.3.2.1) Streamlines With No Inlet Correction ($R_e = R_{ec} = 10$)

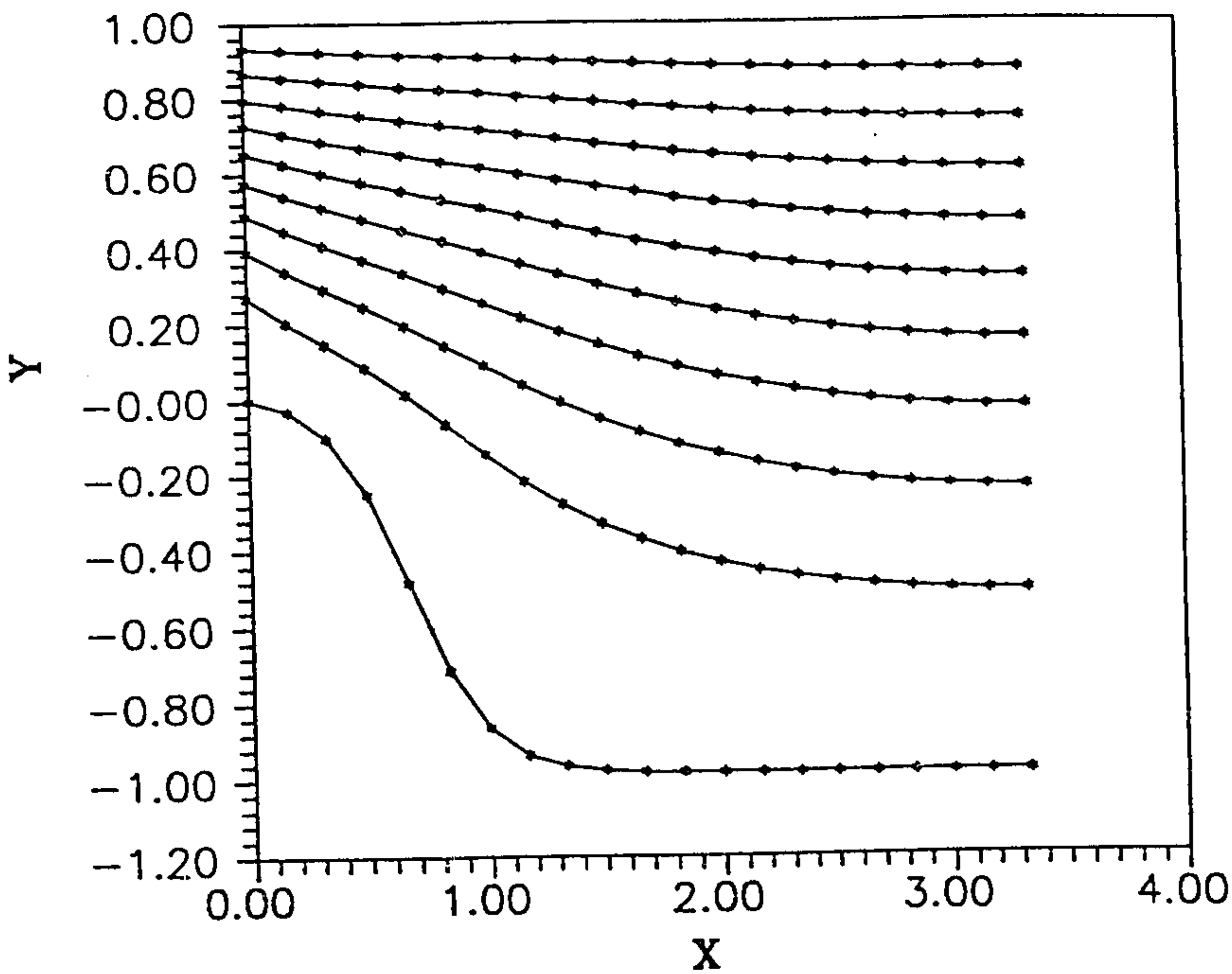

Figure (3.3.2.2) Streamlines With Inlet Correction ($R_e = R_{ec} = 10$)

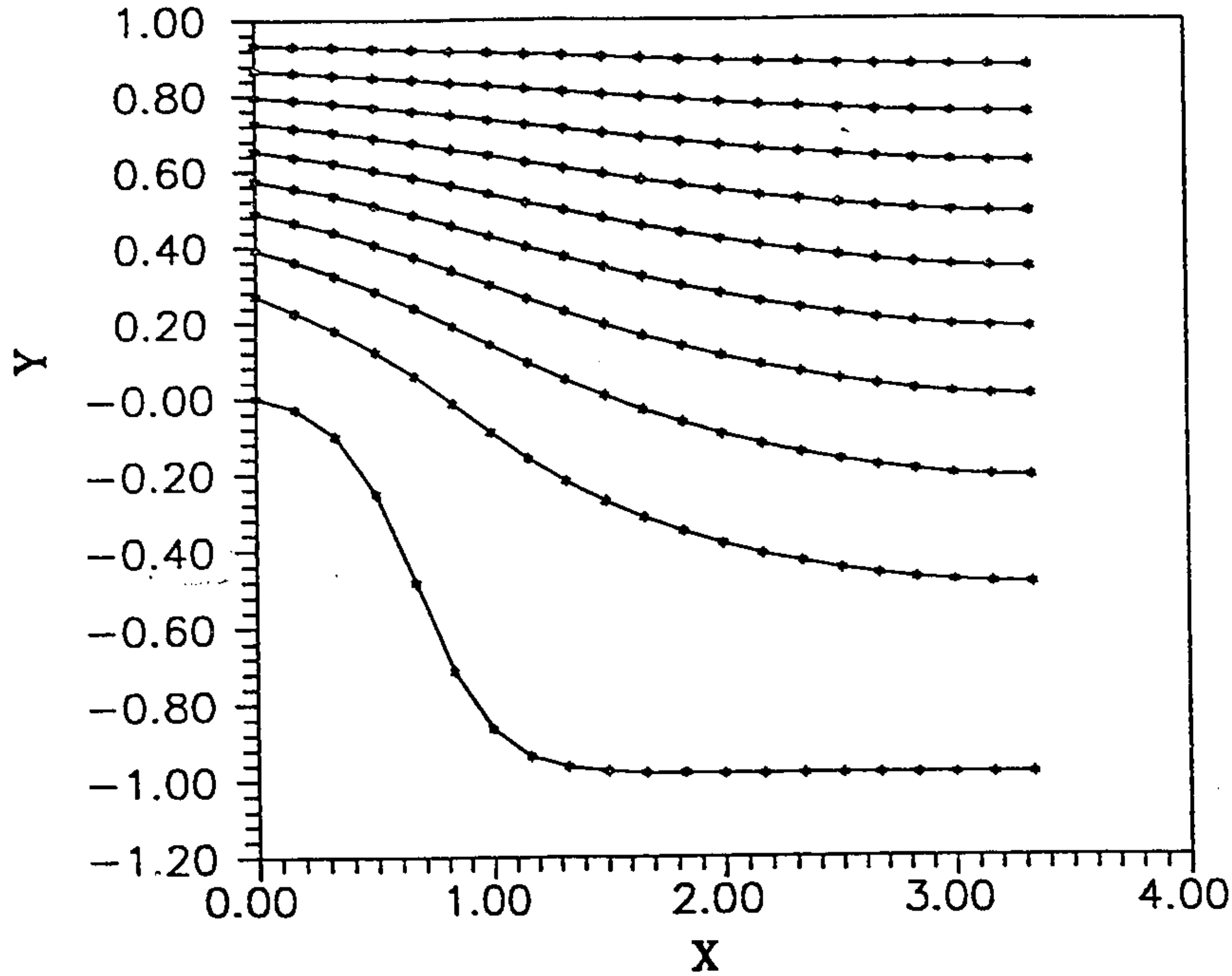

Figure (3.3.2.3) Streamlines With Boundary Condition Correction ($R_e = R_{\infty} = 10$)

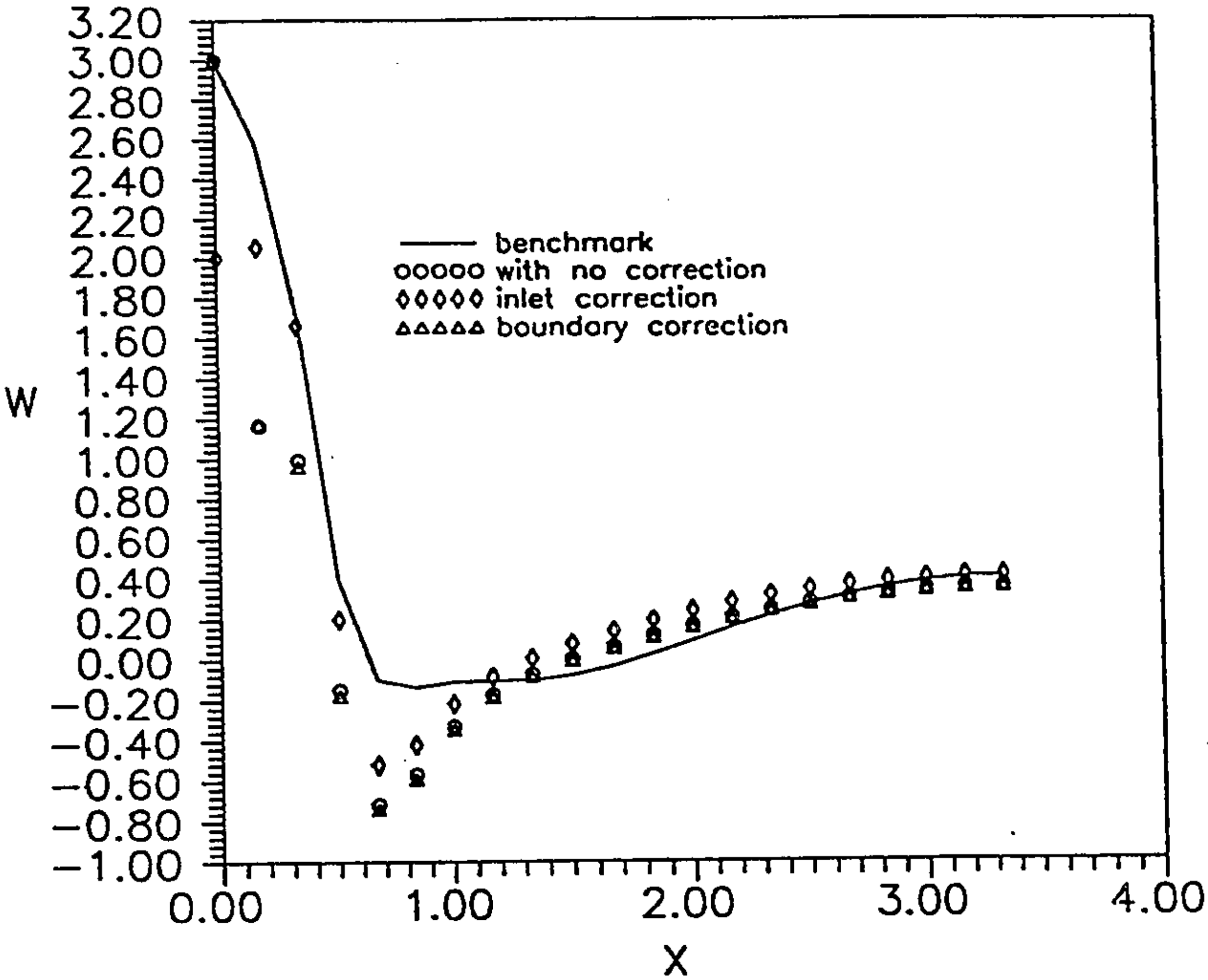

Figure (3.3.2.4) Wall Vorticity (R_e = R_∞ = 10)

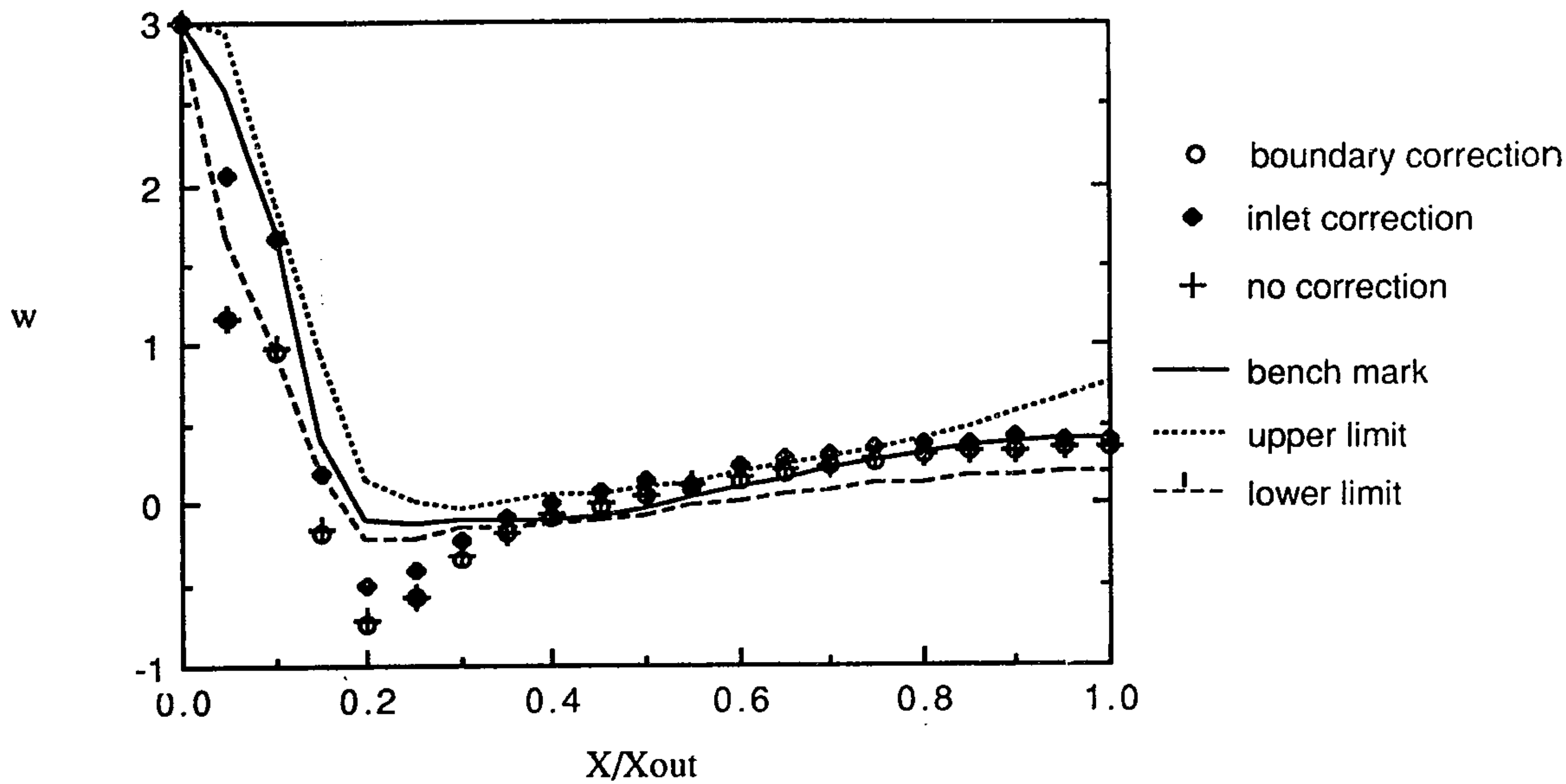

Figure (3.3.2.5) Worst Case Wall Vorticity Values in [III.3] vs. Results in Figure (3.3.2.4) ($R_\epsilon = R_{\epsilon c} = 10$)

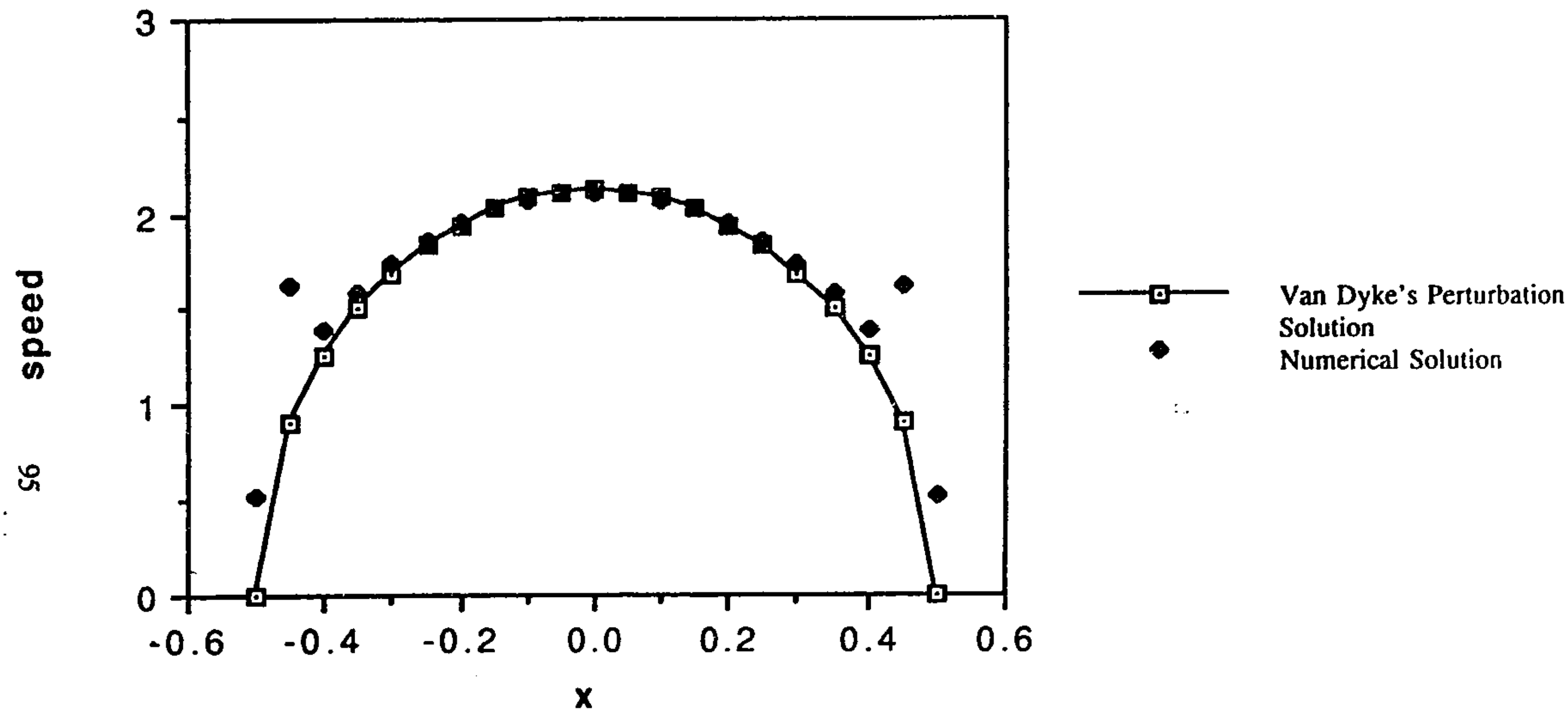

Figure (4.3.1.1) Speed on Surface of Circular Cylinder: Analytic Solution Using Equation (4.2.3.1) (Van Dyke's Perturbation Solution) vs. Numerical Solution

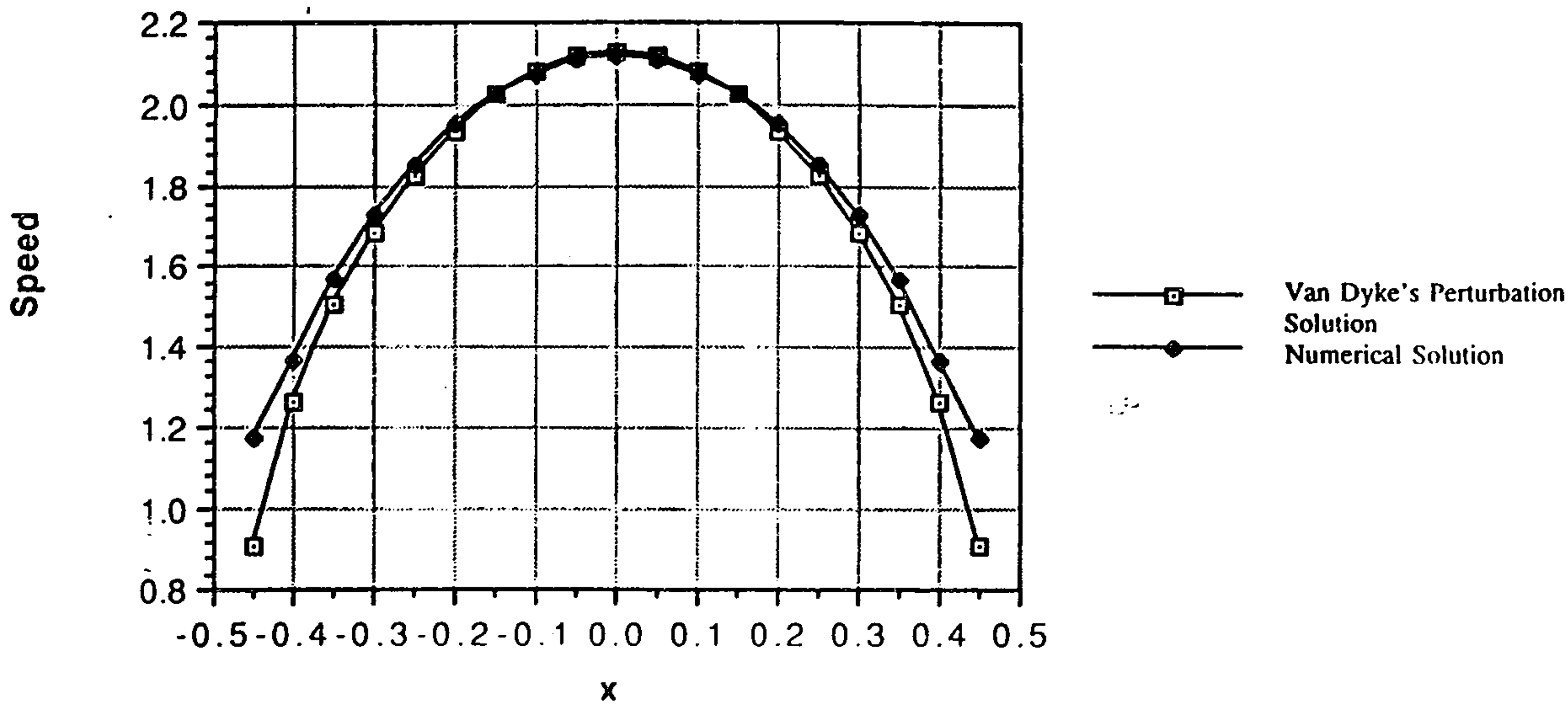

Figure (4.3.1.2) Speed on Surface of Circular Cylinder: Analytic Solution Using Equation (4.2.3.2) (Van Dyke's Perturbation Solution) vs. Numerical Solution

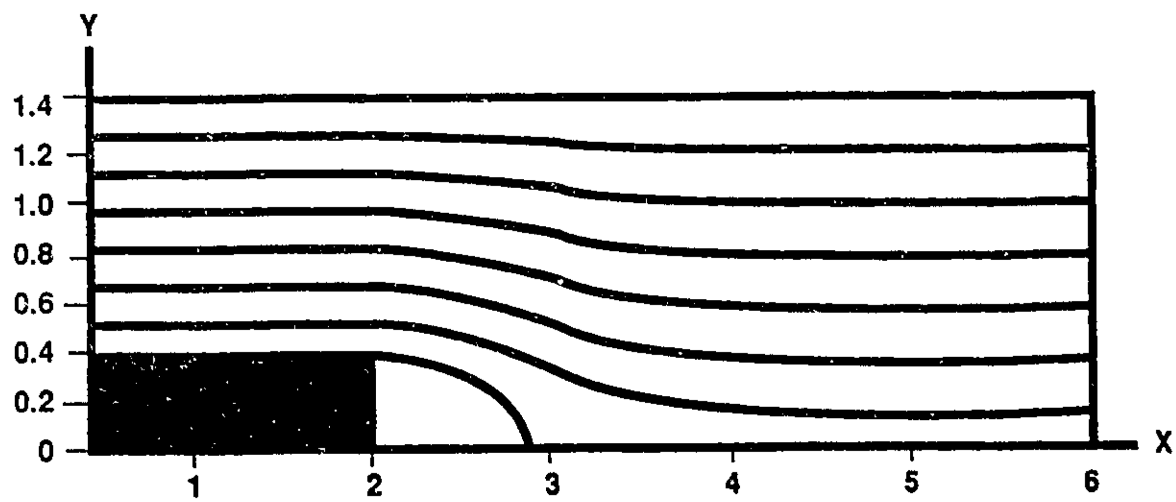

Figure (5.3.2.1)   Streamlines for BFS

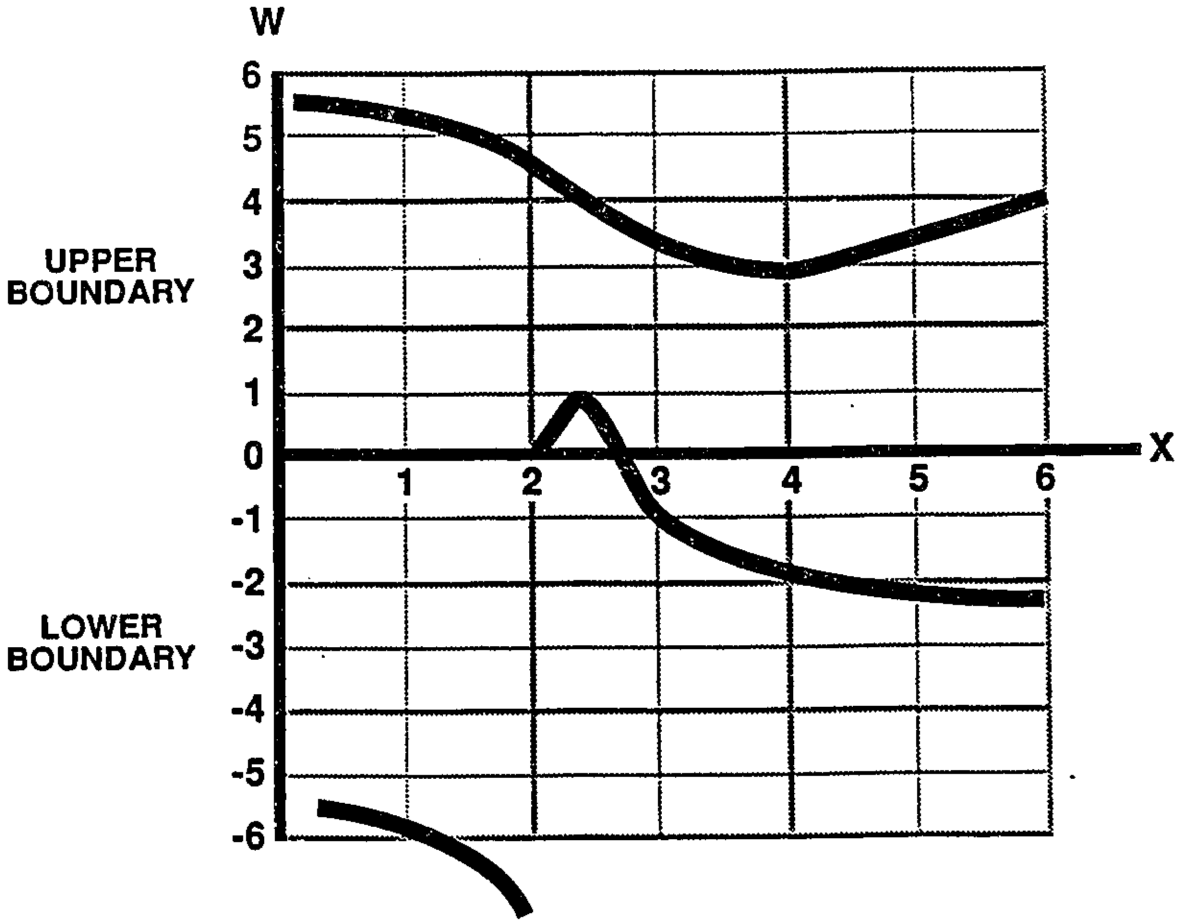

Figure (5.3.2.2) Vorticity Distribution for BFS

TABLES

Table (3.3.2.1) Parameters for $R_e = R_{ec} = 10$

Parameter	Value
$R_e = R_{ec}$	10
x_{MIN}	0.00
x_{MAX}	3.333
ψ_{MIN}	0.00
ψ_{MAX}	1.00
δ	0.40
β_y	1.80
β_ω	0.20
ε_y	1×10^{-4}
ε_ω	1×10^{-4}

Table (3.3.2.2) Vorticity with No Inlet Correction
($R_e = R_{ec} = 10$)

x	x/x_{out}	Vorticity ω_{i1CJG}	Vorticity ω_{i1}	Relative Error x 100%
0.000	0.00	3.000	3.000	0.000
0.167	0.05	2.575	1.164	0.548
0.333	0.10	1.706	0.990	0.419
0.500	0.15	0.399	-0.150	1.376
0.667	0.20	-0.100	-0.718	6.175
0.883	0.25	-0.135	-0.570	3.222
1.000	0.30	-0.108	-0.330	2.055
1.167	0.35	-0.106	-0.175	0.654
1.333	0.40	-0.103	-0.076	0.265
1.500	0.45	-0.079	-0.001	0.991
1.667	0.50	-0.033	0.062	2.876
1.833	0.55	0.027	0.117	3.325
2.000	0.60	0.092	0.166	0.800
2.167	0.65	0.157	0.209	0.331
2.333	0.70	0.217	0.247	0.139
2.500	0.75	0.272	0.280	0.030
2.667	0.80	0.319	0.308	0.035
2.833	0.85	0.357	0.330	0.077
3.000	0.90	0.385	0.345	0.103
3.167	0.95	0.402	0.355	0.117
3.333	1.00	0.408	0.358	0.122
AVERAGE PERCENTAGE ERROR				124.5%
NUMBER OF ITERATIONS				381

Table (3.3.2.3) Vorticity with Inlet Correction
($R_e = R_{cc} = 10$)

x	x/x_{out}	Vorticity ω_{i1CJG}	Vorticity ω_{i1}	Relative Error x 100%
0.000	0.00	3.000	3.000	0.000
0.167	0.05	2.575	2.055	0.202
0.333	0.10	1.706	1.661	0.027
0.500	0.15	0.399	0.200	0.498
0.667	0.20	-0.100	-0.520	4.195
0.833	0.25	-0.135	-0.420	2.107
1.000	0.30	-0.108	-0.217	1.011
1.167	0.35	-0.106	-0.086	0.190
1.333	0.40	-0.103	0.004	1.041
1.500	0.45	-0.079	0.077	1.973
1.667	0.50	-0.033	0.140	5.234
1.833	0.55	0.027	0.195	6.213
2.000	0.60	0.092	0.243	1.637
2.167	0.65	0.157	0.284	0.807
2.333	0.70	0.217	0.319	0.469
2.500	0.75	0.272	0.348	0.278
2.667	0.80	0.319	0.371	0.164
2.833	0.85	0.357	0.390	0.091
3.000	0.90	0.385	0.420	0.045
3.167	0.95	0.402	0.410	0.020
3.333	1.00	0.408	0.413	0.120
AVERAGE PERCENTAGE ERROR				138.5%
NUMBER OF ITERATIONS				365

Table (3.3.2.4) Vorticity with Boundary Condition Correction
($R_e = R_{ec} = 10$)

x	x/x_{out}	Vorticity ω_{i1CJG}	Vorticity ω_{i1}	Relative Error x 100%
0.000	0.00	3.000	3.000	0.000
0.167	0.05	2.575	1.175	0.544
0.333	0.10	1.706	0.962	0.436
0.500	0.15	0.399	-0.176	1.442
0.667	0.20	-0.100	-0.741	6.405
0.833	0.25	-0.135	-0.590	3.370
1.000	0.30	-0.108	-0.345	2.194
1.167	0.35	-0.106	-0.187	0.763
1.333	0.40	-0.103	-0.086	0.169
1.500	0.45	-0.079	-0.010	0.873
1.667	0.50	-0.033	0.053	2.600
1.833	0.55	0.027	0.108	2.991
2.000	0.60	0.092	0.157	0.703
2.167	0.65	0.157	0.200	0.276
2.333	0.70	0.217	0.239	0.101
2.500	0.75	0.272	0.272	0.001
2.667	0.80	0.319	0.300	0.059
2.833	0.85	0.357	0.322	0.097
3.000	0.90	0.385	0.338	0.121
3.167	0.95	0.402	0.348	0.134
3.333	1.00	0.408	0.352	0.138
AVERAGE PERCENTAGE ERROR				123.3%
NUMBER OF ITERATIONS				375

Table (3.3.2.5) Separation and Reattachment
($R_e = R_\alpha = 10$)

Method	Separation x	Error (%)	Reattachment x	Error (%)
CJG	0.634	Benchmark	1.759	Benchmark
No Inlet Correction	0.478	24.6	1.503	14.6
Inlet Correction	0.546	13.8	1.327	24.6
Boundary Condition Correction	0.474	25.2	1.527	13.2

Table (4.3.1.1) Parameters for $R_c = \infty$

Parameter	Value
R_c	∞
x_{MIN}	-5.0
x_{MAX}	5.0
ψ_{MIN}	0.0
ψ_{MAX}	2.5
δ	---
B_y	1.8
B_ω	---
ϵ_y	1×10^{-4}
ϵ_ω	---

Table (4.3.1.2) Speed on Surface of Circular Cylinder: Analytic Solution Using Equation (4.2.3.1) (Van Dyke's Perturbation Solution) vs. Numerical Solution

x	Analytic Results	Numerical Results	Relative Error (%)
0.00	2.127	2.117	0.47
±0.05	2.116	2.107	0.43
±0.10	2.082	2.077	0.24
±0.15	2.025	2.027	0.01
±0.20	1.942	1.956	0.72
±0.25	1.831	1.861	1.64
±0.30	1.687	1.737	2.96
±0.35	1.501	1.579	5.20
±0.40	1.257	1.393	10.8
±0.45	0.909	1.618	78.0
±0.50	0.000	0.526	∞
Number of Iterations			351

Table (4.3.1.3) Speed on Surface of Circular Cylinder: Analytic Solution Using Equation (4.2.3.2) (Van Dyke's Perturbation Solution) vs. Numerical Solution

x	Analytic Results	Numerical Results	Relative Error (%)
0.00	2.127	2.117	0.47
±0.05	2.116	2.107	0.43
±0.10	2.082	2.077	0.24
±0.15	2.025	2.027	0.01
±0.20	1.942	1.954	0.62
±0.25	1.831	1.857	1.42
±0.30	1.687	1.730	2.55
±0.35	1.501	1.564	4.20
±0.40	1.257	1.356	7.87
±0.45	0.909	1.174	29.2
±0.50	0.000	0.082	∞
Number of Iterations			341

Table (5.3.2.1) Parameters for $R_e = 50$

Parameter	Value
R_e	50
x_{MIN}	0.0
x_{MAX}	6.0
ψ_{MIN}	0.00
ψ_{MAX}	1.00
δ	0.40
β_y	1.80
β_ω	0.20
ε_y	1×10^{-3}
ε_ω	1×10^{-2}
$\Delta\eta$	0.17-0.18

DIAGRAMS

Diagram (2.1.1) (ϕ,ψ) Coordinate System

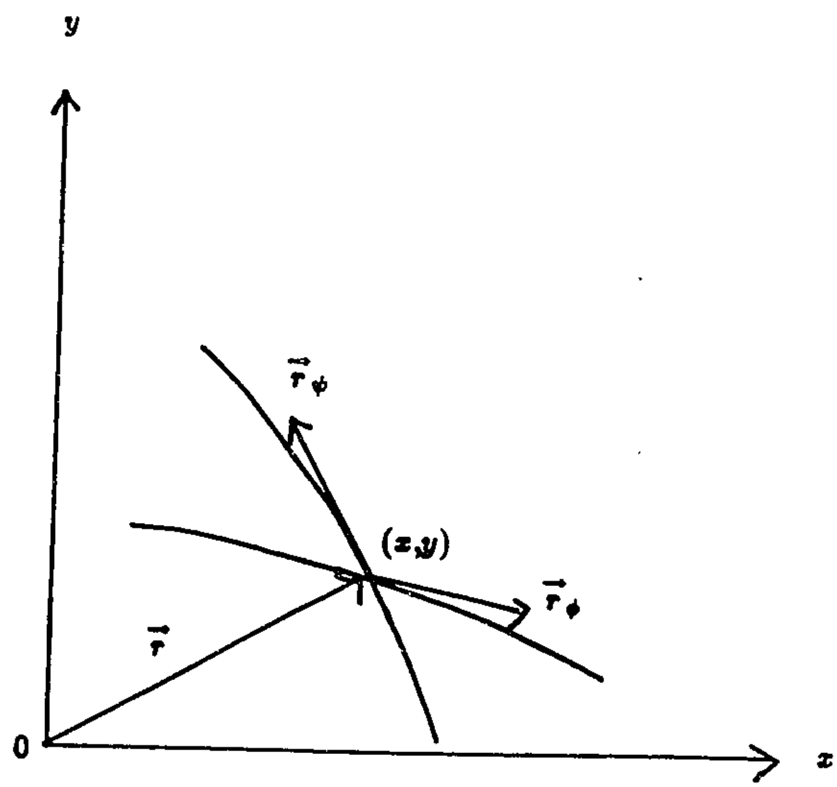

Diagram (3.1.1) Physical Domain

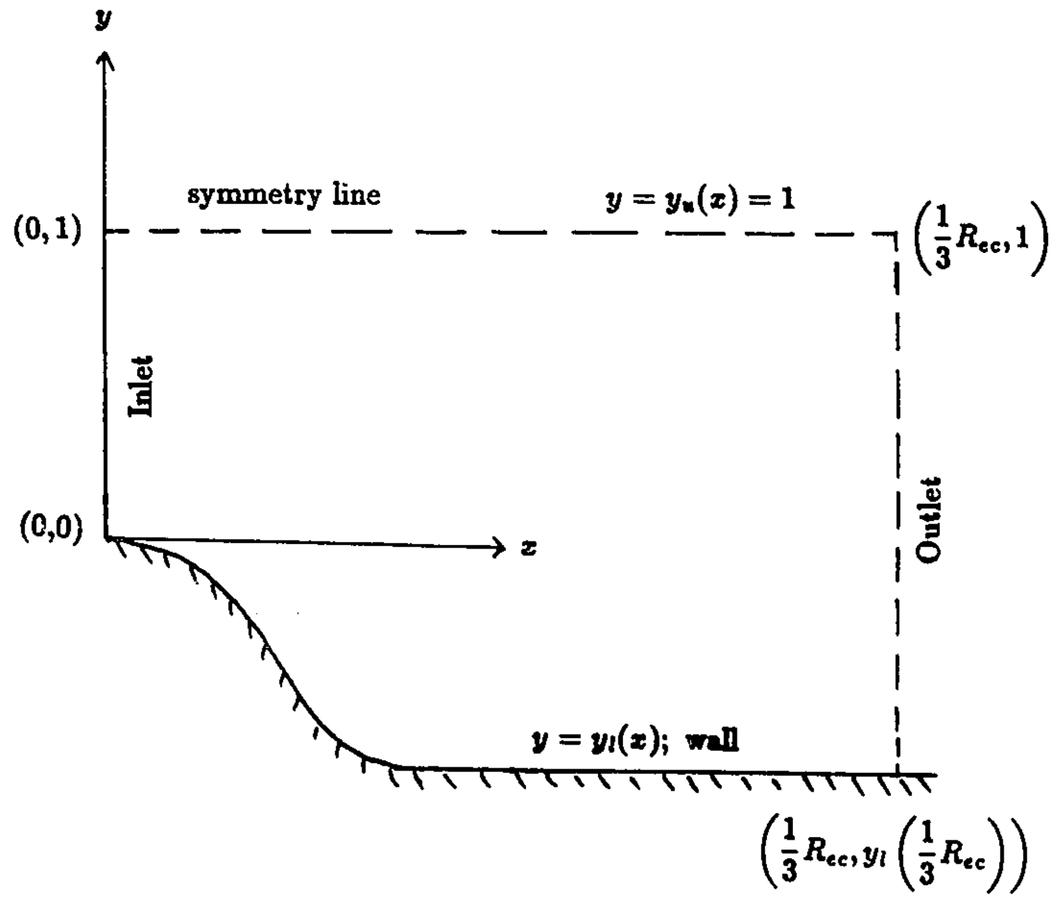

Diagram (3.1.2) Computational Domain

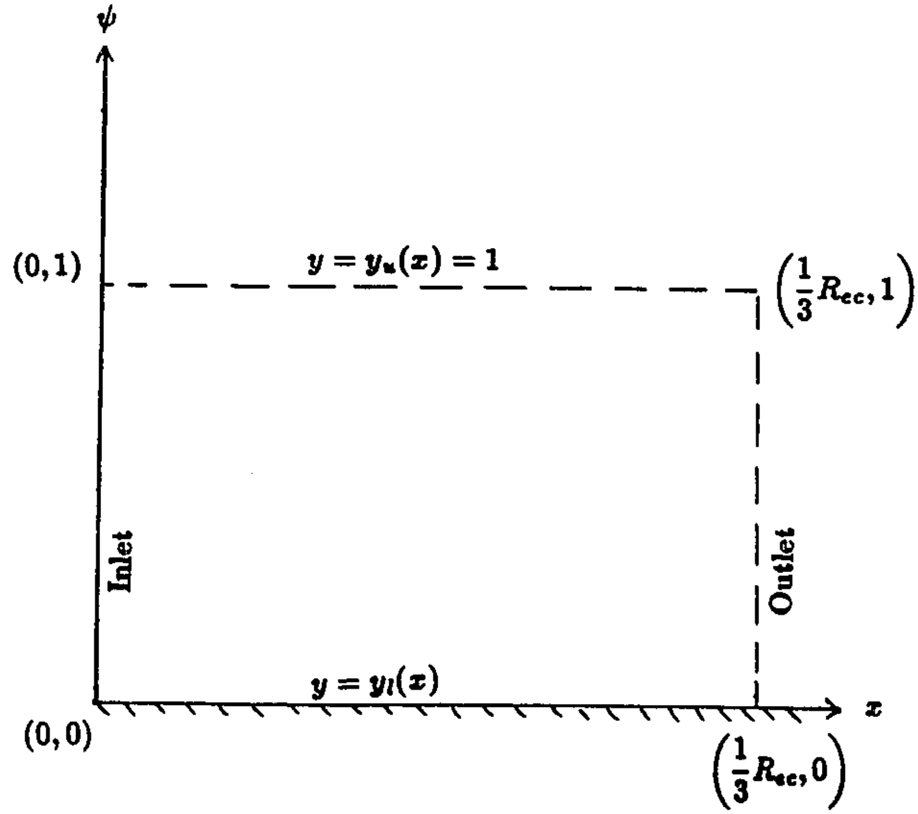

Diagram (L1) Slight Shear Flow Past a Circular Cylinder

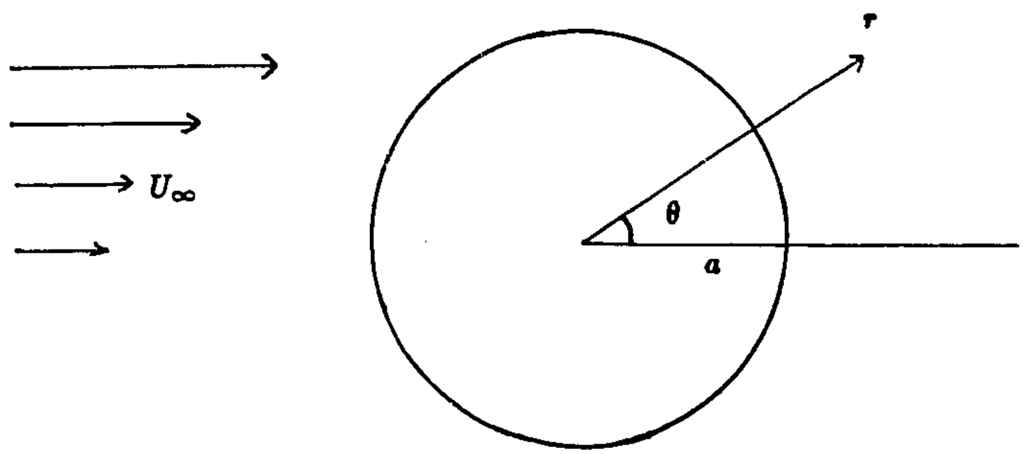

Diagram (4.2.3.1) Computational Domain

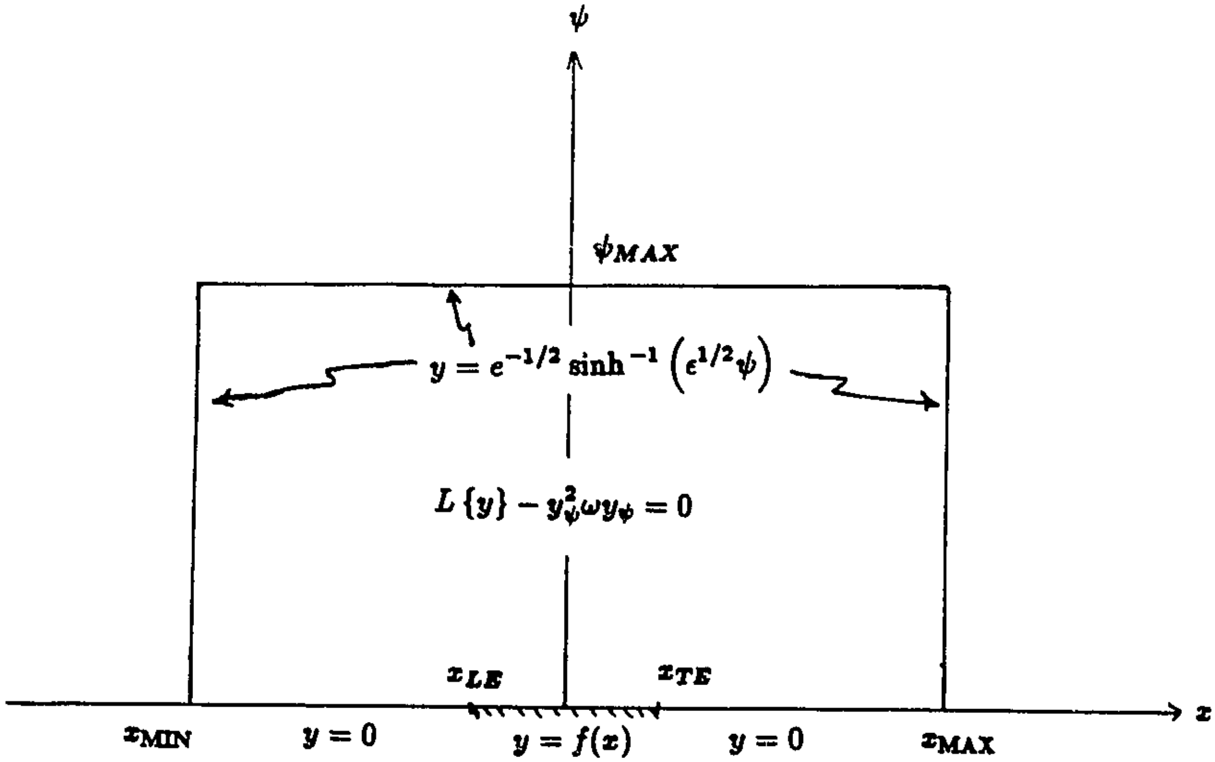

For a circular cylinder of radius $r = a = \frac{1}{2}$ $\quad y = f(x) = \sqrt{0.25 - x^2}$

Diagram (5.1.1) Physical Domain

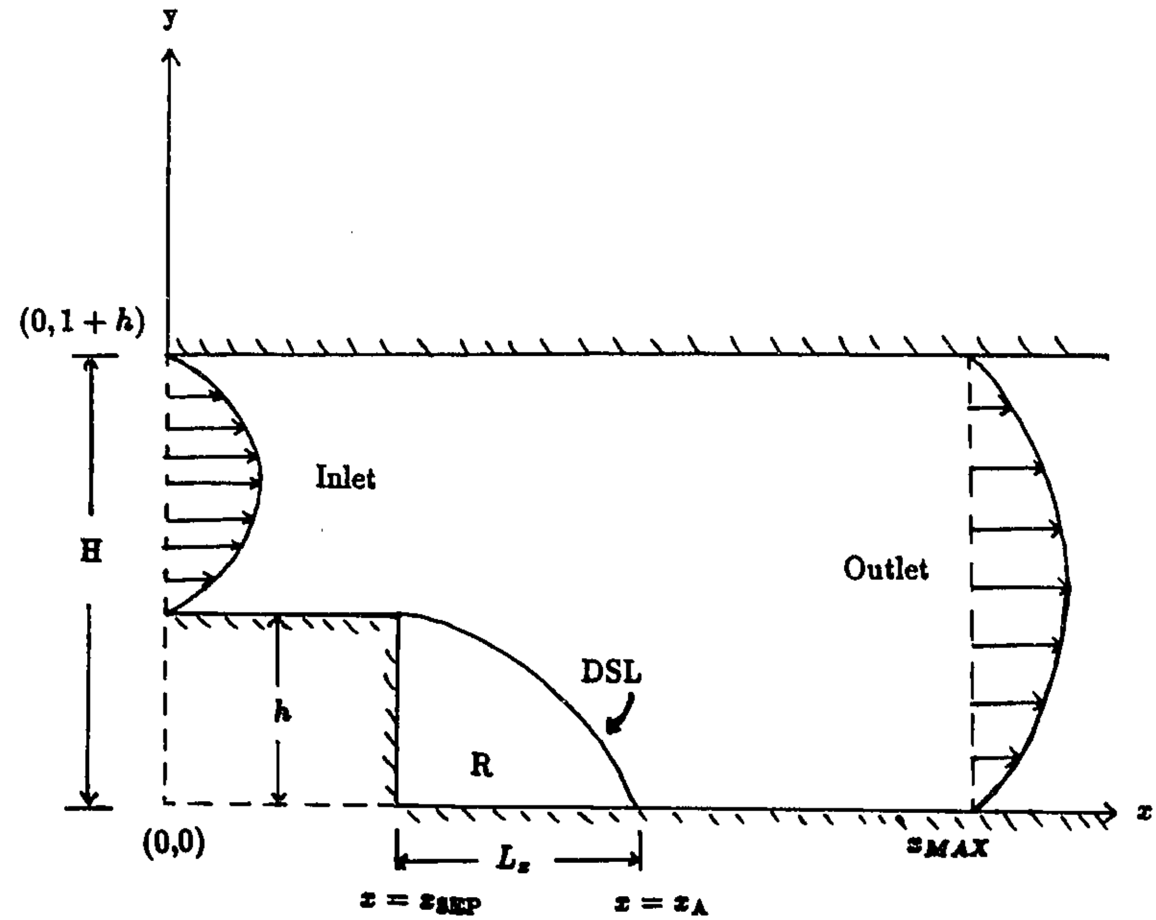

R = recirculating region

Length of channel = 6

Height of channel = H = 1+h = 1.4

Backward Facing Step (BFS) located at x = 2

Height of BFS h = 0.4

Length of R vortex length or reattachment length = L_x

Reynolds number R_e = 50

Expansion ratio $E = \frac{h}{H} = \frac{h}{1+h}$

Inlet: u = equation (5.2.2.4b)

v = 0

Outlet: u = equation (5.2.2.6b)

v = 0

Diagram (5.1.2) Computational Domain

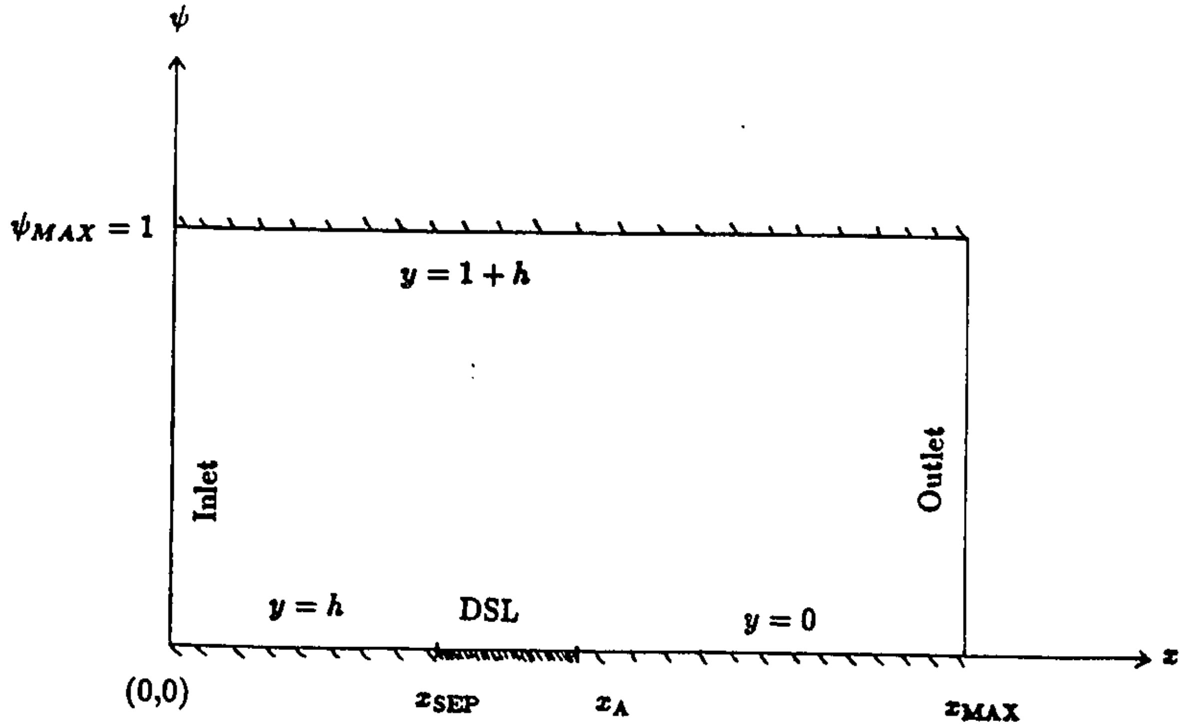

Inlet

y = y(ψ) = equation (5.2.2.8b)

Outlet

y = y(ψ) = equation (5.2.2.10b)

APPENDICES

APPENDIX A

Presentation of equations (2.2.2c) and (2.2.3b) using equation (2.2.6) in an alternate form

From equations (2.2.2c)

$$h_{xy} - (v\omega)_y = -\frac{1}{R_e}\omega_{yy}$$

$$h_{yx} + (u\omega)_x = \frac{1}{R_e}\omega_{xx}$$

Subtracting, we get

$$\frac{1}{R_e}\nabla^2\omega = (u\omega)_x + (v\omega)_y$$

$$= (u_x + v_y)\omega + u\omega_x + v\omega_y$$

$$= u\omega_x + v\omega_y \qquad \text{using (2.2.1b)}$$

Hence, using (2.2.6), $\nabla^2\omega + R_e(\psi_x\omega_y - \psi_y\omega_x) = 0$.

From equation (2.2.3b), using (2.2.6) again, we get

$$\omega = -\nabla^2\psi \tag{A1}$$

APPENDIX B

Derivation of equations (2.2.2e) from (2.2.2d)

Equations (2.2.2d) are

$$Gh_\phi - F(h_\psi + \omega) = -\frac{1}{R_e} J\omega_\psi \tag{B1}$$

$$-Fh_\phi + E(h_\psi + \omega) = -\frac{1}{R_e} J\omega_\phi \tag{B2}$$

Dividing (B1) by G, (B2) by F, and adding gives

$$(h_\psi + \omega)\left[\frac{F}{G} - \frac{E}{F}\right] - \frac{1}{R_e}\frac{J}{G}\omega_\psi + \frac{1}{R_e}\frac{J}{F}\omega_\phi = 0 \tag{B3}$$

But $\frac{F}{G} - \frac{E}{F} = \frac{-J^2}{FG}$. Dividing (B3) by this quantity, and noting that

$$\left[\frac{-J}{G}\right]\left[-\frac{FG}{J^2}\right] = \frac{F}{J}$$

$$\left[\frac{J}{F}\right]\left[-\frac{FG}{J^2}\right] = \frac{-G}{J}$$

we get

$$h_\psi = -\omega + \frac{1}{R_e}\frac{G}{J}\omega_\phi - \frac{1}{R_e}\frac{F}{J}\omega_\psi \tag{B4}$$

From (B1) and (B4)

$$h_\phi = \frac{1}{R_e}\frac{F}{J}\omega_\phi - \frac{1}{R_e}\left[\frac{F^2}{GJ} + \frac{J}{G}\right]\omega_\psi$$

Using

$$\frac{F^2}{GJ} + \frac{J}{G} = \frac{F^2 + EG - F^2}{GJ} = \frac{E}{J}$$

yields

$$h_\phi = \frac{1}{R_e}\frac{F}{J}\omega_\phi - \frac{1}{R_e}\frac{E}{J}\omega_\psi$$

APPENDIX C

Demonstration that Gauss' equation (2.2.7) is automatically satisfied

We have, from (2.2.7),

$$\left[\frac{J}{E}\Gamma^2_{11}\right]_{\psi} - \left[\frac{J}{E}\Gamma^2_{12}\right]_{x} = 0 \tag{C1}$$

By definition,

$$\Gamma^2_{11} = \frac{-FE_x + 2EF_x - EE_{\psi}}{2J^2}$$

$$= \frac{-y_x y_{\psi} 2y_x y_{xx} + 2(1+y_x^2)(y_x y_{\psi x} + y_{\psi} y_{xx}) - (1+y_x^2)2y_x y_{x\psi}}{2y_{\psi}^2}$$

$$= \frac{y_{xx}}{y_{\psi}}$$

if we assume that $y_{x\psi} = y_{\psi x}$.

Hence,

$$\frac{J}{E}\Gamma^2_{11} = \frac{y_{\psi}}{1+y_x^2}\frac{y_{xx}}{y_{\psi}} = \frac{y_{xx}}{1+y_x^2}$$

Also, by definition,

$$\Gamma^2_{12} = \frac{EG_x - FE_{\psi}}{2J^2}$$

$$= \frac{(1+y_x^2)2y_{\psi} y_{\psi x} - y_x y_{\psi} 2y_x y_{x\psi}}{2y_{\psi}^2}$$

$$= \frac{y_{\psi x}}{y_{\psi}}$$

Hence,

$$\frac{J}{E}\Gamma_{12}^2 = \frac{y_\psi}{1+y_x^2}\,\frac{y_{\psi x}}{y_\psi} = \frac{y_{\psi x}}{1+y_x^2}$$

Substituting into the left-hand side of equation (C1) gives

$$\left[\frac{J}{E}\Gamma_{11}^2\right]_\psi - \left[\frac{J}{E}\Gamma_{12}^2\right]_x = \left[\frac{y_{xx}}{1+y_x^2}\right]_\psi - \left[\frac{y_{\psi x}}{1+y_x^2}\right]_x$$

$$= \frac{(1+y_x^2)y_{xx\psi} - 2y_x y_{xx} y_{x\psi} - (1+y_x^2)y_{\psi xx} + 2y_x y_{xx} y_{x\psi}}{(1+y_x^2)^2}$$

$$= 0$$

if we assume that $y_{x\psi} = y_{\psi x}$ and $y_{xx\psi} = y_{\psi xx}$ for all (x,ψ).

APPENDIX D

Derivation of equation (2.3.7b) from equations (2.3.7a)

From the first equation of (2.3.7a), differentiating with respect to ψ,

$$R_e h_{x\psi} = y_x \omega_{x\psi} + y_{x\psi}\omega_x - \frac{(1+y_x^2)}{y_\psi}\omega_{\psi\psi} - \frac{2y_x y_{x\psi}\omega_\psi}{y_\psi}$$

$$+ \frac{(1+y_x^2)}{y_\psi^2} y_{\psi\psi}\omega_\psi \tag{D1}$$

From the second equation of (2.3.7a), differentiating with respect to x,

$$R_e h_{\psi x} = -R_e \omega_x + y_\psi \omega_{xx} + y_{\psi x}\omega_x - y_x \omega_{\psi x} - y_{xx}\omega_\psi \tag{D2}$$

Equating (D1) and (D2) and reordering, we get

$$y_\psi^2 \omega_{xx} - 2y_x y_\psi \omega_{x\psi} + (1+y_x^2)\omega_{\psi\psi} - R_e y_\psi \omega_x$$

$$+ 2y_x y_{x\psi}\omega_\psi - \frac{(1+y_x^2)}{y_\psi} y_{\psi\psi}\omega_\psi - y_{xx} y_\psi \omega_\psi = 0 \tag{D3}$$

Now, from (2.3.7b), writing the equation out in full

$$y_\psi^2 \omega_{xx} - 2y_x y_\psi \omega_{x\psi} + (1+y_x^2)\omega_{xx} - R_e y_\psi \omega_x - y_\psi^2 \omega\omega_\psi = 0 \tag{D4}$$

(D3) and (D4) will be the same equation if we can show that

$$-y_\psi^2 \omega\omega_\psi = 2y_x y_{x\psi}\omega_\psi - \frac{(1+y_x^2)}{y_\psi} y_{\psi\psi}\omega_\psi - y_{xx} y_\psi \omega_\psi$$

$$\text{RHS} = \frac{2y_x y_\psi y_{x\psi}\omega_\psi - (1+y_x^2)y_{\psi\psi}\omega_\psi - y_{xx}y_\psi^2\omega_\psi}{y_\psi}$$

$$= \frac{-[y_\psi^2 y_{xx} - 2y_x y_\psi y_{x\psi} + (1+y_x^2)y_{\psi\psi}]\omega_\psi}{y_\psi}$$

$$= \frac{-L\{y\}\omega_\psi}{y_\psi} \quad \text{from definition of operator L}$$

$$= \frac{-y_\psi^3\omega\omega_\psi}{y_\psi} \quad \text{using (2.3.8c)}$$

$$= -y_\psi^2\omega\omega_\psi$$

$$= \text{LHS}$$

APPENDIX E

Derivation of the equation for energy $h = h(x,\psi)$, and hence pressure $p = p(x,\psi)$, from equations (2.3.7a)

From definition of the operator L,

$$L\{h\} = y_\psi^2 h_{xx} - 2y_x y_\psi h_{x\psi} + \left(1+y_x^2\right)h_{\psi\psi}$$

$$- \frac{y_\psi^2}{R_e}\left[y_x\omega_{xx}+y_{xx}\omega_x-\left\{\frac{y_\psi\left[(1+y_x^2)\omega_{x\psi}+2y_xy_{xx}\omega_\psi\right] - (1+y_x^2)\omega_\psi y_{x\psi}}{y_\psi^2}\right\}\right]$$

$$- \frac{2y_xy_\psi}{R_e}\left[y_x\omega_{x\psi}+y_{x\psi}\omega_x-\left\{\frac{y_\psi\left[(1+y_x^2)\omega_{\psi\psi}+2y_xy_{x\psi}\omega_\psi\right]-(1+y_x^2)\omega_\psi y_{\psi\psi}}{y_\psi^2}\right\}\right]$$

$$+(1+y_x^2)\left[-\omega_\psi+\frac{1}{R_e}\{y_\psi\omega_{x\psi}+y_{\psi\psi}\omega_x-y_x\omega_{\psi\psi}-y_{x\psi}\omega_\psi\}\right]$$

$$= \omega_x\left[\frac{y_{xx}y_\psi^2}{R_e}-\frac{2y_xy_{x\psi}}{R_e}y_\psi+\frac{(1+y_x^2)}{R_e}y_{\psi\psi}\right]$$

$$+ \omega_\psi\left[\frac{-y_\psi^2}{R_e}\frac{1}{y_\psi}2y_xy_{xx}+\frac{y_\psi^2}{R_e}\frac{(1+y_x^2)}{y_\psi^2}\,y_{x\psi}+\frac{2y_xy_\psi}{R_e}\frac{1}{y_\psi}2y_xy_{x\psi}\right.$$

$$\left.-\frac{2y_xy_\psi}{R_e}\frac{(1+y_x^2)}{y_\psi^2}y_{\psi\psi}-(1+y_x^2)-\frac{(1+y_x^2)}{R_e}y_{x\psi}\right]$$

$$+ \; y_x \left[\frac{y_\psi^2}{R_e}\omega_{xx} - \frac{2y_x y_\psi}{R_e}\omega_{x\psi} - \frac{(1+y_x^2)}{R_e}\omega_{\psi\psi} \right]$$

$$+ \; y_\psi \left[\frac{-y_\psi^2}{R_e}\frac{1}{y_\psi^2}(1+y_x^2)\omega_{x\psi} + \frac{2y_x y_\psi}{R_e}\frac{1}{y_\psi^2}(1+y_x^2)\omega_{\psi\psi} \; + \; \frac{(1+y_x^2)}{R_e}\omega_{x\psi} \right]$$

$$- \; \frac{\omega_x}{R_e}\left[y_\psi^2 y_{xx} - 2y_x y_\psi y_{x\psi} + (1+y_x^2)y_{\psi\psi}\right]$$

$$+ \; \omega_\psi \left[-(1+y_x^2) + \frac{1}{R_e}\left\{ -2y_x y_\psi y_{xx} + 4y_x^2 y_{x\psi} - \frac{2y_x}{y_\psi}(1+y_x^2)y_{\psi\psi} \right\} \right]$$

$$+ \; \frac{y_x}{R_e}\left[y_\psi^2\omega_{xx} - 2y_x y_\psi \omega_{x\psi} - (1+y_x^2)\omega_{\psi\psi}\right]$$

$$+ \; \frac{y_\psi(1+y_x^2)}{R_e}\left(-\omega_{x\psi} + \frac{2y_x\omega_{\psi\psi}}{y_\psi} + \omega_{x\psi} \right)$$

$$- \; \frac{\omega_x y_\psi^3 \omega}{R_e} + \omega_\psi \; \left[-(1+y_x^2) + \frac{2y_x}{R_e y_\psi}\left\{ -y_\psi^2 y_{xx} + 2y_x y_\psi y_{x\psi} - (1+y_x^2)y_{\psi\psi} \right\} \right]$$

$$+ \; \frac{y_x}{R_e}\left[y_\psi^2\omega_{xx} - 2y_x y_\psi \omega_{x\psi} + (1+y_x^2)\omega_{\psi\psi}\right]$$

$$= \frac{\omega_x y_\psi^3 \omega}{R_c} + \omega_\psi \left[-(1+y_x^2) - \frac{2 y_x y_\psi^3 \omega}{R_c y_\psi} \right] + \frac{y_x}{R_c}\left(R_c y_\psi \omega_x + y_\psi^2 \omega \omega_\psi \right)$$

$$= \omega_x \left\{ \frac{y_\psi^3 \omega}{R_c} + y_x y_\psi \right\} + \omega_\psi \left[-(1+y_x^2) - \frac{2 y_x y_\psi^2 \omega}{R_c} + \frac{y_x y_\psi^2 \omega}{R_c} \right]$$

Hence,

$$L\{h\} = y_\psi \left\{ y_x + \frac{y_\psi^2 \omega}{R_c} \right\} \omega_x - \left\{ 1 + y_x^2 + \frac{y_x y_\psi^2}{R_c} \omega \right\} \omega_\psi$$

APPENDIX F

Derivation of boundary conditions for vorticity equations (2.4.5.7b) and (2.4.5.7d)

1. $\omega_{11} = aq_{13}^2 + bq_{12}^2 = -\frac{1}{2}(q_\psi^2)_{11}$

Expand in a Taylor Series about i1

	$(q^2)_{11}$	$(q_\psi^2)_{11}$	$(q_{\psi\psi}^2)_{11}$	$(q_{3\psi}^2)_{11}$	$(q_{4\psi}^2)_{11}\ldots$
aq_{13}^2	$a[1(1)$	$1(2\Delta\psi)$	$\frac{1}{2}(2\Delta\psi)^2$	$1/6(2\Delta\psi)^3$	$1/24(2\Delta\psi)^4\ldots]$
$=$	a	$2a\Delta\psi$	$2a\Delta\psi^2$	$(4/3)a\Delta\psi^3$	$2/3a\Delta\psi^4\ldots$
bq_{12}^2	$b[1(1)$	$1(\Delta\psi)$	$\frac{1}{2}(\Delta\psi)^2$	$1/6(\Delta\psi)^3$	$1/24(\Delta\psi)^4\ldots]$
$=$	b	$b\Delta\psi$	$\frac{1}{2}b\Delta\psi^2$	$1/6b\Delta\psi^3$	$1/24b\Delta\psi^4\ldots$
$\frac{1}{2}(q_\psi^2)_{11}$		$\frac{1}{2}$			
Σ	$a + b$	$(2a + b)\Delta\psi + \frac{1}{2}$	$(2a + \frac{1}{2}b)\Delta\psi^2$	$(4a/3 + b/6)\Delta\psi^3$	$(2a/3 + b/24)\Delta\psi^4\ldots$

Setting the first two coefficient sums equal to zero gives

$$a + b = 0$$

$$(2a + b)\Delta\psi + ½ = 0$$

Solving these equations,

$$b = ½\Delta\psi \qquad a = -½\Delta\psi$$

and

$$\omega_{i1} \approx -(½\Delta\psi)(q_{i3}^2 - q_{i2}^2)$$

Then, the truncation error E_T is given by

$$E_T + (2a + ½b)\Delta\psi^2 = 0$$

that is,

$$E_T = 3/4\Delta\psi$$

$$= 0(\Delta\psi)$$

2. $\omega_{11} \approx aq_{13}^2 + bq_{12}^2 + cq_{11}^2 \approx -\frac{1}{2}(q_\psi^2)_{11}$

· Expand in a Taylor Series about i1

	$(q^2)_{11}$	$(q_\psi^2)_{11}$	$(q_{\psi\psi}^2)_{11}$	$(q_{3\psi}^2)_{11}$	$(q_{4\psi}^2)_{11}\ldots$
aq_{13}^2	a[1(1)	$1(2\Delta\psi)$	$\frac{1}{2}(2\Delta\psi)^2$	$1/6(2\Delta\psi)^3$	$1/24(2\Delta\psi)^4\ldots]$
=	a	$2a\Delta\psi$	$2a\Delta\psi^2$	$(4/3)a\Delta\psi^3$	$(2/3)a\Delta\psi^4\ldots$
bq_{12}^2	b[1(1)	$1(\Delta\psi)$	$\frac{1}{2}(\Delta\psi)^2$	$1/6(\Delta\psi)^3$	$1/24(\Delta\psi)^4\ldots]$
=	b	$b\Delta\psi$	$\frac{1}{2}b\Delta\psi^2$	$(1/6)b\Delta\psi^3$	$(1/24)b\Delta\psi^4\ldots$
cq_{11}^2	c				
$\frac{1}{2}(q_\psi^2)_{11}$		$\frac{1}{2}$			
Σ	a + b + c	$(2a+b)\Delta\psi+\frac{1}{2}$	$(2a+\frac{1}{2}b)\Delta\psi^2$	$(4a/3+b/6)\Delta\psi^3$	$(2a/3+b/24)\Delta\psi^4\ldots$

Set the first three coefficient sums equal to zero:

$$a + b + c = 0$$

$$(2a + b)\Delta\psi + \tfrac{1}{2} = 0$$

$$2a + \tfrac{1}{2}b = 0$$

Hence,

$$b = -1/\Delta\psi$$

$$a = 1/4\Delta\psi$$

$$c = 3/4\Delta\psi$$

and

$$\omega_{i1} \approx (1/\Delta\psi)(q_{i3}^2/4 - q_{i2}^2 + 3q_{i1}^2/4)$$

$$= (1/4\Delta\psi)(q_{i3}^2 - 4q_{i2}^2) \text{ when } q_{i1}^2 = 0$$

As before,

$E_T + (4a/3 + b/6)\Delta\psi^3 = 0$ where E_T is the truncation error.

Therefore, $E_T = -[(4/3)(1/4\Delta\psi) - (1/6)(1/\Delta\psi)]\Delta\psi^3$

$= (-1/6)\Delta\psi^2$

$= 0(\Delta\psi^2)$

APPENDIX G

Derivation of equations in stretched coordinates

From equation (2.4.6.1), for the transformation $\psi = fn(\eta)$ only, $\Delta\psi$ transforms to $\Delta\eta$ and we have

$$\begin{aligned}
\partial/\partial\psi &= (d\psi/d\eta)^{-1}(\partial/\partial\eta) \\
\partial^2/\partial\psi^2 &= (d\psi/d\eta)^{-2}(\partial^2/\partial\eta^2) - (d\psi/d\eta)^{-3}(d^2\psi/d\eta^2)(\partial/\partial\eta) \\
\partial^2/\partial x\partial\psi &= (d\psi/d\eta)^{-1}(\partial^2/\partial x\partial\eta)
\end{aligned} \tag{G1}$$

From equations (2.4.1.1) and (2.4.1.2) using (G1) we get

$$\begin{aligned}
\{&A_{ij}^{(k)}\delta_{xx} + B_{ij}^{(k)}(d\psi/d\eta)^{-1}_{j}\delta_{x\eta} \\
&+ C_{ij}^{(k)}[(d\psi/d\eta)^{-2}_{j}\delta_{\eta\eta} - (d\psi/d\eta)^{-3}_{j}(d^2\psi/d\eta^2)_j\delta_\eta] \\
&+ \alpha R_e D_{ij}^{(k)}\delta_x + E_{ij}^{(k)}(d\psi/d\eta)^{-1}_{j}\delta_\eta\}\phi_{ij}^{(n+1)} = 0
\end{aligned}$$

Therefore,

$$\begin{aligned}
\{&A_{ij}^{(k)}\delta_{xx} + B_{ij}^{(k)}(d\psi/d\eta)^{-1}_{j}\delta_{x\eta} + C_{ij}^{(k)}(d\psi/d\eta)^{-2}_{j}\delta_{\eta\eta} \\
&+ \alpha R_e D_{ij}^{(k)}\delta_x \\
&+ [E_{ij}^{(k)}(d\psi/d\eta)^{-1}_{j} - C_{ij}^{(k)}(d\psi/d\eta)^{-3}_{j}(d^2\psi/d\eta^2)_j]\delta_\eta\}\phi_{ij}^{(n+1)} = 0
\end{aligned}$$

where $\phi = \begin{cases} y(x,\eta) & \text{if } \alpha = 0 \\ \omega(x,\eta) & \text{if } \alpha = 1 \end{cases}$ are the unknowns,

$$\begin{aligned}
A_{ij}^{(k)} &= (d\psi/d\eta)^{-2}_{j}(\delta_\eta y)^2_{ij} \\
B_{ij}^{(k)} &= -2(\delta_x y)_{ij}(d\psi/d\eta)^{-1}_{j}(\delta_\eta y)_{ij} \\
C_{ij}^{(k)} &= 1 + (\delta_x y)^2_{ij} \\
D_{ij}^{(k)} &= -(d\psi/d\eta)^{-1}(\delta_\eta y)_{ij} \\
E_{ij}^{(k)} &= -(d\psi/d\eta)^{-2}_{j}(\delta_\eta y)^2_{ij}\omega_{ij}
\end{aligned}$$

Simplifying we obtain

$$(\overline{A}_{ij}^{(k)}\delta_{xx} + \overline{B}_{ij}^{(k)}\delta_{x\eta} + \overline{C}_{ij}^{(k)}\delta_{\eta\eta} + \alpha R_e\overline{D}_{ij}^{(k)}\delta_x + \overline{E}_{ij}^{(k)}\delta_\eta)\phi_{ij}^{(n+1)} = 0$$

where

$$\overline{A}_{ij}^{(k)} = (d\psi/d\eta)^{-2}_j(\delta_\eta y)^2_{ij}$$

$$\overline{B}_{ij}^{(k)} = -2(d\psi/d\eta)^{-2}_j(\delta_x y)_{ij}(\delta_\eta y)_{ij}$$

$$\overline{C}_{ij}^{(k)} = (d\psi/d\eta)^{-2}_j[1 + (\delta_x y)^2_{ij}]$$

$$\overline{D}_{ij}^{(k)} = -(d\psi/d\eta)^{-1}_j(\delta_\eta y)_{ij}$$

$$\overline{E}_{ij}^{(k)} = -(d\psi/d\eta)^{-3}_j(\delta_\eta y)^2_{ij}\omega_{ij} - [1 + (\delta_x y)^2_{ij}](d\psi/d\eta)^{-3}_j(d^2\psi/d\eta^2)_j$$

$$= -(d\psi/d\eta)^{-3}_j\{(\delta_\eta y)^2_{ij}\omega_{ij} + (d^2\psi/d\eta^2)_j[1 + (\delta_x y)^2_{ij}]\}$$

Therefore, equations (2.4.2.3a) become

$$\overline{a}_{ij} = \overline{A}_{ij}^{(k)}$$

$$\overline{b}_{ij} = \overline{B}_{ij}^{(k)}(\Delta x/4\Delta\eta)$$

$$\overline{c}_{ij} = \overline{C}_{ij}^{(k)}(\Delta x^2/\Delta\eta^2)$$

$$\overline{d}_{ij} = \alpha R_e\overline{D}_{ij}^{(k)}(\Delta x/2)$$

$$\overline{e}_{ij} = \overline{E}_{ij}^{(k)}(\Delta x^2/2\Delta\eta)$$

From equation (2.4.6.1) Δx transforms to $\Delta\xi$ and $\Delta\psi$ transforms to $\Delta\eta$ and, in addition to the relations in (G1) we have

$$\partial/\partial x = (dx/d\xi)^{-1}(\partial/\partial\xi)$$

$$\partial^2/\partial x^2 = (dx/d\xi)^{-2}(\partial^2/\partial\xi^2) - (dx/d\xi)^{-3}(d^2x/d\xi^2)(\partial/\partial\xi) \qquad \text{(G2)}$$

Again, from equations (2.4.1.1) and (2.4.1.2) using (G1) and (G2) we get

$$\{A_{ij}^{(k)}[(dx/d\xi)_i^{-2}\delta_{\xi\xi} - (dx/d\xi)_i^{-3}(d^2x/d\xi^2)_i\delta_\xi]$$
$$+ B_{ij}^{(k)}(dx/d\xi)_i^{-1}(d\psi/d\eta)_j^{-1}\delta_{\xi\eta}$$
$$+ C_{ij}^{(k)}[(d\psi/d\eta)_j^{-2}\delta_{\eta\eta} - (d\psi/d\eta)_j^{-3}(d^2\psi/d\eta^2)_j\delta_\eta]$$
$$+ \alpha R_e D_{ij}^{(k)}(dx/d\xi)_i^{-1}\delta_\xi + E_{ij}^{(k)}(d\psi/d\eta)_j^{-1}\delta_\eta\}\phi_{ij}^{(n+1)} = 0$$

Therefore,

$$\{A_{ij}^{(k)}(dx/d\xi)_i^{-2}\delta_{\xi\xi} + B_{ij}^{(k)}(dx/d\xi)_i^{-1}(d\psi/d\eta)_j^{-1}\delta_{\xi\eta}$$
$$+ C_{ij}^{(k)}(d\psi/d\eta)_j^{-2}\delta_{\eta\eta} + [\alpha R_e D_{ij}^{(k)}(dx/d\xi)_i^{-1}$$
$$- A_{ij}^{(k)}(dx/d\xi)_i^{-3}(d^2x/d\xi^2)_i]\delta_\xi$$
$$+[E_{ij}^{(k)}(d\psi/d\eta)_j^{-1} - C_{ij}^{(k)}(d\psi/d\eta)_j^{-3}(d^2\psi/d\eta^2)_j]\delta_\eta\}\phi_{ij}^{(n+1)} = 0$$

where $\phi = \begin{cases} y(\xi,\eta), & \text{if } \alpha = 0 \\ \omega(\xi,\eta), & \text{if } \alpha = 1 \end{cases}$ are the unknowns,

and

$$A_{ij}^{(k)} = (d\psi/d\eta)_j^{-2}(\delta_\eta y)_{ij}^2$$

$$B_{ij}^{(k)} = -2(dx/d\xi)_i^{-1}(\delta_\xi y)_{ij}(d\psi/d\eta)_j^{-1}(\delta_\eta y)_{ij}$$

$$C_{ij}^{(k)} = 1 + (dx/d\xi)_i^{-2}(\delta_\xi y)_{ij}^2$$

$$D_{ij}^{(k)} = -(d\psi/d\eta)_j^{-1}(\delta_\eta y)_{ij}$$

$$E_{ij}^{(k)} = -(d\psi/d\eta)_j^{-2}(\delta_\eta y)_{ij}^2\omega_{ij}$$

Simplifying we obtain

$$(\overline{A}_{ij}^{(k)}\delta_{\xi\xi} + \overline{B}_{ij}^{(k)}\delta_{\xi\eta} + \overline{C}_{ij}^{(k)}\delta_{\eta\eta} + \overline{D}_{ij}^{(k)}\delta_\xi + \overline{E}_{ij}^{(k)}\delta_\eta)\phi_{ij}^{(n+1)} = 0$$

where

$$\overline{A}_{ij}^{(k)} = (dx/d\xi)_i^{-2}(d\psi/d\eta)_j^{-2}(\delta_\eta y)_{ij}^2$$

$$\overline{B}_{ij}^{(k)} = -2(dx/d\xi)_i^{-2}(d\psi/d\eta)_j^{-2}(\delta_\xi y)_{ij}(\delta_\eta y)_{ij}$$

$$\overline{C}_{ij}^{(k)} = (d\psi/d\eta)_j^{-2}[1 + (dx/d\xi)_i^{-2}(\delta_\xi y)_{ij}^2]$$

$$\begin{aligned}\overline{D}_{ij}^{(k)} &= -\alpha R_e(d\psi/d\eta)_j^{-1}(\delta_\eta y)_{ij}(dx/d\xi)_i^{-1} \\ &\quad -(d\psi/d\eta)_j^{-2}(\delta_\eta y)_{ij}^2(dx/d\xi)_i^{-3}(d^2x/d\xi^2)_i \\ &= -(dx/d\xi)_i^{-1}[\alpha R_e(d\psi/d\eta)_j^{-1}(\delta_\eta y)_{ij} \\ &\quad +(dx/d\xi)_i^{-2}(d\psi/d\eta)_j^{-2}(d^2x/d\xi^2)_i(\delta_\eta y)_{ij}^2]\end{aligned}$$

$$\begin{aligned}\overline{E}_{ij}^{(k)} &= -(d\psi/d\eta)_j^{-3}(\delta_\eta y)_{ij}^2\omega_{ij} \\ &\quad -[1 + (dx/d\xi)_i^{-2}(\delta_\xi y)_{ij}^2](d\psi/d\eta)_j^{-3}(d^2\psi/d\eta^2)_j \\ &= -(d\psi/d\eta)_j^{-3}\{(\delta_\eta y)_{ij}^2\omega_{ij} + (d^2\psi/d\eta^2)_j[1 + (dx/d\xi)_i^{-2}(\delta_\xi y)_{ij}^2]\}\end{aligned}$$

Therefore, equations (2.4.2.3a) become

$$\overline{a}_{ij} = \overline{A}_{ij}^{(k)}$$

$$\overline{b}_{ij} = \overline{B}_{ij}^{(k)}(\Delta\xi/4\Delta\eta)$$

$$\overline{c}_{ij} = \overline{C}_{ij}^{(k)}(\Delta\xi^2/\Delta\eta^2)$$

$$\overline{d}_{ij} = \overline{D}_{ij}^{(k)}(\Delta\xi/2)$$

$$\overline{e}_{ij} = \overline{E}_{ij}^{(k)}(\Delta\xi^2/2\Delta\eta)$$

APPENDIX H

Channel shape

The channel shape for this study was chosen by Roache [III.1]. It was desirable to have separated flow with a nearly constant channel height at outflow, and a shape defined by a single-valued smooth analytic function. The shape of the lower wall was defined by a shifted hyperbolic tangent function, given by

$$y = y_\ell(x) = \frac{1}{2}\left[1 - \tanh\left\{sc\frac{x - x_F}{L_c}\right\}\right] + \delta \tag{H1}$$

where L_c = length of the channel;

x_F = location of the inflection point in the tanh profile;

sc = scale factor;

δ = small adjustment set to give $y_\ell(0) = 0$.

For the parametric cases considered, L_c is scaled with Reynolds number $R_c = R_{cc}$ as $L_c = \dfrac{R_{cc}}{C_{L_c}}$. Again, this scaling is necessary to keep the separated flow region within the computational mesh, and results in the self-similarity of the solutions at high R_c. The particular channel parameters used were:

$$sc = 10, \quad \frac{x_F}{L_c} = 0.2 \quad \text{so that } x_F = \frac{R_{cc}}{15} \text{ and } C_{L_c} = 3 \tag{H2}$$

Substituting (H2) into (H1) and taking $y_t(0) = 0$, we obtain

$$y_t(x) = \frac{1}{2}\left[1 - \tanh\left(10\frac{x-x_F}{\frac{R_{cc}}{3}}\right)\right] + \delta$$

$$= \frac{1}{2}\left[\tanh\left(2 - \frac{30x}{R_{cc}}\right) + 1\right] + \delta$$

$$= \frac{1}{2}\left[\tanh\left(2 - \frac{30x}{R_{cc}}\right) - \tanh 2\right]$$

APPENDIX I

Justification of the boundary conditions at the channel outlet

The slope of the lower wall at is given by

$$y_\ell' = \frac{1}{2}\mathrm{sech}^2\left(2 - \frac{30x}{R_{cc}}\right)\left(-\frac{30}{R_{cc}}\right)$$

Hence, at $x = x_{out} = \dfrac{R_{cc}}{3}$,

$$y_\ell'\left(\frac{R_{cc}}{3}\right) = \frac{-15}{R_{cc}}\mathrm{sech}^2\left(2-10\right)$$

$$\approx 7\times10^{-7} \text{ for } R_{cc} = 10$$

$$\approx 7\times10^{-8} \text{ for } R_{cc} = 100$$

The channel shape has a height that is constant to five figures over the last 20% of the channel. Hence, using the condition commonly used in straight-channel calculations, i.e., parabolic velocity profile, would be acceptable. In any case, the lower wall is virtually parallel to the x-axis at the outlet, and we can reasonably assume that $v = 0$ at the outlet. To further support the above argument, consider the following:

$$u = \psi_y$$

$$v = -\psi_x$$

Hence, $u_x = 0$ implies $\psi_{yx} = 0$, i.e., $(\psi_x)_y = 0$. Similarly, $v_x = 0$ implies $-\psi_{xx} = 0$, i.e., $(-\psi_x)_x = 0$.

Therefore, we can conclude that $\psi_x = -v = \text{constant}$. Since $v = 0$ at the walls, this constant is zero, and hence $v = 0$ at $x = x_{out}$ for all y. Also, $v = uy_x = \frac{y_x}{y_\psi} = 0$

implies $y_x = 0$ for $x = x_{out}$ and $y_\ell\left(\frac{R_\infty}{3}\right) \le y \le 1$.

Finally, $\omega = v_x - u_y$, so

$$\omega \mid_{x=x_{out}} = -u_y = -\psi_{yy}$$

Hence,

$$\omega_x \mid_{x=x_{out}} = -\psi_{yyx} = \left(-\psi_{yx}\right)_x = 0$$

Therefore, $\omega_x = 0$ for $x = x_{out}$ and $y_\ell\left(\frac{R_\infty}{3}\right) \le y \le 1$.

APPENDIX J

Derivation of equation (3.2.3.1)

We want to solve $\psi = \frac{1}{2}(3y^2 - y^3)$ explicitly for $y = y(\psi)$. Rewrite this equation as

$$y^3 - 3y^2 + 2\psi = 0 \tag{J1}$$

Let $p = -3$, $y = x - \frac{p}{3} = x+1$. Then

$$(x + 1)^3 - 3(x + 1)^2 = 2\psi = 0$$

or,

$$x^3 - 3x - 2 + 2\psi = 0 \tag{J2}$$

Let $a = -3$, $b = -2 + 2\psi$, then $ab = -3(-2 + 2\psi) \neq 0$ provided $\psi \neq 1$.

The solution of (J2) is given by

$$x = m\cos\theta$$

where

$$m = 2\sqrt{\frac{-a}{3}} = 2$$

and

$$\cos 3\theta = \frac{3b}{9m} = 1-\psi$$

Hence, the solution of (J1) is

$$
\begin{aligned}
y &= m\cos\theta + 1 \\
&= 2\cos\theta + 1
\end{aligned}
\tag{J3}
$$

where

$$
\theta = \begin{cases} \theta_1 \\ \theta_1 + \dfrac{2\pi}{3} \\ \theta_1 + \dfrac{4\pi}{3} \end{cases}
\tag{J4}
$$

and θ_1 is defined as

$$
\theta_1 \equiv \frac{1}{3}\cos^{-1}(1-\psi)
\tag{J5}
$$

Several possibilities occur for the value of θ. To determine the appropriate choice, consider the following cases:

1. When $\psi = 0$, we require that $y = 0$. From (J1), $\psi = 0$ yields

   $$y^2(y-3) = 0$$

   This implies that $y = 0$ or $y = 3$, so we can select $y = 0$. Using $\psi = 0$ in (J5) gives

   $$\theta_1 = \frac{1}{3}\cos^{-1}(1) = 0$$

Then, (J4) gives

$$\theta = \begin{cases} 0 \\ \dfrac{2\pi}{3} \\ \dfrac{4\pi}{3} \end{cases}$$

We find that $y = 0$ for $\theta = \dfrac{2\pi}{3}$ and $\dfrac{4\pi}{3}$.

2. Equation (J1) is also satisfied at the channel centreline, $y = 1$, at which $\psi = 1$. Hence, using (J5)

$$\theta_1 = \frac{1}{3}\cos^{-1}(0) = \frac{\pi}{6}$$

Using (J4),

$$\theta = \begin{cases} \dfrac{\pi}{6} \\ \dfrac{\pi}{6} + \dfrac{2\pi}{3} \\ \dfrac{\pi}{6} + \dfrac{4\pi}{3} \end{cases}$$

We find that $y = 1$ for $\theta = \dfrac{\pi}{6} + \dfrac{4\pi}{3}$ only.

Combining these results, we see that the only choice for θ is $\theta = \theta_1 + \dfrac{4\pi}{3}$. Hence, we arrive at the solution

$$y = 2\cos\left[\theta_1 + \frac{4\pi}{3}\right] + 1$$

where

$$\theta_1 = \frac{1}{3}\cos^{-1}(1-\psi)$$

APPENDIX K

Difference formulas used for v_x in equation (3.2.4.1)

We have $u = \dfrac{1}{y_\psi}$ and $v = uy_x = \dfrac{y_x}{y_\psi}$.

The derivative v_x is approximated by forward differencing,

$$(v_x)_{ij} \approx (\delta_x v)_{ij} = \frac{v_{i+1,j} - v_{ij}}{\Delta x} \qquad \text{2-point, } 0(\Delta x)$$

or

$$(\delta_x v)_{ij} = \frac{-v_{i+2,j} + 4v_{i+1,j} - 3v_{ij}}{2\Delta x} \qquad \text{3-point, } 0(\Delta x)$$

We use a forward (downwind) difference for y_x, but a central difference for y_ψ, to compute values of v,

$$v_{ij} \approx \left[\frac{\delta_x y}{\delta_\psi y}\right]_{ij} = \frac{y_{i+1,j} - y_{ij}}{\Delta x}\,\frac{2\Delta\psi}{y_{i,j+1} - y_{i,j-1}}, \qquad 0(\Delta x)0(\Delta\psi)$$

or

$$v_{ij} \approx \frac{-y_{i+2,j} + 4y_{i+1,j} - 3y_{ij}}{2\Delta x}\,\frac{\Delta\psi^2}{y_{i,j+1} - 2y_{ij} + y_{i,j-1}}, \qquad 0(\Delta x)0(\Delta\psi^2)$$

The above formulas are valid for $i = 1$ only, $j = 2,3,\ldots,J1$.

At $j = 1$, the solid wall no-slip condition gives $(v_x)_{11} = 0$.

At $j = JX$, the centreline symmetry condition implies $(v_x)_{1,Jx} = 0$.

APPENDIX L

Derivation of the solution for a circular cylinder in hyperbolic-cosine shear flow

Problem A: Flow about a circular cylinder of radius $r = a$

Consider steady plane (2-dimensional) motion of an incompressible, inviscid fluid past a circular cylinder without circulation (irrotational).

DE: (Differential Equation)

$\nabla^2\psi = -\omega(\psi) \equiv 0$, since the flow is irrotational.

ψ is the stream function with velocity components in cartesian coordinates given by $u = \psi_y$, $v = -\psi_x$, and $\omega = \omega(\psi)$ is the vorticity.

BC's: (Boundary Conditions)

Upstream: Uniform flow far upstream at infinity, implying that the vorticity vanishes.

Speed:

$$\left.\begin{array}{l} u = U_\infty = \text{constant} \\ v = 0 \end{array}\right\} \text{ at infinity.}$$

Stream function: Integrating $\psi_{\infty y} = U_\infty$ gives

$\psi_\infty = U_\infty y = U_\infty r\sin\theta$ in polar coordinates (r,θ). Hence

$\psi(r,\theta) \rightarrow \psi_\infty = U_\infty r\sin\theta$ as $r \rightarrow \infty$.

Note: We have taken $y = 0$ as the streamline $\psi = 0$ so the arbitrary constant of integration will be zero. This will be the case in the problems to follow.

Surface: Since the surface is a streamline, we can take $\psi = 0$ on $r = a$, i.e., $\psi(a,\theta) = 0$.

Circulation: To rule out circulation and obtain a unique solution, it is assumed that no flow will cross the x axis by assuming symmetry about the line $\theta = 0$ and $\theta = \pi$ ($|r| > a$), i.e., no additional circulation is induced by the body.

Solution:

$$\psi(r,\theta) = U_\infty \left(r - \frac{a^2}{r} \right) \sin\theta$$

i.e., uniform stream plus a dipole at the centre of the circle.

Problem B: Circular cylinder in slight shear flow (same as problem A except as noted below)

DE: $\nabla^2\psi = -\omega(\psi) \neq 0$, since the flow is rotational. (L1)

BC's: Upstream: Consider a slight or small linear perturbation to the uniform flow boundary condition far upstream at infinity. Let the oncoming stream be a parallel flow with small constant vorticity.

Speed:

$$\left.\begin{matrix} u = U_\infty\left[1+\epsilon\dfrac{y}{a}\right] \\ v = 0 \end{matrix}\right\} \quad \text{at infinity.}$$

Stream function: Integrating $\psi_{\infty y} = U_\infty\left[1+\epsilon\dfrac{y}{a}\right]$ gives

$$\psi_\infty = U_\infty\left[y+\frac{1}{2}\epsilon\frac{y^2}{a}\right]$$

That is, $\psi(r,\theta;\epsilon) \rightarrow \psi_\infty = U_\infty\left[r\sin\theta+\dfrac{1}{4}\epsilon\dfrac{r^2}{a}(1-\cos2\theta)\right]$

as $r \rightarrow \infty$.

Vorticity: $\omega_\infty = -\nabla^2\psi_\infty = -\dfrac{\epsilon U_\infty}{a} = \text{constant}.$

Hence, $\omega(\psi) \equiv \omega_\infty = -\dfrac{\epsilon U_\infty}{a}$.

DE: Equation (L1) becomes

$$\nabla^2\psi = \frac{\epsilon U_\infty}{a}$$

Solution: If the dimensionless "vorticity number" ϵ is small (slight vorticity), it seems likely that the flow will depart only slightly from the solution in problem A for irrotational motion.

Hence, by perturbing the solution to problem A, we get

$$\psi(r,\theta;\epsilon) = U_\infty\left[r-\frac{a^2}{r}\right]\sin\theta + \frac{1}{4}\epsilon U_\infty\left[\frac{r^2}{a}(1-\cos 2\theta)+\frac{a^3}{r^2}\cos 2\theta - a\right]$$

The basic solution consists of a uniform stream (a dipole at infinity) plus its image in the circle (a dipole at the origin) as before. The first order perturbation solution consists of the rotational part of the stream, its image in the circle and a constant to adjust the stream function to zero on the surface.

Note: Since the vorticity is constant everywhere, this problem is not difficult to solve.

Problem C: Circular cylinder in parabolic and hyperbolic-cosine shear (same as problem A except as noted below)

BC's: Upstream: Consider a circular cylinder of radius a symmetrically placed in a parallel stream of incompressible, inviscid fluid having the following velocity profiles far upstream.

a) Parabolic velocity profile

Speed:

$$\left.\begin{aligned} u &= U_\infty\left[1+\frac{1}{2}\epsilon\frac{y^2}{a^2}\right] \\ v &= 0 \end{aligned}\right\} \quad \text{at infinity.}$$

Stream Function: Integrating $\psi_{\infty y} = U_\infty\left[1+\frac{1}{2}\epsilon\frac{y^2}{a^2}\right]$ and choosing $\psi = 0$ along $y = 0$ gives

$$\psi_\infty = U_\infty\left[y+\frac{1}{6}\epsilon\frac{y^3}{a^2}\right]$$

That is, $\psi(r,\theta;\epsilon) \to \psi_\infty = U_\infty\left[r\sin\theta+\frac{1}{6}\epsilon\frac{r^3\sin^3\theta}{a^2}\right]$

as $r \to \infty$.

Vorticity:

$$\omega_\infty = -\nabla^2\psi_\infty = -\frac{\epsilon}{a^2}U_\infty y \neq \text{constant.}$$

In inviscid motion we have the physical fact that vorticity is constant along streamlines in the absence of viscosity.

Hence, writing $\omega(\psi) = \omega \equiv \omega_\infty$

and $\psi(r,\theta;\epsilon) = \psi \equiv \psi_\infty$

we have $y = -\frac{a^2}{\epsilon}\frac{\omega}{U_\infty}$ and, therefore,

$$\psi = U_\infty\left[-\frac{a^2}{\epsilon}\frac{\omega}{U_\infty} - \frac{1}{6}\frac{a^4}{\epsilon^2}\frac{\omega^3}{U_\infty^3}\right]$$

$$= \frac{a^2}{\epsilon}\left[-\omega - \frac{1}{6}\frac{a^2\omega^3}{\epsilon U_\infty^2}\right]$$

Reverting this series gives

$$-\omega = \omega(\psi) = \frac{\epsilon}{a^2}\psi - \frac{1}{6}\frac{\epsilon^2}{U_\infty^2 a^4}\psi^3 + 0(\epsilon^3)$$

D.E.: Equation (L1) now becomes

$$\nabla^2\psi = \frac{\epsilon}{a^2}\psi + \frac{1}{6}\frac{\epsilon^2}{a^4\ U_\infty^2}\psi^3 + 0(\epsilon^3)$$

Solution: $$\psi(r,\theta;\epsilon) = U_\infty\left[r-\frac{a^2}{r}\right]\sin\theta + \epsilon U_\infty\left[\frac{1}{6}\frac{r^3}{a^2}\sin^3\theta - \frac{1}{2}r\ell n\frac{r}{a}\sin\theta + \chi\right] + 0(\epsilon^2)$$

where χ is a solution of the homogeneous equation (complementary solution) that restores the boundary conditions. However, the term in the particular integral or solution that contains a logarithm gives velocity perturbations that are logarithmically infinite at infinity and no harmonic function χ will cancel them, i.e., no solution exists with disturbances dying out to satisfy the upstream condition.

Hence, there is no analytic solution here to verify numerically.

Therefore, we consider a profile which is almost the same near the cylinder.

b) Hyperbolic-cosine profile

Speed:
$$\left.\begin{array}{l} u = U_\infty \cosh\left[\dfrac{\epsilon^{\frac{1}{2}}}{a}y\right] \\ v = 0 \end{array}\right\} \quad \text{at infinity.}$$

Stream function: Integrating $\psi_{\infty y} = U_\infty \cosh\left[\dfrac{\epsilon^{\frac{1}{2}}}{a}y\right]$ gives

$$\psi_\infty = \frac{U_\infty a}{\epsilon^{\frac{1}{2}}}\sinh\left[\frac{\epsilon^{\frac{1}{2}}}{a}y\right]$$

$$= U_\infty\left[y+\frac{1}{6}\frac{\epsilon y^3}{a^2}+\ldots\right]$$

Thus,

$$\psi(r,\theta;\epsilon) \to \psi_\infty = U_\infty\left[r\sin\theta+\frac{1}{6}\epsilon r^3\frac{\sin^3\theta}{a^2}+\ldots\right]$$

as $r \to \infty$.

Vorticity:
$$\omega_\infty = -\nabla^2\psi_\infty = -\frac{\epsilon}{a^2}\psi_\infty \neq \text{constant}.$$

Hence, writing $\omega(\psi) = \omega \equiv \omega_\infty$ and $\psi(r,\theta;\epsilon) = \psi \equiv \psi_\infty$, we have

$$-\omega = -\omega(\psi) = \frac{\epsilon}{a^2}\psi$$

DE: Equation (L1) now becomes exactly

$$\nabla^2\psi = \frac{\epsilon}{a^2}\psi$$

Solution: $$\psi(r,\theta;\epsilon) = U_\infty\left[r-\frac{a^2}{r}\right]\sin\theta+\epsilon U_\infty\left[\frac{1}{6}\frac{r^3}{a^2}\sin^3\theta-\frac{1}{2}r\ell n\frac{r}{a}\sin\theta+\chi\right]+0(\epsilon^2) \qquad \text{(L2)}$$

where a solution χ can now be found that disturbs the distant flow upstream as little as possible.

We find,

$$\chi(r,\theta) = -\frac{1}{8}\frac{a^2}{r}\sin\theta+\frac{1}{24}\frac{a^4}{r^3}\sin3\theta+c\left[r-\frac{a^2}{r}\right]\sin\theta$$

where $c = \frac{1}{4}\left[\ell n\frac{4}{\epsilon}-2\gamma+1\right]$; $\gamma = 0.577$

Speed: $$q^2 = q_r^2+q_\theta^2 = \frac{1}{r^2}\left[\frac{\partial\psi}{\partial\theta}\right]^2+\left[\frac{\partial\psi}{\partial r}\right]^2$$

From equation (L2)

$$\frac{\partial\psi}{\partial\theta} = U_\infty\left[r-\frac{a^2}{r}\right]\cos\theta+\epsilon U_\infty\left[\frac{1}{2}\frac{r^3}{a^2}\sin^2\theta\cos\theta-\frac{1}{2}r\ell n\frac{r}{a}\cos\theta+\frac{\partial\chi}{\partial\theta}\right]+0(\epsilon^2)$$

$$\frac{\partial\chi}{\partial\theta} = -\frac{1}{8}\frac{a^2}{r}\cos\theta+\frac{1}{8}\frac{a^4}{r^3}\cos3\theta+c\left[r-\frac{a^2}{r}\right]\cos\theta$$

$$\frac{\partial\psi}{\partial r} = U_\infty\left[1+\frac{a^2}{r^2}\right]\sin\theta+\epsilon U_\infty\left[\frac{1}{2}\frac{r^2}{a^2}\sin^3\theta-\frac{1}{2}\ell n\frac{r}{a}\sin\theta-\frac{1}{2}\sin\theta+\frac{\partial\chi}{\partial r}\right]+0(\epsilon^2)$$

$$\frac{\partial\chi}{\partial r} = \frac{1}{8}\frac{a^2}{r^2}\sin\theta-\frac{1}{8}\frac{a^4}{r^4}\sin3\theta+c\left[1+\frac{a^2}{r^2}\right]\sin\theta$$

In order to obtain expressions in nondimensional variables, we can take $U_\infty = a = 1$.

Then, $u = \cosh(\epsilon^{\frac{1}{2}}y)$

$$\psi_\infty = \frac{1}{\epsilon^{\frac{1}{2}}}\sinh\left(\epsilon^{\frac{1}{2}}y\right) \quad \text{or} \quad y = \frac{1}{\epsilon^{\frac{1}{2}}}\sinh^{-1}\left(\epsilon^{\frac{1}{2}}\psi_\infty\right) \tag{L3}$$

$$\omega = -\epsilon\psi = -\epsilon^{\frac{1}{2}}\sinh\left(\epsilon^{\frac{1}{2}}y\right) \tag{L4}$$

The preceeding solution is obtained with considerable difficulty using the method of matched asymptotic expansions. A perturbation solution is required, one valid far away from the body, termed the outer solution and another valid near the body, termed the inner solution. Both of these solutions contain arbitrary constants which have to be matched using some form of matching principle to obtain a unique solution. A uniformly valid composite approximation can be obtained by finding the common part of the inner and outer solutions and subtracting it from the inner plus outer solution using additive composition.

APPENDIX M

Derivation of the initial guess for equation (5.2.4.4)

We have $2 = x_{sep} < x < x_A = 2 + L_x$

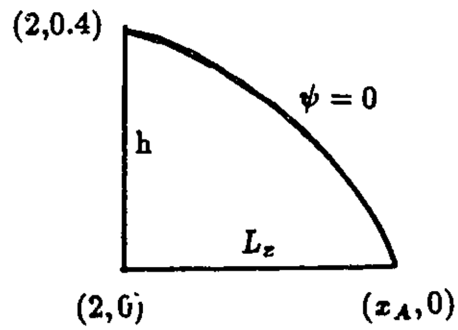

For an ellipse we take $a = L_x$, $b = h = 0.4$ to get the equation

$$\frac{(x-2)^2}{L_x^2} + \frac{y^2}{h^2} = 1$$

Solving for y gives $y = h\left[1 - \frac{(x-2)^2}{L_x^2}\right]^{\frac{1}{2}}$

$$= y_{i1}^{(1)}$$

in equation (5.2.4.4). This gives the initial guess for y, for some initial value of the reattachment length L_x.

APPENDIX N

Computer program

```
      PROGRAM SLOR
      IMPLICIT DOUBLE PRECISION (A-H, O-Z)
c       EXTERNAL DELXY,DELPSY
       PARAMETER (IMAX=61, JMAX=21, IMM1 = IMAX - 1, JMM1 =
      #   JMAX - 1, IMM2 = IMAX - 2, JMM2 = JMAX - 2)
       DIMENSION A(JMM1), B(JMM1), C(JMM1), D(JMM1), R(JMM1),
      #   WOLD(IMAX,JMAX), WNEW(IMAX,JMAX),BENCH(JMAX,2),
      #   YOLD(IMAX,JMAX), YNEW(IMAX,JMAX)
C    , F(JMAX,2), G(JMAX,2)
       COMMON /BND/DELX, DELPSI, XMIN, PSIMIN, REY
         COMMON   /WVALUE/WOLD,   WNEW/YVALUE/YOLD,
YNEW/WCH/WCHECK/WA/HSTEP
       LOGICAL CHECK, WCHECK
C
C      DEFINITION OF STATEMENT FUNCTIONS
C
       A1(I,J) = DELPSY(I,J) ** 2
       A2(I,J) = -2.0 * DELXY(I,J) * DELPSY(I,J)
       A3(I,J) = 1.0 + DELXY(I,J) ** 2
       A4(I,J) = -DELPSY(I,J)
       A5(I,J) = -A1(I,J) * WOLD(I,J)
       Q(I,J) = A3(I,J) / A1(I,J)
      VK(I) = (YOLD(I+1,1)-YOLD(I-1,1)) / (YOLD(I,2)-YOLD(I,1)) *
      #          DELPSI * 0.5 / DELX
C
C      FORMULA 1 OF W
       W1(I) = (3.0 * Q(I, 4) - 8.0 * Q(I, 3)
      #          + 5.0 * Q(I, 2)) / (4.0 * DELPSI)
       W2(I) = -(3.0 * Q(I, JMAX-3) - 8.0 * Q(I, JMM2)
      #          + 5.0 * Q(I, JMM1)) / (4.0 * DELPSI)
       W3(I) = -(2.0 * Q(I, 4) - 9.0 * Q(I, 3)
      #            + 18.0 * Q(I, 2) - 11.0 * Q(I, 1) ) / (12.0 *
DELPSI)
C
C      FORMULA 2 OF W
C       W1(I) = -(2.0 * Q(I, 4) - 9.0 * Q(I, 3)
C      #          + 18.0 * Q(I, 2)) / (12.0 * DELPSI)
C       W2(I) = (2.0 * Q(I, JMAX-3) - 9.0 * Q(I, JMM2)
C      #          + 18.0 * Q(I, JMM1)) / (12.0 * DELPSI)
C     W3(I) = 0.5* ((VK(I+1) - VK(I-1)) / DELX -
C      #            (Q(I,2) - Q(I,1)) / DELPSI )
C
C      FORMULA 3 OF W
C       W(I) = -(11.0 * Q(I,5) - 42.0 * Q(I, 4) + 57.0 * Q(I, 3)
C      #          - 26.0 * Q(I, 2)) / (12.0 * DELPSI)
C
C       READ THE MINIMUM AND MAXMUM X AND PSI VALUES. READ THE
C       VALUE OF EPSILON TO BE USED
C
      WRITE(*,*)' Input Reynolds Number'
      READ(*,*)REY
      WRITE(*,*)' Input Beta for y'
      READ(*,*)BETAY
```

```
       WRITE(*,*)' Input Beta for w'
       READ(*,*)BETAW
       WRITE(*,*)' Input delta for w'
       READ(*,*)DELTA
       WRITE(*,*)' Input epsilon for error tolerance'
       READ(*,*)EPSILY,EPSILW
       WRITE(*,*)' Input maximum iteration Number'
       READ(*,*)NMAX
       WRITE(*,*)' Input starting point for delta calculation'
       READ(*,*)MMU
      WRITE(*,*)' Input index for reattachment'
      READ(*,*)IRETACH, ISTEP
      read(*,*)CF
C       OPEN(UNIT = 1, FILE = 'TEST.DAT', STATUS = 'NEW')
C
C DATA INITIALIZATION
C
       DO 10 I=1,IMAX
       DO 10 J=1,JMAX
          WOLD(I,J)=0.0
          YOLD(I,J)=0.0
10     CONTINUE
C
C       CALCULATE DELTA X AND DELTA PSI
C
      HSTEP = 0.4
C
C     ASSUMING AN INDEX FOR REATTACHMENT,
C     WHICH IS CLOSE TO THE OUTLET
C
       XMIN = 0.0
       XMAX = 6.0
       PSIMIN = 0.0
       PSIMAX = 1.0
       DELX = (XMAX - XMIN) / IMM1
       DELPSI = (PSIMAX - PSIMIN) / JMM1
       RAT = DELX / DELPSI
       RAT2 = RAT * RAT
       RATD = RAT * DELX * 0.5
       RATF = RAT * 0.25
       REY2 = 0.5 * REY * DELX

       WRITE(1,111)XMIN, XMAX, PSIMIN, PSIMAX, REY,
      #          DELTA, BETAY, BETAW, EPSILY, EPSILW
111    FORMAT(1X,'========================================='/
      #       4X,'Xmin = ',F5.2,'   Xmax = ',F5.2/
      #       4X,'Pmin = ',F5.2,'   Pmax = ',F5.2/
      #       4X,'Re   = ',F5.2,'   delta= ',F5.2/
      #       4X,'By   = ',F5.2,'   Bw   = ',F5.2/
      #       4X,'Ey   = ',E12.5,'   Ew   = ',E12.5/
      #       1X,'=========================================')
C
C CALCULATE THE BOUNDARY CONDITIONS WHICH REMAIN UNCHANGED DURING
ITERATION
```

```
C THEY ARE I<>IMAX FOR Y AND I=1 AND J=JMAX FOR W
C
C     BOUNDARY CONDITIONS FOR Y ON THE LOWER AND UPPER BOUNDARIES
C
       DO 20 I=1, IMAX
          YOLD(I,1) = YBND(I,1)
          YOLD(I,JMAX) = YBND(I,JMAX)
          WOLD(I,1) = WBND(I,1)
          WOLD(I,JMAX) = WBND(I,JMAX)
20     CONTINUE
C
C     BOUNDARY CONDITIONS OF THE INLET AND OUTLET
C
       DO 30 J=1,JMAX
          YOLD(1,J) = YBND(1,J)
          YOLD(IMAX,J) = YBND(IMAX, J)
      WOLD(1,J) = WBND(1,J)
      WOLD(IMAX,J) = WBND(IMAX, J)
30     CONTINUE
C     DO 33 J = 2, JMM1
C     DO 33 I=2,IMM1
C          WOLD(I,J) = WOLD(1,J) + (WOLD(IMAX,J) - WOLD(1,J)) *
C      #              FLOAT(I-1) / 60.0
C33   CONTINUE
C
C DO ITERATIONS
C
C     DO 32 I=21,29
C32   WRITE(1,*)K,I,YOLD(I,1)
       DO 899 K = 1, NMAX, ISTEP
C
C       SET OR RESET THE FLAG IF THE VORTICITY IS COMPUTED
C
         WCHECK = MOD(K,2) .EQ. 0
C
C       CALCULATE THE BOUNDARY CONDITIONS FOR W ON LOWER AND UPPER
BOUNDARIES
C     (J=1 OR J=JMAX), WHICH CHANGES DURING THE ITERATIONS
C
      IF(WCHECK) THEN
C          IF (K.EQ.2) THEN
           DO 31 J=1,JMAX
C              WOLD(1,J) = WBND(1,J)
31              WOLD(IMAX,J) = WBND(IMAX, J)
C          ENDIF
          DO 40 I = 2, IMM1
C          WRITE(*,*)YOLD(I,2),YOLD(I,3),YOLD(I,4)
C          WRITE(*,*)YOLD(I,JMAX-3),YOLD(I,JMM2),YOLD(I,JMM1)
C           IF ( I .GT. 21 .AND. I .LT. IRETACH ) THEN
C                WOLD(I, 1) = (1.0 - DELTA) *  WOLD(I,1) + DELTA *
W3(I)
C           ELSE
C                WOLD(I, 1) = (1.0 - DELTA) *  WOLD(I,1) + DELTA *
W1(I)
```

```
C          ENDIF
C                 WOLD(I, JMAX) = (1.0 - DELTA) *WOLD(I,JMAX) +
DELTA*W2(I)
C         WRITE(*,'(I3,3F10.4)')I,W1(I),W2(I),W3(I)
          WOLD(I,1) = WBND(I,1)
          WOLD(I,JMAX) = WBND(I,JMAX)
C     WRITE(*,*)I,WOLD(I,1),WOLD(I,JMAX)
40        CONTINUE
C     WRITE(*,'(A)')' OK'
      ELSE
          DO 32 J=1,JMAX
32             YOLD(IMAX,J) = YBND(IMAX, J)
          WRITE( 1, *)'K=', K
      ENDIF
C
C     DO 41 I = 1, IMAX
C     WRITE( *,'(4F10.4)') YOLD(I,1), YOLD(I, JMAX), WOLD(I,1),
C      #        WOLD(I, JMAX)
C41   CONTINUE
C     WRITE(*,'(A)')'***'
C     DO 42 J=1,JMAX
C     WRITE(*,'(4F10.4)') YOLD(1,J),YOLD(IMAX,J), WOLD(1,J),
C      #        WOLD(IMAX,J)
C42   CONTINUE
         DO 300 I = 2, IMM1
C          IF ( K .EQ. 1 .AND. I.GT.21 .AND. I.LT.IRETACH) THEN
C               YOLD(I,1) = YOLD(I-1,1)
C          ENDIF
           DO 100 J = 2, JMM1
C
C       CALCULATE THE VALUE NEEDED IN THE PRESENT ROW OF THE
C       COEFFICIENT MATRIX
C
             C1 = A1(I,J)
             C2 = A2(I,J) * RATF
             C3 = A3(I,J) * RAT2
             IF(WCHECK) THEN
               C4 = A4(I,J) * REY2
             ELSE
               C4 = 0.0
             END IF
             C5 = A5(I,J) * RATD
C     WRITE(*, '(I5,5F10.5)')I, C1,C2,C3,C4,C5
C
C       CALCULATE THE COEFFICIENT MATRIX
C
             IF(J .GT. 2) THEN
               A(J) = C3 - C5
             ENDIF
             B(J) = -2.0 * (C1 + C3)
             IF(J .LT. JMM1) THEN
               C(J) = C3 + C5
             ENDIF
C
```

```
C
C       FIND THE SOLUTION FOR THE PRESENT I-TH LINE
C
C     WRITE(*,'(I5, 4F10.3)')(I, A(J),B(J),C(J),D(J),J=2,JMM1)
         CALL TRID(A,B,C,D,R,2,JMM1)
C     WRITE(1,*)(R(J),J=1,JMAX)
C
C       UPDATE NEW VALUES
C
         IF(WCHECK) THEN
           DO 200 J = 2, JMM1
             WNEW(I,J) = (1.0 - BETAW) * WOLD(I,J) + BETAW * R(J)
C     WRITE(1,*)WNEW(I,J)
200        CONTINUE
C          WRITE(1,*)WNEW(I,2)
         ELSE
           DO 201 J = 2, JMM1
             YNEW(I,J) = (1.0 - BETAY) * YOLD(I,J) + BETAY * R(J)
C     WRITE(1,*)YNEW(I,J)
201        CONTINUE
C          WRITE(1,*)YNEW(I,2)
C
C      MODIFY THE BOUNDARY CONDITIONS FOR Y ON LOWER BOUNDARY ( J=1
)
C
        IF ( I .GT. 21 .AND. I .LE. IRETACH ) THEN
C          WRITE(*,*) I, YOLD(I,1), YNEW(I,2), YNEW(I,3)
C     AAA = 0.0
C     DO J = 3, JMM1
C          AAA = AAA + 2.0 * DELPSI / (YNEW(I,J+1) - YNEW(I,J-1))
C     ENDDO
C     BBB = DELPSI * ( 1.0 / YNEW(I,2) + 4.0 / YNEW(I,3) )
C*    YOLD(I,1) = 0.4 * (1.0 - AAA) / DELPSI -
C*      #         0.2 * ( YNEW(I,2) + YNEW(I,3) * 4.0 )
C     YOLD(I,1) = 2.0 * (1.0 - AAA) / BBB - 1.0
C               YOLD(I,1) = 2.0 * YNEW(I, 2) - YNEW(I,3) -
C      #        CF * (YNEW(I,3) - YNEW(I,2))
c     YOLD(I,1) = (6.0*(1.0-CF)*YOLD(I,2)-(3.0-2.0*CF)*YOLD(I,3))/
c      #         (3.0-4.0*CF)
      WRITE(1,*) I, YOLD(I,1), YOLD(I,2)
c     IF (I.EQ.IRETACH)THEN
c          IF (YOLD(IRETACH,1) .LT. 0.0 .AND.
c      #             YOLD(IRETACH-1,1).GT.0.0) THEN
c               STOP
c          ENDIF
c     ENDIF
            IF ( YOLD(I,1) .LT. 0.0 ) THEN
           IF (I.LT.IRETACH) THEN
                YOLD(I,1) = 0.0
           ENDIF
C               IRETACH = I
        ENDIF
         ENDIF
      ENDIF
```

```
C
C               ELSE IF(I .GT. 21 .AND. I .LE. IRETACH ) THEN
C                 IF(J. EQ. 2) THEN
C                   RB = 0.0
C                 END IF
C           ENDIF
C             END IF
C
C      CALCULATE THE RIGHT HAND SIDE OF THE SYSTEM EQUATION
C      WHICH DEPENDS ON THE INITIAL CONDITIONS (INTERIOR VALUE)
C
            RI = -(C1 - C4) * PNEW(I-1, J)
     #                    - (C1 + C4) * POLD(I+1, J)
            IF(J .EQ. 2) THEN
                 RI = RI + C2 * (PNEW(I-1,3) - POLD(I+1,3))
            ELSE IF(J .EQ. JMM1) THEN
                 RI = RI - C2 * (PNEW(I-1,JMM2) - POLD(I+1,JMM2))
            ELSE
                 RI = RI + C2 * (PNEW(I-1, J+1) - PNEW(I-1, J-1)
     #                      + POLD(I+1, J-1) - POLD(I+1, J+1))
            ENDIF
            IF(I .EQ. 2) THEN
              RI = -(C1 + C4) * POLD(3, J)
              IF(J .EQ. 2) THEN
                 RI = RI - C2 * POLD(3,3)
              ELSE IF(J .EQ. JMM1) THEN
                 RI = RI + C2 * POLD(3,JMM2)
              ELSE
                 RI = RI + C2 * (POLD(3, J-1) - POLD(3, J+1))
              ENDIF
            ELSE IF(I .EQ. IMM1) THEN
              RI = -(C1 - C4) * PNEW(IMM2, J)
              IF(J .EQ. 2) THEN
                 RI = RI + C2 * PNEW(IMM2,3)
              ELSE IF(J .EQ. JMM1) THEN
                 RI = RI - C2 * PNEW(IMM2,JMM2)
              ELSE
                 RI = RI + C2 * (PNEW(IMM2, J+1) - PNEW(IMM2, J-1))
              ENDIF
         ENDIF
C
C     THIS IS THE RECIRCULATING REGION AND THE REATTACHMENT POINT
C
C        IF ( .NOT. WCHECK ) THEN
C              IF( I .GT. 21 .AND. I .LT. IRETACH ) THEN
C                IF ( J .EQ. 2 ) THEN
C             RI = -( C1 + 2.0*C2 ) * PNEW( I-1, J ) -
C      #                     ( C1 - 2.0*C2 ) * POLD( I+1, J ) +
C      #                     2.0 * C2 * ( PNEW(I-1,3) - POLD(I+1,3) )
C          ENDIF
C           ENDIF
C             END IF
         R(J) = RB + RI
100           CONTINUE
```

```
C     THE RECIRCULATING REGION HAS DIFFERENT MATRIX
C
C         IF ( .NOT. WCHECK ) THEN
C          IF( I .GT. 21 .AND. I .LT. IRETACH )THEN
C                IF ( J .EQ. 2 ) THEN
C                    B(J) = -2.0 * ( C1 + C5 )
C                    C(J) = 2.0 * C5
C                ENDIF
C          ENDIF
C         ENDIF
C
C       CALCULATE THE RIGHT HAND SIDE OF THE SYSTEM EQUATION
C       WHICH DEPENDS ON THE BOUNDARY CONDITIONS (RHSi)
C
            IF(J .EQ. 2) THEN
                RB = C2 * (PBND(I+1,1) - PBND(I-1,1))
     #                  - (C3 - C5) * PBND(I,1)
            ELSE IF(J. EQ. JMM1) THEN
                RB = C2 * (PBND(I-1,JMAX) - PBND(I+1,JMAX))
     #                  - (C3 + C5) * PBND(I,JMAX)
            ELSE
                RB = 0.0
            END IF

            IF(I .EQ. 2) THEN
              RB = C2 * (PBND(1, J+1) - PBND(1, J-1))
     #               - (C1 - C4) * PBND(1, J)
              IF(J .EQ. 2) THEN
                RB = RB + C2 * PBND(3,1) - (C3 - C5) * PBND(I,1)
              ELSE IF(J. EQ. JMM1) THEN
                RB = RB - C2 * PBND(3,JMAX)
     #                  - (C3 + C5) * PBND(I,JMAX)
              END IF
            ELSE IF(I .EQ. IMM1) THEN
              RB = C2 * (PBND(IMAX, J-1) - PBND(IMAX, J+1))
     #                - (C1 + C4) * PBND(IMAX, J)
              IF(J .EQ. 2) THEN
                RB = RB - C2 * PBND(IMM2,1)
     #                  - (C3 - C5) * PBND(I,1)
              ELSE IF(J. EQ. JMM1) THEN
                RB = RB + C2 * PBND(IMM2,JMAX)
     #                 - (C3 + C5) * PBND(I,JMAX)
              END IF
            ENDIF
C         IF ( .NOT. WCHECK ) THEN
C
C     THIS IS THE SEPARATION POINT
C
C              IF( I .EQ. 21 ) THEN
C                IF(J .EQ. 2) THEN
C                  RB = -C2 * HSTEP
C                END IF
C
C     THIS IS THE RECIRCULATING REGION AND THE REATTACHMENT POINT
```

```
300       CONTINUE
      IF(WCHECK)THEN
C
C     CHECK THE CONVERGENCE ACCORDING TO THE OUTER CONVERGENCE
C     CRITERIA
C
C        IF(CHECK(WNEW,WOLD,IMAX,JMAX,EPSILW)) THEN
C
C     SOLUTION HAS CONVERGED, RECORD NUMBER OF ITERATIONS AND
C     EXIT THE DO-LOOP
C
C          N = K
C          GOTO 999
C        ENDIF
      ELSE
C
C     CALCULATE THE DAMPING FACTOR FOR THE INNER CONVERGENCE
C     CRITERIA
C
        IF(CHECK(YNEW,YOLD,IMAX,JMAX,EPSILY)) THEN
C
C     SOLUTION HAS CONVERGED, RECORD NUMBER OF ITERATIONS AND
C     EXIT THE DO-LOOP
C
          N = K
          GOTO 999
        ENDIF
         IF(K .GT. MMU)THEN
            YE=0.0
            DO 102 I=2,IMM1
               DO 101 J=2,JMM1
                  YE=AMAX1(YE,ABS(YNEW(I,J) -YOLD(I,J)))
101            CONTINUE
102         CONTINUE
            IF(YEOLD.EQ.0.0)YEOLD=1.0
            RHO = YE /YEOLD
            DELTA=RHO/(RHO+2.0)
            YEOLD=YE
            WRITE(1,*)DELTA
         ENDIF
      ENDIF
C
C     TRANSFER THE NEW PHI'S TO THE OLD PHI'S
C
C     TRANSFER THE BOUNDARIES IF IT IS THE FIRST STEP
C
      IF(WCHECK) THEN
C
C     TRANSFER THE BOUNDARIES
C
C      DO 810 I=1,IMAX
C         WOLD(I,1)=WBND(I,1)
C         WOLD(I,JMAX)=WBND(I,JMAX)
C810   CONTINUE
```

```
C        DO 710 J=1,JMAX
C           WOLD(1,J)=WBND(1,J)
C           WOLD(IMAX,J)=WBND(IMAX,J)
C710     CONTINUE
C
C       TRANSFER THE INTERIOR VALUES
C
          DO 700 I = 2, IMM1
            DO 800 J = 2, JMM1
              WOLD(I,J)  =  WNEW(I,J)
800         CONTINUE
700       CONTINUE
C
C        CALCULATE THE RELATIVE ERROR AGAINST THE BENCH VALUES
C
C          WRITE(1,*)K,(WOLD(I,1),I=1,IMAX),ERROR
        ELSE
C
C       TRANSFER THE BOUNDARIES
C
C        DO 815 I=1,IMAX
C           YOLD(I,1)=YBND(I,1)
C           YOLD(I,JMAX)=YBND(I,JMAX)
C815     CONTINUE
C        DO 715 J=1,JMAX
C           YOLD(1,J)=YBND(1,J)
C           YOLD(IMAX,J)=YBND(IMAX,J)
C
C
C       TRANSFER THE INTERIOR VALUES
C
          DO 701 I = 2, IMM1
            DO 801 J = 2, JMM1
              YOLD(I,J)  =  YNEW(I,J)
C     WRITE(*,*)I,J,YOLD(I,J)
801         CONTINUE
701       CONTINUE
        ENDIF
C
C        INCREMENT NUMBER OF ITERATIONS
C
899          CONTINUE
      N = K
C
C       SOLUTION FAILS TO CONVERGE
C
        WRITE(1,'(A)')' SOLUTION APPARENTLY FAILS TO CONVERGE'
C        GOTO 1100
999     CONTINUE
C
C        W VALUES HAVE CONVERGED, PRINT SOLUTION
C
        WRITE(1,199)N
199        FORMAT(' NUMBER OF ITERATIONS = ',I4)
```

```
      WRITE(1,97)
97    FORMAT(10X,' SOLUTION'/3(9X,'I',3X,'X',6X,'Y',2X))
         DO 600 I = 1,20
                WRITE(1,99)I,X(I), YOLD(I,1),I+20,X(I+20),
     #                 YOLD(I+20,1),I+40,X(I+40),YOLD(I+40,1)
600      CONTINUE
99    FORMAT(3(I10,F5.1,F8.5))
1100        CONTINUE
      CLOSE(UNIT=1)
      STOP
      END

      LOGICAL FUNCTION CHECK(A,B,IL,IU,E)
C
C      THIS FUNCTION CHECKS TO SEE IF (A(I,J) - B(I,J)) < E
C      FOR ALL I,J
C
     IMPLICIT DOUBLE PRECISION (A-H, O-Z)
      DIMENSION A(IL,IU), B(IL,IU)
      CHECK = .TRUE.
      DO 200 I = 2, IL-1
        DO 100 J = 2, IU-1
          IF(ABS(A(I, J) - B(I, J)) .GE. E)THEN
            CHECK = .FALSE.
            RETURN
          ENDIF
100        CONTINUE
200      CONTINUE
      RETURN
      END

      SUBROUTINE TRID(A,B,C,D,F,NL,NU)
C
C      SCALAR TRIDIAGONAL SOLVE (THOMAS ALGORITHM)
C      NL AND NU ARE INDEX LIMITS, NL <= N <= NU
C      A,B,C ARE TRIDIAGONAL ELEMENTS WITH B ARRAY ON THE
C      MAIN DIAGONAL
C      D IS SCRATCH OR DUMMY ARRAY
C      F IS FHS FORCING FUNCTION, THE SOLUTION IS OVERLOADED IN F
C
     IMPLICIT DOUBLE PRECISION (A-H, O-Z)
      DIMENSION A(1),B(1), C(1), D(1), F(1)
      D(NL) = C(NL) / B(NL)
      F(NL) = F(NL) / B(NL)
      NLP = NL + 1
      DO 10 N = NLP, NU
         Z = 1.0 / (B(N) - A(N) * D(N - 1))
         D(N) = C(N) * Z
         F(N) = (F(N) - A(N) * F(N - 1)) * Z
10      CONTINUE
C
C      BACK SWEEP
C
      NUP = NU + NL
```

```
      DO 20 NN = NLP, NU
         N = NUP - NN
         F(N) = F(N) - D(N) * F(N + 1)
20      CONTINUE
      RETURN
      END

      double precision FUNCTION PBND(I,J)
C
C       THIS FUNCTION RETURNS THE BOUNDARY VALUE OF AN ELEMENT OF
THE
C         PHI ARRAY WHICH COULD BE EITHER Y BOUNDARY VALUE OR W
BOUNDARY VALUE
C
C       COMMON /WCH/WCHECK
C       LOGICAL WCHECK
C       IF(WCHECK) THEN
C         PBND = WBND(I,J)
C       ELSE
C         PBND = YBND(I,J)
C       ENDIF
      IMPLICIT DOUBLE PRECISION (A-H, O-Z)
       PBND = POLD(I,J)
       RETURN
       END

       double precision FUNCTION PNEW(I,J)
C
C       THIS FUNCTION RETURNS THE FUNCTION VALUE AT A NEW ITERATION
LEVEL OF
C       PHI ARRAY WHICH COULD BE EITHER Y OR W
C
      IMPLICIT DOUBLE PRECISION (A-H, O-Z)
       PARAMETER (IMAX = 61, JMAX = 21)
       DIMENSION WOLD(IMAX,JMAX), WNEW(IMAX,JMAX),
      #      YOLD(IMAX,JMAX), YNEW(IMAX,JMAX)
       COMMON /WVALUE/WOLD, WNEW/YVALUE/YOLD, YNEW/WCH/WCHECK
       LOGICAL WCHECK
       IF(WCHECK) THEN
         PNEW = WNEW(I,J)
       ELSE
         PNEW = YNEW(I,J)
       ENDIF
       RETURN
       END

       double precision FUNCTION POLD(I,J)
C
C       THIS FUNCTION RETURNS THE FUNCTION VALUE AT A OLD ITERATION
LEVEL OF
C       PHI ARRAY WHICH COULD BE EITHER Y OR W
C
      IMPLICIT DOUBLE PRECISION (A-H, O-Z)
       PARAMETER (IMAX = 61, JMAX = 21)
```

```
       DIMENSION WOLD(IMAX,JMAX), WNEW(IMAX,JMAX),
     #       YOLD(IMAX,JMAX), YNEW(IMAX,JMAX)
       COMMON /WVALUE/WOLD, WNEW/YVALUE/YOLD, YNEW/WCH/WCHECK
       LOGICAL WCHECK
       IF(WCHECK) THEN
         POLD = WOLD(I,J)
       ELSE
         POLD = YOLD(I,J)
       ENDIF
       RETURN
       END

       double precision FUNCTION YBND(I,J)
C
C       THIS FUNCTION RETURNS THE BOUNDARY VALUE OF Y AT I,J.
C       I MUST EQUAL 1 OR IMAX, OR J MUST EQUAL 1 OR JMAX
C
      IMPLICIT DOUBLE PRECISION (A-H, O-Z)
       PARAMETER (IMAX=61, JMAX = 21)
       DIMENSION YOLD(IMAX,JMAX), YNEW(IMAX,JMAX)
       COMMON /YVALUE/YOLD, YNEW
       COMMON /BND/DELX, DELPSI, XMIN, PSIMIN, REY
       DATA PI/3.1415927/
       IF(I .EQ. 1) THEN
          THETA = ACOS(1.0 - 2.0*PSI(J)) / 3.0
          YBND = COS(THETA + 4.0 * PI / 3.0) + 0.9
       ELSE IF (I.EQ.IMAX) THEN
C          THETA = ACOS(1.0 - 2.0*PSI(J)) / 3.0
C          YBND = 1.4 * COS(THETA + 4.0 * PI / 3.0) + 0.7
        YBND = YOLD(I-1,J)
       ELSE IF (J .EQ. JMAX) THEN
          YBND = 1.4
       ELSE IF(J .EQ. 1) THEN
      IF ( I .LE. 21 ) THEN
           YBND = 0.4
      ELSE IF ( I .GE. 29 ) THEN
           YBND = 0.0
      ELSE
           YBND = 0.4 * SQRT( 1.0 - ( ( X(I) - 2.0 ) / 0.8 ) ** 2 )
      ENDIF
       ENDIF
       RETURN
       END

       double precision FUNCTION WBND(I,J)
C
C       THIS FUNCTION RETURNS THE BOUNDARY VALUE OF W AT I,J.
C       I MUST EQUAL 1 OR IMAX, OR J MUST EQUAL 1 OR JMAX
C
      IMPLICIT DOUBLE PRECISION (A-H, O-Z)
       PARAMETER (IMAX=61, JMAX = 21)
       DIMENSION WOLD(IMAX,JMAX), WNEW(IMAX,JMAX),
     #       YOLD(IMAX,JMAX), YNEW(IMAX,JMAX)
       COMMON /WVALUE/WOLD, WNEW/YVALUE/YOLD, YNEW/WA/HSTEP
```

```
      IF (I .EQ. 1) THEN
         WBND = 12.0 * YBND(I,J) - 10.8
      ELSE IF (I.EQ.IMAX) THEN
      WBND = WOLD(I-1,J)
C4.373177843 * YBND(I,J) - 3.06122449
      ELSE IF (J.EQ.1) THEN
     IF ( I .GT. 21 .AND. I .LT. 29 ) THEN
       WBND = 0.0
     ELSE
       WBND = 3.0 * ( FLOAT(I-1) / 60.0 - 2.0 )
     ENDIF
      ELSE IF (J.EQ.JMAX) THEN
      WBND = WOLD(I,J-1)
c-3.0 * ( FLOAT(I-1) / 60.0 - 2.0 )
      ENDIF
      RETURN
      END

      double precision FUNCTION PSI(J)
     IMPLICIT DOUBLE PRECISION (A-H, O-Z)
      COMMON /BND/DELX, DELPSI, XMIN, PSIMIN, REY
      PSI = PSIMIN + (J - 1) * DELPSI
      RETURN
      END

      double precision FUNCTION X(I)
     IMPLICIT DOUBLE PRECISION (A-H, O-Z)
      COMMON /BND/DELX, DELPSI, XMIN, PSIMIN, REY
      X = XMIN + (I - 1) * DELX
      RETURN
      END

      double precision FUNCTION DELXY(I,J)
     IMPLICIT DOUBLE PRECISION (A-H, O-Z)
      PARAMETER (IMAX=61, JMAX=21)
      DIMENSION YOLD(IMAX,JMAX), YNEW(IMAX,JMAX)
      COMMON /BND/DELX, DELPSI, XMIN, PSIMIN, REY
      COMMON /YVALUE/YOLD, YNEW
      IF(I .EQ. 1) THEN
         DELXY = (YOLD(I+1, J) - YOLD(I, J)) / DELX
      ELSE IF(I .EQ. IMAX) THEN
         DELXY = (YOLD(I, J) - YOLD(I-1, J)) / DELX
      ELSE
         DELXY = (YOLD(I+1, J) - YOLD(I-1, J)) / (2.0 * DELX)
      END IF
      RETURN
      END

      double precision FUNCTION DELPSY(I,J)
     IMPLICIT DOUBLE PRECISION (A-H, O-Z)
      PARAMETER (IMAX=61, JMAX=21)
      DIMENSION YOLD(IMAX,JMAX), YNEW(IMAX,JMAX)
      COMMON /BND/DELX, DELPSI, XMIN, PSIMIN, REY
      COMMON /YVALUE/YOLD, YNEW
```

```
IF(J .EQ. 1) THEN
   DELPSY = (YOLD(I, J+1) - YOLD(I, J)) / DELPSI
ELSE IF(J .EQ. JMAX) THEN
   DELPSY = (YOLD(I, J) - YOLD(I, J-1)) / DELPSI
ELSE
   DELPSY = (YOLD(I, J+1) - YOLD(I, J-1)) / (2.0 * DELPSI)
END IF
RETURN
END
```

VITA AUCTORIS

Paul Carson graduated from the University of Windsor in Honours Mathematics in 1969 (B.Sc.) and in Applied Mathematics in 1970 (MSc.). He received a Master's Degree in Aeronautical Engineering (M.Eng.) in 1977 from Carleton University and his P.Eng. from the Association of Professional Engineers in 1981. He holds both senior Airline Transport Pilot Licences (ATPL) issued by Canada and the United States. He has worked for the Defence Research Board of Canada, the Federal Department of Transport and Bell Canada in a number of capacities, including research scientist, engineer and pilot. Mr. Carson is a member of several professional organizations and associations including the Canadian Aeronautics and Space Institute, the Association of Professional Engineers of Ontario, the Canadian Airline Pilots' Association, the International Society for Air Safety Investigators, and most recently, the Human Factors Association of Canada. He is currently studying towards an honours B.A. degree in Psychology at the University of Ottawa.